REACTION KINETICS IN ENVIRONMENTALLY BENIGN NOVEL SOLVENT SYSTEMS

A Thesis
Presented to
The Academic Faculty

by

Heather Patrick Lesutis

In Partial Fulfillment
of the Requirements for the Degree
Doctor of Philosophy in Chemical Engineering

Georgia Institute of Technology
April 2000

REACTION KINETICS IN ENVIRONMENTALLY
BENIGN NOVEL SOLVENT SYSTEMS

Approved:

Charles A. Eckert, Chairperson

Charles L. Liotta

Agaram S. Abhiraman

Dennis W. Hess

Amyn S. Teja

Date Approved 4/6/00

DEDICATION

I dedicate this thesis to my family, without whose love and encouragement this work would not have been possible. This is dedicated to Mike, for his unending love and support in every imaginable way; to Mom and Dad, for always encouraging me to do the best I can; to Grandpa, for being a wonderful role model; to Grandma, for always being proud of me; and to Casey, for always bringing a smile to my face.

ACKNOWLEDGEMENTS

I would like to thank my advisor, Professor Charles Eckert, for his invaluable guidance and support of this research. I would also like to thank Professor Charles Liotta for always sharing his knowledge of and excitement about organic chemistry. Additionally, I would like to thank Professors Agaram Abhiraman, Dennis Hess, and Amyn Teja for their time and assistance as members of my thesis committee.

I would like to thank Dr. David Schiraldi at KoSa for his input and enthusiasm in the work focusing on the supercritical fluid promoted esterification of terephthalic acid. I would also like to thank Dr. Laura Babcock and Dr. Michael Jones at Hercules for their assistance in the nearcritical water polymerizations. I also acknowledge Charles Kizer at Celanese Acetate for his contribution to the research focusing on the treatment of cellulose and cellulose acetate with nearcritical water. Dr. Walter Partenheimer and Dr. Michael Vincent from DuPont assisted greatly with the phase-transfer catalytic oxidation of *p*-xylene. I also appreciate the many hours Jeff Andrews spent to machine the titanium tube reactors used in the nearcritical water research.

I would like to thank the Eckert and Liotta research groups for their friendship and for their contributions to this work. In particular, I gratefully acknowledge the contributions from Dr. Roger Gläser, Richard Coelho, James Brown, Kris Griffith, Christy Culp, Kevin West, Dr. David Lamb, Dr. Barry West, and Dr. David Bush. Finally, I would like to thank Greg Ladzinske for his assistance in the lab.

TABLE OF CONTENTS

LIST OF TABLES

LIST OF FIGURES

SUMMARY

Many conventional organic solvents used in commercial processes carry the distinct disadvantages of being both expensive and deleterious to the environment. Replacement solvent systems are required if the products of these processes are to be produced in a sustainable fashion. These replacement solvent systems must not introduce substantial cost over the systems they replace. They must allow for facile separation after the reaction is run, and they must be environmentally benign. Most importantly, these replacement solvent systems must allow the desired reaction to run at an acceptable rate.

This thesis presents kinetic data for reactions run in three types of replacement solvent systems. First, supercritical fluids are studied as a means of accomplishing simultaneous reaction and extraction. A desired intermediate in a series reaction was produced and isolated by running the reaction in scDME, in which the desired intermediate is soluble. Nearcritical water is then evaluated as a catalytic solvent for reactions, including polymerizations and Beckmann rearrangements, which are currently run with large amounts of Lewis acid catalysts. Finally, a low temperature phase-transfer catalytic system is assessed for the environmentally benign oxidation of *p*-xylene to terephthalic acid and its precursors.

CHAPTER I

INTRODUCTION

For both economic and environmental reasons, solvent selection is one of the most important tasks in the design of any chemical process. A solvent system must allow reactants and catalysts to come together efficiently in a single phase, so that reaction can take place. It also must not yield prohibitive resistance to mass transfer. After a reaction has taken place, the solvent system must be removed with minimal cost, both economically and environmentally. The solvent must be removed so that it can be recycled and, in many cases, so that traces of residual solvent do not contaminate the final product. This work explores three fields that offer great opportunities for the replacement of many commonly used toxic, organic solvents. First, supercritical fluids are studied as a means of accomplishing simultaneous reaction and extraction. Nearcritical water is then evaluated as a catalytic solvent for reactions that are currently run with large amounts of Lewis acid catalysts. Finally, a low temperature phase-transfer catalytic system is assessed for the potential replacement of an environmentally deleterious system.

Chapter II reports the successful production and isolation of an intermediate in a series reaction, accomplished by running the reaction in supercritical dimethyl ether (T_c = 126.9°C, P_c = 52.4 bar). In this work, mono (2-hydroxyethyl terephthalate), a potential monomer in the production of poly(ethylene terephthalate), was synthesized from

terephthalic acid (TA) and ethylene oxide in the presence of several quaternary ammonium salt catalysts. Supercritical dimethyl ether is a good solvent here because, while neither the reactant TA nor the catalyst is soluble in it, MHET is quite soluble. When this reaction was run semi-batch, the MHET dissolved in the solvent upon its formation. It was then removed from the packed bed of TA and catalyst before it could react further to the undesired diester. The solvent was removed from the product by simply depressurizing. Here, the liquid-like solvent power and gas-like transport properties of supercritical fluids were employed to achieve a simultaneous reaction and extraction in order to stop a reaction at the desired intermediate product.

Chapter III investigates liquid water in the nearcritical region for applications as both a benign solvent and a self-neutralizing catalyst. Because both salts and organic compounds are soluble in nearcritical water, many reactions can be run homogeneously in it. Also, the dissociation constant of water in the nearcritical region is high enough that it is a significant source of both hydronium and hydroxide ions. It is possible to run acid- and base-catalyzed reactions in nearcritical water without the addition of any acid or base. Water neutralizes itself upon cooling, eliminating the need to dispose of large quantities of salt waste. Here, the rates of hydrolyses of several benzoic acid esters and several substituted anisoles are measured. Examination of Hammett plots allows analysis of the competitive catalysis from the two ions formed from the dissociation of water.

In Chapter III, catalytic ester and anisole hydrolyses were run successfully in nearcritical water without the addition of any acid or base. Following this achievement, the kinetics of several commercially important acid-catalyzed reactions were studied in

nearcritical water. Styrene and 1,3-pentadiene are commonly polymerized in a cationic polymerization in the presence of Lewis acid catalysts such as $AlCl_3$ or BF_3. These catalysts must eventually be neutralized with the addition of base, and the resulting salts leave the plant as a waste byproduct. These polymerizations were evaluated in nearcritical water, both neat and with added traces of acetic acid, to determine the viability of solvent replacement for these reactions. The acid-catalyzed redistribution of acetyl groups in cellulose acetate, as well as the acetylation of cellulose with acetic acid, was also attempted in nearcritical water. A process run in hot water could eliminate the need for sulfuric acid catalyst, which would improve the process both financially and from a sustainability standpoint. Finally, the Beckmann rearrangement of cyclohexanone oxime to ε-caprolactam, a precursor to nylon 6, was investigated in nearcritical water. The results of these commercially important studies are given in Chapter IV.

In Chapter V, a phase-transfer catalytic system is investigated as a potential replacement for the current high temperature oxidation of *p*-xylene to terephthalic acid in acetic acid. Because this reaction is catalyzed by bromide anion, acetic acid is utilized to bring the organic reactant component and the catalyst salt into the same phase. Here, a quaternary ammonium salt, which can transport bromide ions between an aqueous phase and an organic phase, makes the use of acetic acid obsolete. Water is the solvent for the bromide catalyst, and the phase-transfer catalyst carries the oxidation catalyst into the *p*-xylene phase.

Finally, recommendations for continuing work on solvent system replacement are made in Chapter VI. Some suggestions are made for the continuation and improvement

of the work presented in this thesis. Several other acid-catalyzed reactions are also proposed for their study in nearcritical water. Finally, nearcritical water as a benign medium for thermal polymerizations and oxidation reactions is suggested.

CHAPTER II

SUPERCRITICAL FLUID SEPARATION FOR SELECTIVE QUATERNARY AMMONIUM SALT PROMOTED ESTERIFICATION OF TEREPHTHALIC ACID

Introduction

Poly(ethylene terephthalate) (PET) can be produced from an atypical monomer, mono (2-hydroxyethyl terephthalate) (MHET). This polymerization is superior to the current process, which uses ethylene glycol and terephthalic acid (TA), for two reasons. First, the proposed process has lower heat-flux and mass-flux loads in the polymerizer. Because the polymerization is diffusion controlled, MHET will yield a faster polymerization. Also, polymerization of MHET will require the removal of only half the water removed in the conventional polymerization, yielding a more economical polymerization. While this polymerization does require more precise feed control, this is within the capabilities of modern process equipment.

In this work, MHET was synthesized from the esterification of TA and ethylene oxide (EO) in the presence of a quaternary ammonium salt catalyst. The desired product, MHET, was continuously extracted by a supercritical fluid before a second esterification could occur (Figure 2-1).

We examined several pure and modified supercritical fluids because of their tunable solvent power (Brennecke and Eckert, 1989; Gurdial and Foster, 1991; Eckert and Knutson, 1993; McHugh and Krukonis, 1994). This tunability allowed us to remove

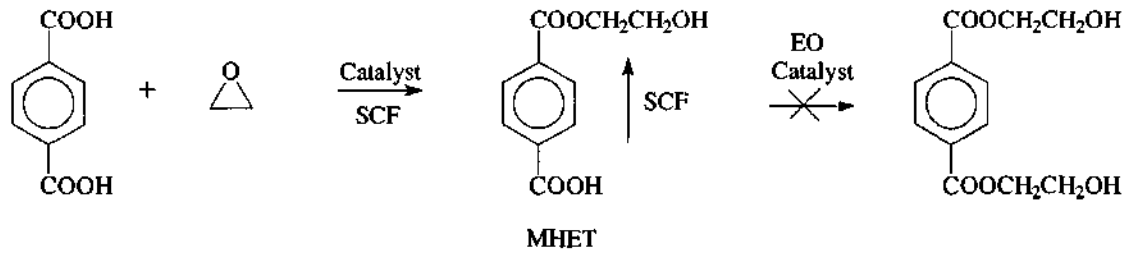

Figure 2-1. Selective ethoxylation of terephthalic acid to MHET.

selectively the intermediate product from the insoluble catalyst/terephthalic acid bed before subsequent reaction. This extraction was followed by facile separation of the product from the SCF by depressurization.

The catalyst was required to be stable at the reaction conditions (100-150°C), to be insoluble in the supercritical solvent, and to have a readily accessible anion to lower the activation energy of the reaction. Because current commercially available quaternary ammonium salts do not meet the first criterion, novel thermally stable quaternary ammonium salt catalysts were synthesized specifically for this reaction.

Supercritical Fluids as Separation and Reaction Solvents

Supercritical fluids are pure fluids or mixtures above both their critical temperature (T_c) and their critical pressure (P_c) (Figure 2-2). Supercritical fluids have a unique set of thermophysical properties, making them candidates for solvent use in many processes, including separations and reactions. Possible separations include decaffeination of coffee and extraction of edible oils (McHugh and Krukonis, 1994). Suggested reactions range from polymerizations in supercritical fluids to the destruction of toxic organic waste in scH_2O (Brennecke and Eckert, 1989; McHugh and Krukonis, 1994).

A fluid near its critical point has a density near that of a liquid and, thus, makes a good solvent (Figure 2-3). Supercritical fluids are very compressible, so they undergo large changes in density with small changes in temperature or pressure (Figure 2-4)

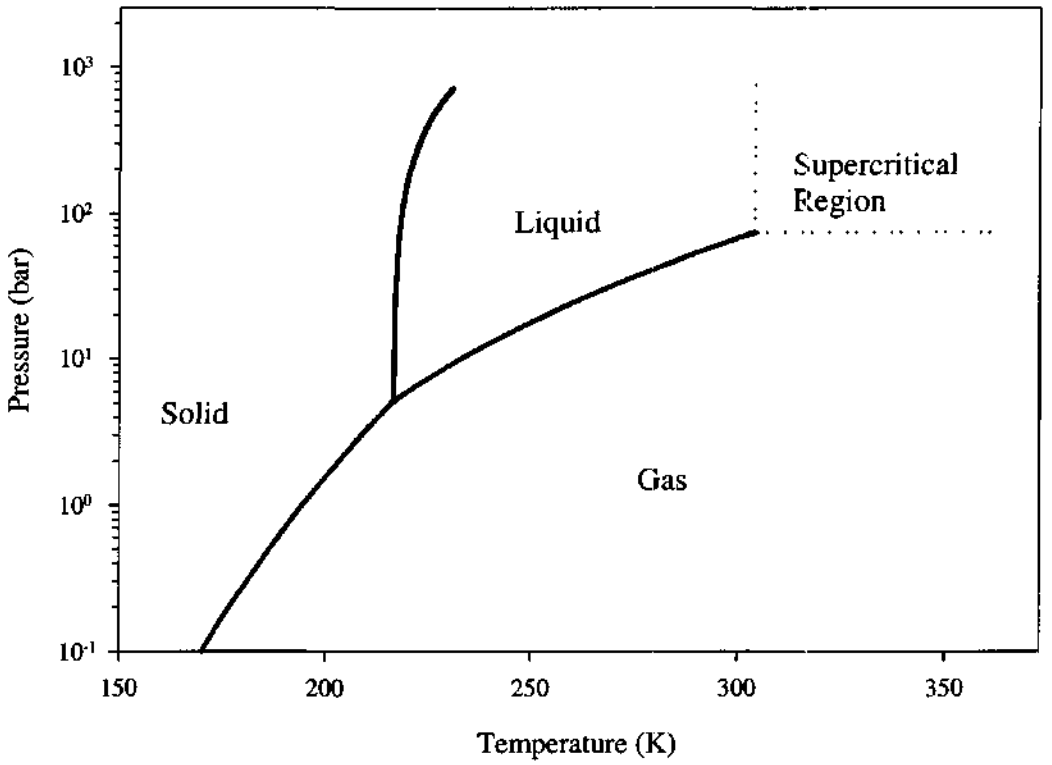

Figure 2-2. Phase diagram of CO_2 (Angus et al., 1976).

(Gurdial and Foster, 1991; Eckert and Knudson, 1993; McHugh and Krukonis, 1994).

These changes in density make supercritical fluids ideal solvents for tuning solubilities, reaction equilibria, and kinetics. Solubilities can change dramatically with slight changes in pressure; the solubility of naphthalene in CO_2 at 318K changes by over an order of magnitude with only a 20% increase in pressure (Tsekhanskaya et al., 1964). Kim and Johnston (1988) used pressure to alter product selectivity in the Diels-Alder addition of methyl acrylate to cyclopentadiene in $scCO_2$. They tuned the endo- to exo- equilibrium constant by changing the pressure of CO_2. Reaction rates can also be controlled by adjusting pressure. Johnston and Haynes (1987) used pressure to alter the rate constant for the thermal decomposition of α-chlorobenzyl methyl ether in supercritical 1,1-difluoroethane. They increased the rate constant by an order of magnitude with only a 30% increase in pressure near the critical point.

The addition of cosolvents can also greatly affect solubilities, equilibria, and kinetics in supercritical fluids. Solubilities in supercritical fluids can increase by orders of magnitude with the addition of a few percent of a cosolvent (Brennecke and Eckert, 1989). Equilibria can also shift with the addition of a small amount of cosolvent. Dillow et al. (1997) found that the tautomeric equilibrium for the Schiff base 4-(methoxyl)-1-(N-phenylforminidoyl)-2-naphthol was affected by the type, concentration, and density of a hydrogen bonding cosolvent when run in supercritical ethane. Finally, Knutson et al. (1995) used cosolvents to alter reaction rates in the Diels-Alder reaction of maleic anhydride and 2,3-dimethyl-1,3-butadiene.

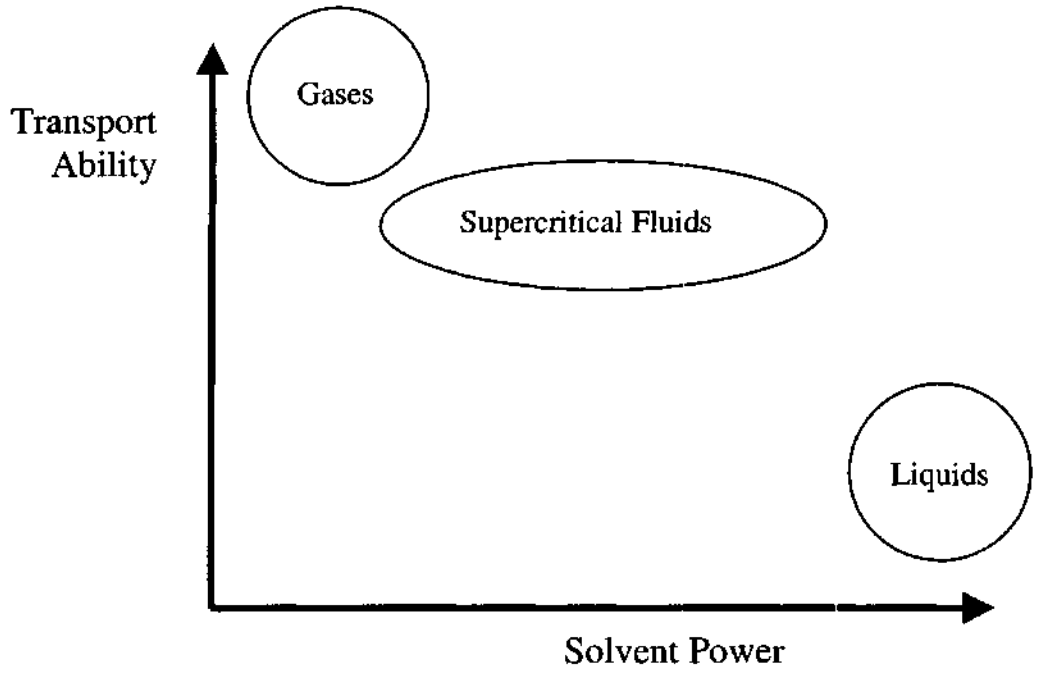

Figure 2-3. Solvent power and transport properties of supercritical fluids.

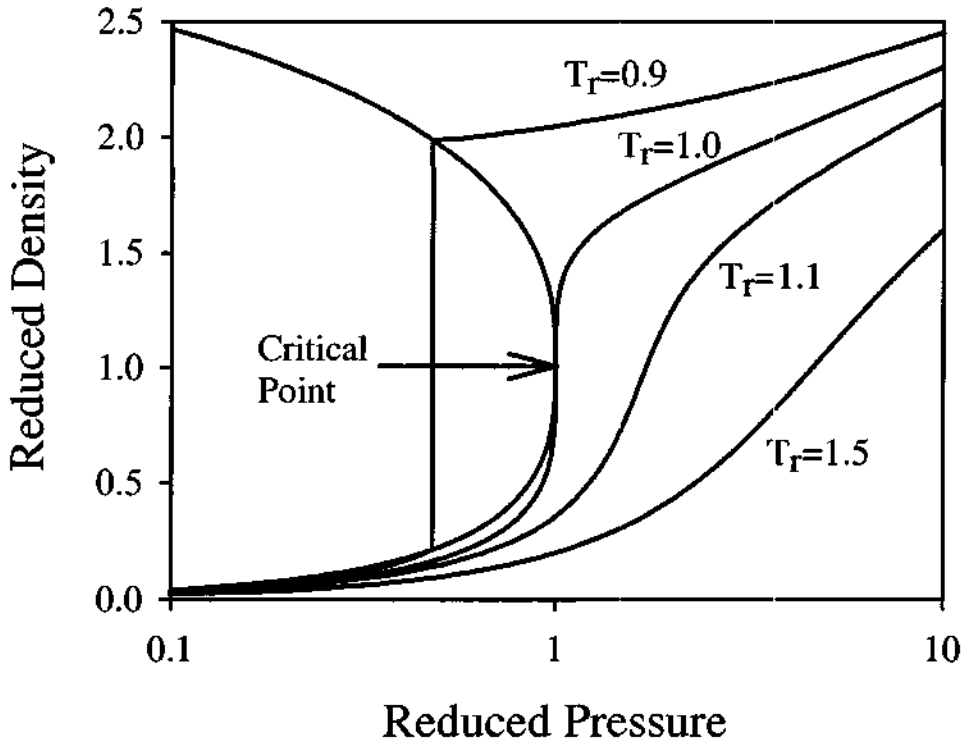

Figure 2-4. Reduced density of CO_2 as a function of reduced pressure and reduced temperature (Ely et al., 1989).

While supercritical fluids have solvating strengths near those of liquids, they have transport properties similar to those of gases (Figure 2-3). They have high diffusivities and low viscosities, making them ideal candidates for use as solvents in the previously mentioned separations and reactions (Brennecke and Eckert, 1989; Tsekhanskaya, 1968, 1971).

These unique thermophysical properties of supercritical fluids make them useful for simultaneous reaction and separation. Their liquid-like, tunable densities encourage applications as reaction solvents, while their compressibilities, which make removal by depressurization a facile process, encourage applications in separations. Kiran and Saraf (1990) utilized supercritical fluids for simultaneous polymerization and separation of styrene in supercritical n-butane. When a polystyrene molecule became sufficiently large, it dropped out of solution, and polymerization stopped. They found that, as solvent density decreased, the polymer solubility decreased, and polymer chain length decreased.

Experimental Methods

Materials

Chemicals used in the experiments and calibrations were the following: acetone (Aldrich, HPLC, 99.9+%), anthracene (Aldrich, 99+%), benzyl viologen dichloride (BVDC; Aldrich, 97%), carbon dioxide (Matheson Gas Products, 99.8+%), [(diethylamino)methyl]-polystyrene (PSDEA; Fluka), dimethyl ether (DME; Matheson

Gas Products, 99.8+%), ethylene oxide (Aldrich, 99.5%), hexadimethrine bromide (HMDB; Aldrich), propane (Matheson Gas Products, 99.97+%), tetrahexylammonium bromide (THAB; Aldrich, 99%) and terephthalic acid (KoSa). Novel quaternary ammonium salt catalysts were synthesized as described in Appendix A (Figure 2-5).

Experimental Procedure

Prior to reaction, dimethyl ether and ethylene oxide were added to a high-pressure syringe pump (ISCO 500D). The syringe pump was pressurized to 70 bar with 200 ml of fluid. Ethylene oxide was metered in as a liquid (0.5 mol% with respect to the supercritical fluid) with a pressure generator (High Pressure Products model 62-6-10). Sufficient DME was then added through the same port to flush all of the EO into the pump cylinder and to improve mixing. The contents were thoroughly mixed by coupling an external magnet with a Teflon-coated magnetic stir bar (Fisher Scientific) previously placed in the pump. Mixing was verified by performing multiple runs with identical conditions with the same pump mixture.

The catalyst/terephthalic acid solid mixture was prepared by combining 10 grams of terephthalic acid, catalyst (5 mol% with respect to the terephthalic acid), and a sufficient volume of methylene chloride to dissolve all of the catalyst (~100 ml). The mixture was shaken in a round bottom flask, and the methylene chloride was removed by rotary evaporation to ensure a uniform coating of catalyst on the terephthalic acid.

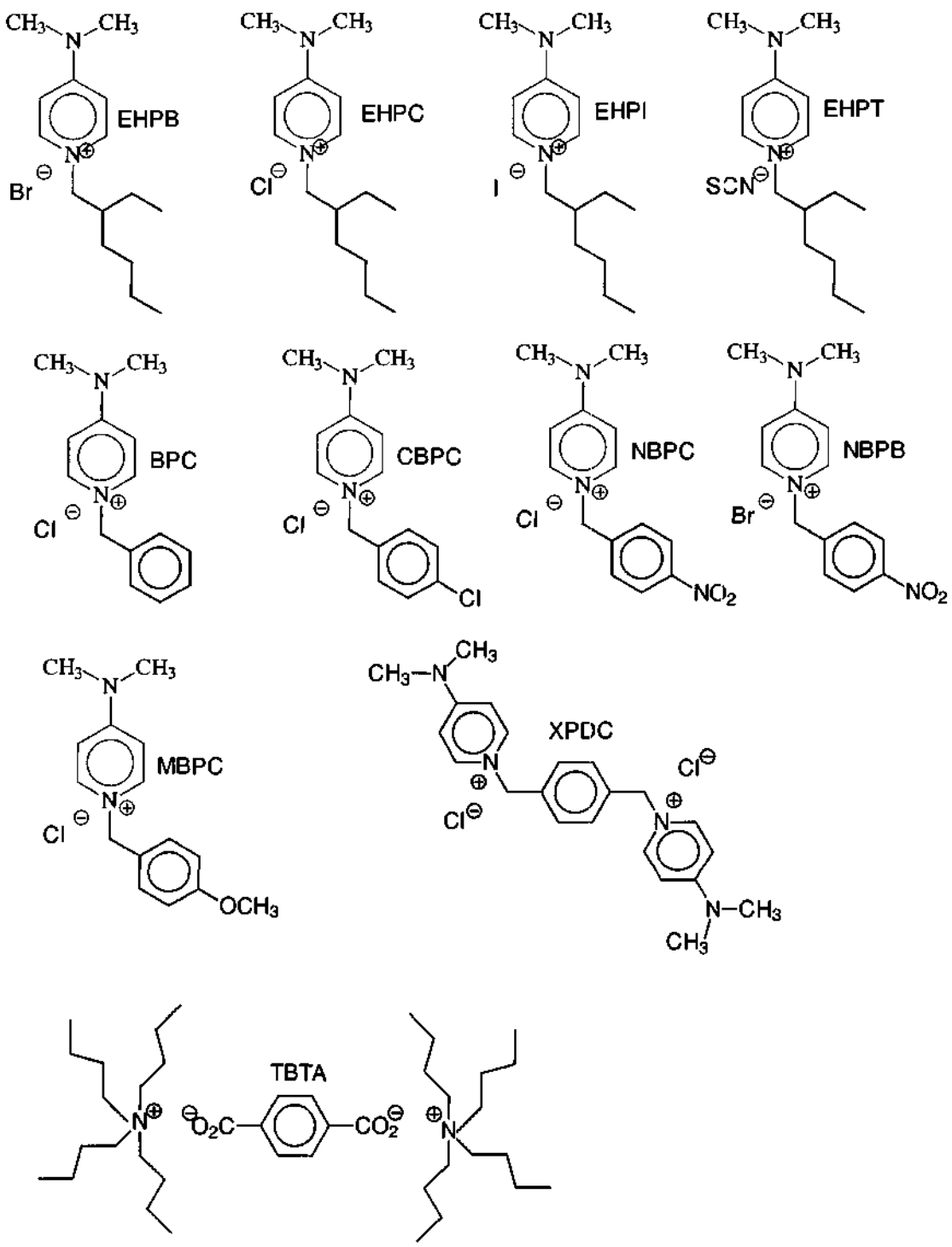

Figure 2-5. Synthesized catalysts with structures and abbreviations.

The particle size was on the order of 10 to 100 μm. A total of 0.2 grams of the terephthalic acid/catalyst mixture was loaded into a 6 mm diameter reaction thimble and held in place with glass wool. The thimbles were placed in a dessicator until required for reaction.

The reactions were performed in a Hewlett Packard 7680T supercritical fluid extractor modified to accept a variety of solvents. The DME / EO mixture was pumped at 70 bar and 25°C at a flowrate of 5 ml/min for 15 minutes (Figure 2-6).

All catalysts were evaluated in dimethyl ether at 130°C and 70 bar with 0.5 mol% ethylene oxide with respect to dimethyl ether. Reaction products have a significantly higher solubility than either the solid reactant or the solid catalyst in supercritical DME. These products were carried out with the supercritical dimethyl ether and collected in a trap during depressurization. The trap was rinsed with a known volume of acetone containing the external standard anthracene at a concentration of 0.5 mg/ml. This solution was analyzed by gas chromatograph with a flame ionization detector (Hewlett Packard Model 6890).

Tetrahexylammonium bromide was used as a reference catalyst. A reaction was performed with this catalyst every few runs to ensure that the system was behaving normally. Two to three replicates of each synthesized catalyst were performed.

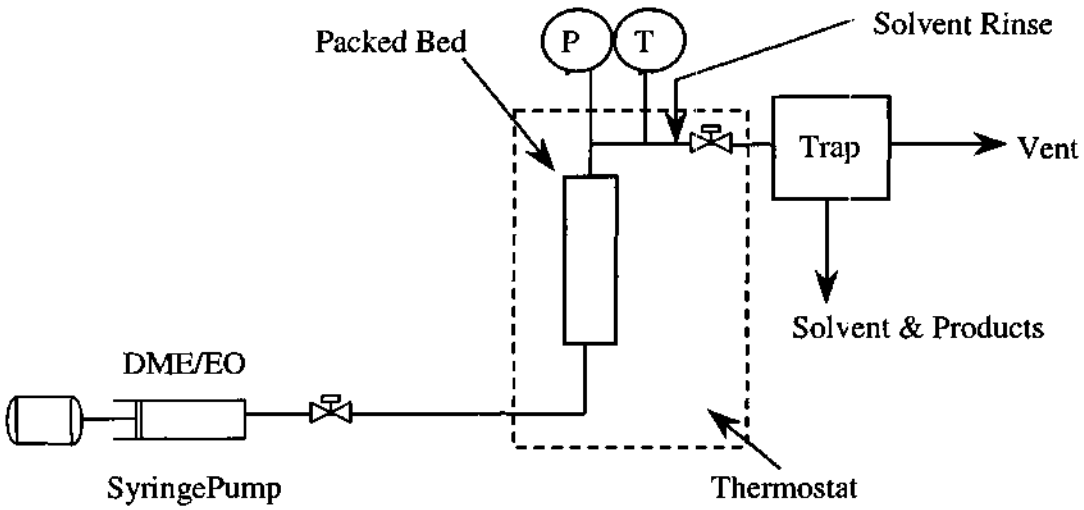

Figure 2-6. Differential flow apparatus.

Results and Discussion

Because the success of this process relies on the ability to extract MHET from the catalyst bed as it is formed, the process must be run in a solvent system in which MHET is very soluble. The solubility of MHET in several fluids was measured with a transpiration-sampling technique similar to that used by Dobbs and Johnston (Dobbs and Johnston, 1987). The data are shown in Figure 2-7. MHET is more soluble in dimethyl ether (T_c = 126.9°C, P_c = 52.4 bar) than in the other solvents tested. The solubility of MHET in DME at 130°C and 46 bar is orders of magnitude higher than the solubility in CO_2 (T_c = 31.1°C, P_c = 73.8 bar) at 130°C and 275 bar or that in propane (T_c = 96.6°C, P_c = 42.5 bar) at 130°C and 275 bar. The solubility of MHET in DME at 130°C and 70 bar is quite high, quantitatively beyond the capability of our apparatus. Terephthalic acid and our quaternary ammonium salt catalysts were shown to be virtually insoluble in DME at reaction conditions. For these reasons, DME was chosen as the reaction solvent. Because the reactions were run dilute in EO, the critical properties of the DME/EO mixture are essentially the same as those of pure DME. The measured solubility of MHET is the same in pure DME and in a mixture containing 0.5 mol% EO.

In addition to being insoluble in the reaction solvent, the catalysts must also be thermally stable for an economically viable process. A quaternary ammonium salt can degrade via two separate mechanisms. It can undergo internal displacement to yield trialkylamine and a displacement product, or, in the presence of strong base, it can undergo Hoffman elimination to yield trialkylamine and an olefin (Starks et al., 1994; Dehmlow et al., 1977; Montanari and Tundo, 1982; Landini et al., 1986). Fortunately,

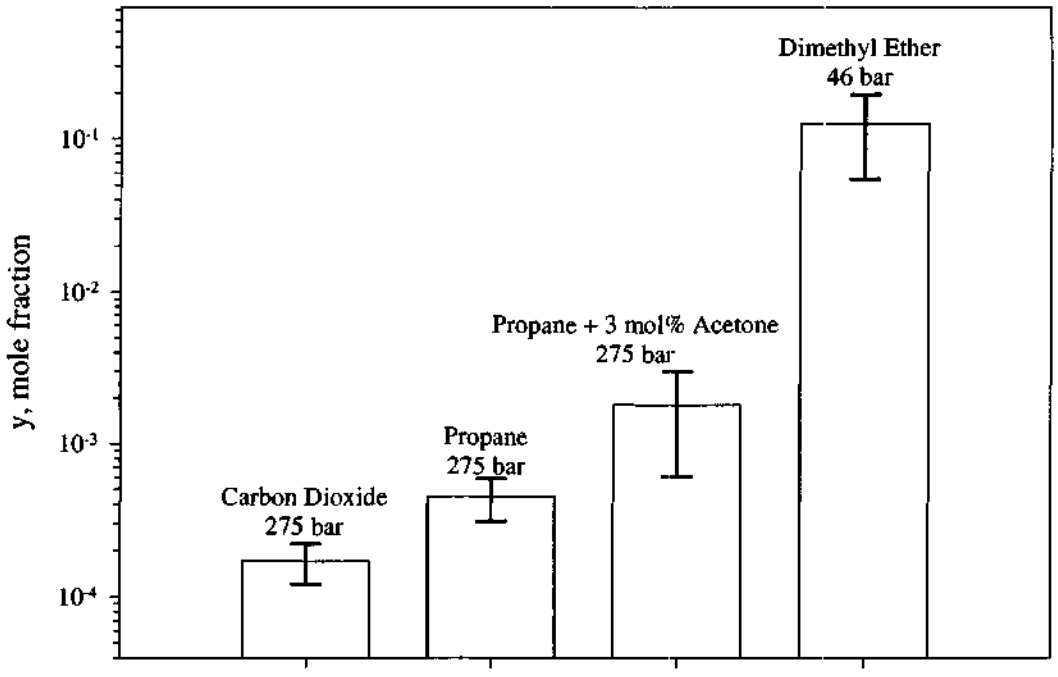

Figure 2-7. Solubility of MHET in various solvents at 130°C.

both degradation pathways can be avoided by designing the quaternary ammonium salt with no β hydrogen or a β hydrogen that is sterically hindered. All catalysts that were designed had either a sterically hindered or no β hydrogen (Figure 2-5). Although tetrahexylammonium bromide does not meet the long-term thermal stability criterion needed for industrial applications, it was not shown to degrade significantly over the course of a single 15-minute experiment.

Catalysts were evaluated on the basis of initial rate in the differential flow reactor shown in Figure 2-6. It was treated as a plug-flow reactor with a differential packed bed of solid. Reactions were stopped after only a small portion of the bed was consumed to avoid channeling in the bed. The concentration of product was measured after 15 minutes of reaction to allow stabilization of temperature, pressure and flow rate of the fluid through the system. The rates of appearance of MHET for each catalyst are shown in Table 2-1. Rates much higher than the highest ones reported were prohibitive because of system plugging. If more active catalysts had been used, a higher flow rate of DME would have been required. We were not certain that results would be comparable at different DME flowrates. Rates of less than 0.01 μmoles per minute were difficult to quantify without a longer reaction time.

The conversion of ethylene oxide was calculated from the initial ethylene oxide concentration and the amount of MHET produced. It was calculated to be approximately 1% or less for all runs. EO was intentionally run in large excess to the catalyst in order to ensure that the reaction was limited by the type and amount of catalyst present. The EO concentration was also kept low and not varied for safety. In

Catalyst	Rate (μmol/min)
EHPT	Above Apparatus Limit
EHPI	1.15 ± 0.20
EHPB	0.80 ± 0.15
EHPC	0.50 ± 0.10
BPC	0.15 ± 0.05
BVDC	0.04 ± 0.02
XPDC	0.03 ± 0.01
TBTA	0.03 ± 0.01
CBPC	0.02 ± 0.01
NBPB	0.05 ± 0.02
NBPC	0.006 ± 0.002
PSDEA	0.170 ± 0.05
THAB	0.75 ± 0.15
MBPC	Above Apparatus Limit
CsBr	Below Detection Limit

Table 2-1. Relative reaction rates for quaternary ammonium salt catalysts.

addition to being a fuel, EO is also an oxidizer and has no upper flammability limit. Besides being flammable at higher concentrations, it is also quite toxic.

While the EO concentration was kept low for proper kinetic measurement and safety measures, the low EO conversion does not rule out economic viability. Normally, with a reactant conversion of less than 1%, the cost of separation and recycle of unreacted product is prohibitively expensive. In this process, the separation of EO is trivial as it is flashed off with the DME. The cost of recycle of 0.5 mol% EO is insignificant compared to the large cost of recycling the DME already encumbered.

To verify that the catalysts activated the system, solvent and ethylene oxide were passed over a bed of terephthalic acid without catalyst; no products were detected. Next, CsBr was used as a catalyst to provide a source of anion, and again no products were detected. To confirm that the reaction was taking place on the surface of the terephthalic acid or in an adsorbed surface phase, a polymerically bound quaternary ammonium salt was tested to ensure near-zero solubility in the fluid phase. The polymeric quaternary hexadimethrine bromide did indeed catalyze the reaction. A polymeric amine [(diethylamino)ethyl]polystyrene was also tested. It is postulated that, in the presence of terephthalic acid, the polymeric amine is protonated and forms a quaternary ammonium salt. This amine/quaternary ammonium salt also catalyzes the reaction.

To verify that experiments were being performed in the kinetic regime, each experiment was performed and the rate was calculated at three temperatures: 130, 140, and 150°C. From the Arrhenius relationship, the activation energy was found to be 20 ±

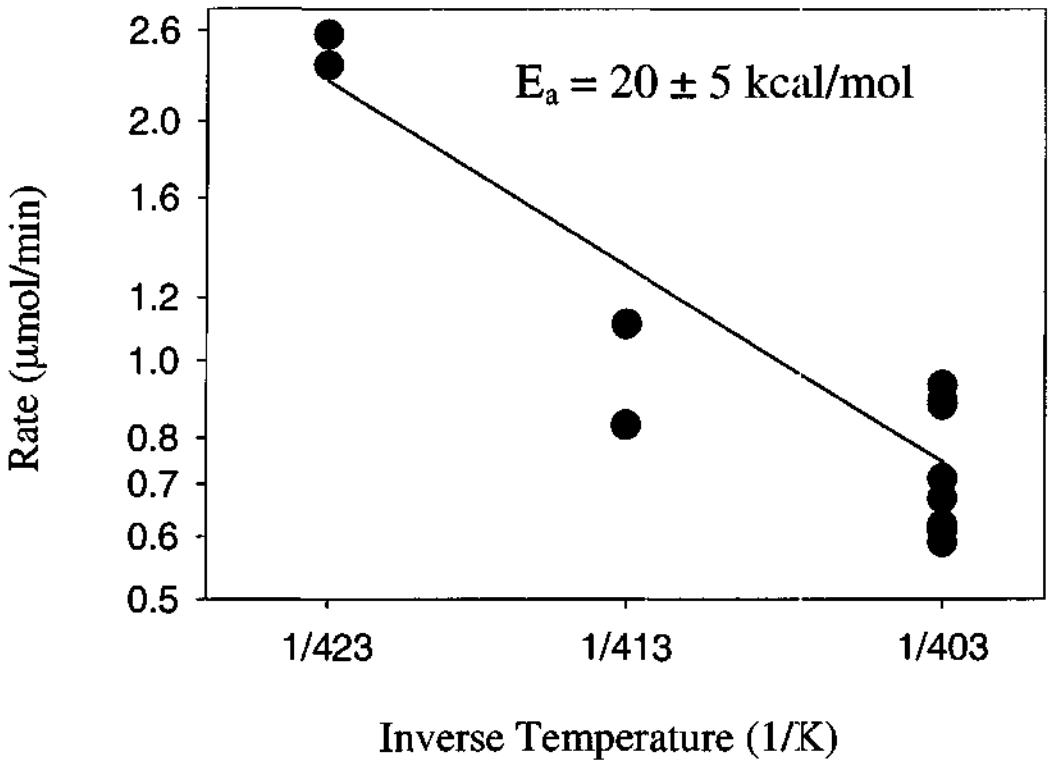

Figure 2-8. Arrhenius relationship for the esterification of terephthalic acid.

5 kcal/mol (Figure 2-8). If the system were mass-transfer-limited, the activation energy would be on the order of 1 kcal/mol. In addition, an increase in catalyst concentration from 0.5 to 2.0 mol% increased the rate from approximately 0.8 +/- 20% to 4.4 +/- 20% μmoles/min.

For the *N*-(2-ethylhexyl)-4-(dimethylamino)pyridinium catalysts, the effect of halide anion on the rate was evaluated to determine the order of nucleophilicity in this system. As shown in Figure 2-9, the reaction rate increased with an increase in the size of the anion: $I^- > Br^- > Cl^-$.

The order of nucleophilicity has been studied in detail in liquid (Edwards and Pearson, 1962) as well as in gaseous systems (Pellerite and Brauman, 1983). The order of nucleophilicity is directly dependent on the tightness of binding of the catalyst ion pair. This tightness of binding is controlled by three factors - the charge density of the cation, the charge density of the anion, and the solvent environment of the ion pair. We looked at the order of nucleophilicity by varying the anion paired with an *N*-(2-ethylhexyl)-4-(dimethylamino)pyridinium cation.

To clarify our discussion of the effect of solvent environment on the order of nucleophilicity, let us classify solvents according to the following four categories: gas, nonpolar, polar aprotic, and polar protic. In polar aprotic liquid solvents and in gas-phase reactions, the order of nucleophilicity is generally $Cl^- > Br^- > I^-$. This order in polar aprotic solvents has been shown to be consistent when tetrabutylammonium halides have been used (Winstein et al., 1960). If the reaction were occurring in the

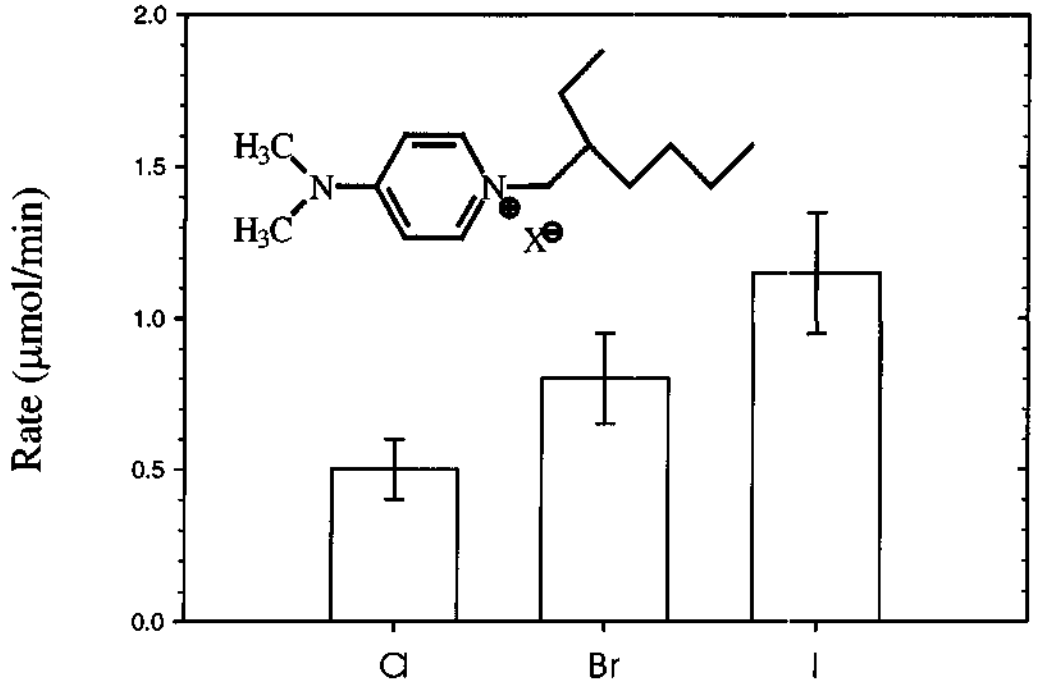

Figure 2-9. Order of anion nucleophilicity.

supercritical fluid dimethyl ether and ethylene oxide, which are both polar aprotic solvents, the reaction order should be the same as that for the tetrabutylammonium halides in the work of Winstein et al., i.e. $Cl^- > Br^- > I^-$. In polar protic and in nonpolar solvents, the order of nucleophilicity is generally $I^- > Br^- > Cl^-$, as nucleophiles with higher charge density are more tightly bound than those with lower charge density because of hydrogen bonding. The order of nucleophilicity that we observe is consistent with that of a reaction in a polar protic or in a nonpolar aprotic solvent and inconsistent with that of a reaction in a gaseous phase or in a polar aprotic solvent.

Because all solvents and reactants in our system are polar, we can rule out a nonpolar aprotic solvent environment. We, therefore, postulate that the reaction is occurring on the polar protic surface of the catalyst/terephthalic acid solid bed.

Our results are also consistent with the mechanism proposed (Figure 2-10). For increased catalyst activity, it is desirable to have a quaternary ammonium salt with an accessible anion, and catalysts were designed accordingly. In the proposed mechanism, the anion of the quaternary ammonium salt performs a nucleophilic attack on ethylene oxide to open the ring and form an oxygen anion. This step is much more favorable if the anion is more loosely associated with the quaternary cation.

The order of nucleophilicity, $I^- > Br^- > Cl^-$, is preserved when the *N*-(2-ethylhexyl) ligand is replaced with an *N*-nitrobenzyl ligand, but, as shown in Figure 2-11, the reaction rates are an order of magnitude lower. This is due to a combination of the electron-withdrawing character of the phenyl ring and the decreased steric hindrance of the nitrobenzyl ligand that increases the tightness of the ion pair.

Initiation and Termination:

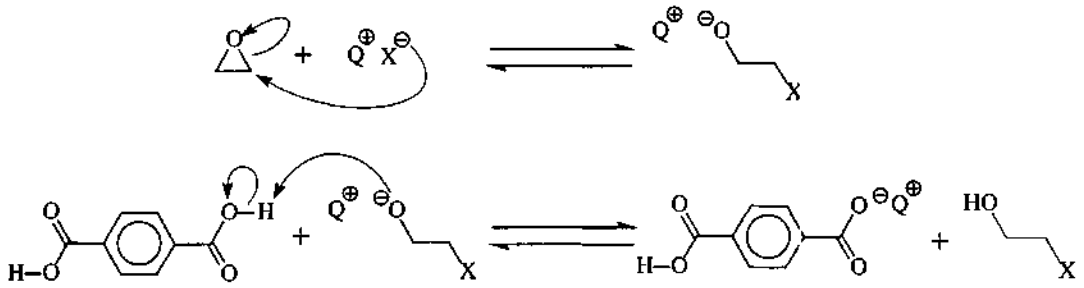

Propagation:

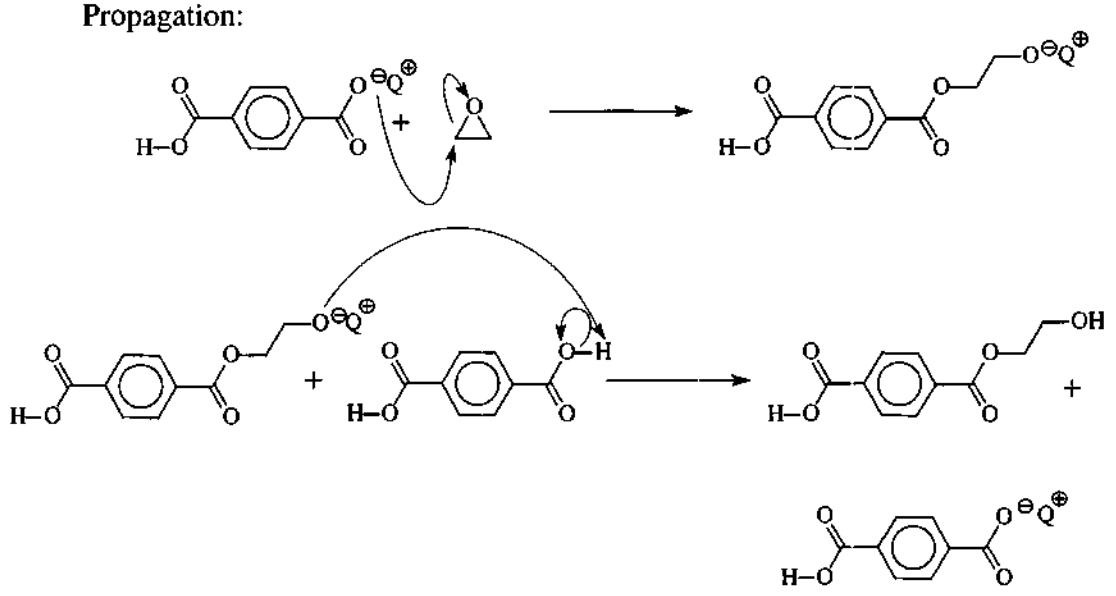

Figure 2-10. Proposed esterification mechanism.

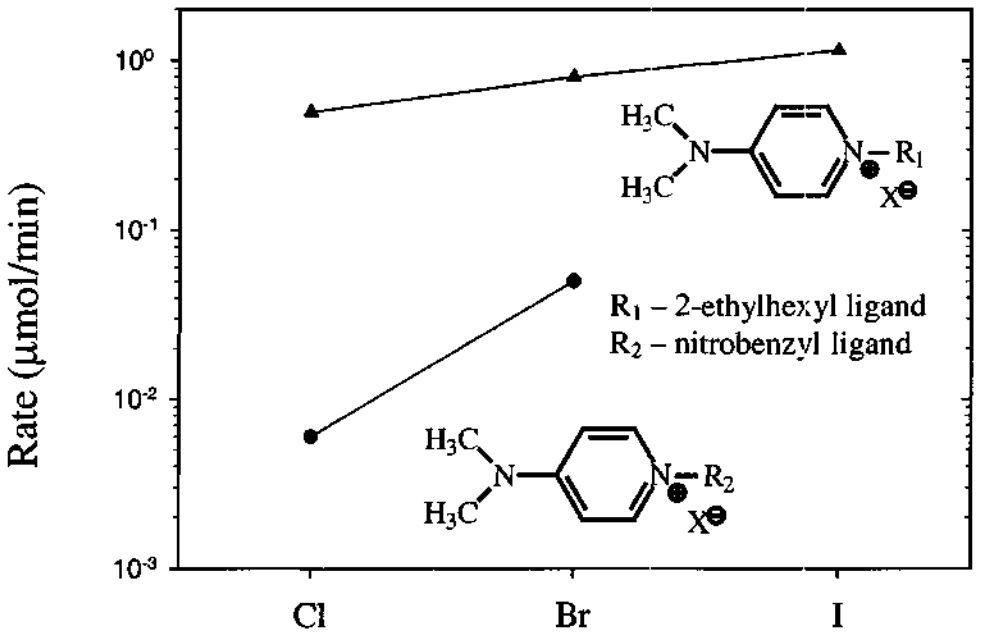

Figure 2-11. Effect of cation on anion reactivity.

Substituents on the pyridine ring have a direct resonance effect. The dimethylamino group on the pyridine ring of each catalyst stabilizes the cation by delocalizing the positive charge on the quaternized nitrogen. This decreases the tightness of the ion pair, which increases the catalyst activity. Substituents on the benzyl ligands of *N-p*-nitrobenzyl-(*N,N*-dimethylamino)pyridinium chloride (NBPC) and *N-p*-nitrobenzyl-(*N,N*-dimethylamino)pyridinium bromide (NBPB), however, are insulated by the methylene groups and therefore have an inductive effect only on the tightness of the ion pair. This allowed us to investigate the inductive effect without interference from resonance effects.

A relationship exists between reaction rate and the inductive effect of the subsitituent, Z, on the phenyl ring, where Z was varied from neutral (hydrogen) on *N*-benzyl-(*N,N*-dimethylamino)pyridinium chloride to slightly withdrawing (chlorine) on *N-p*-chlorobenzyl-(*N,N*-dimethylamino)pyridinium chloride to more withdrawing (nitrogen) on *N-p*-nitrobenzyl-(*N,N*-dimethylamino)pyridinium chloride. A donating group (methoxy) substituted catalyst was tested but caused the test apparatus to plug repeatedly. The white solid produced was characterized and shown to have an NMR spectrum consistent with that of oligamers of poly(ethylene terephthalate). A Hammett plot can be constructed from these relative reactivities (Figure 2-12).

As shown in Figure 2-12, more electron-withdrawing substituents lower relative reactivities, resulting in lower relative rates. This is explained by the fact that a more withdrawing substituent will result in a greater positive charge on the cationic part of the

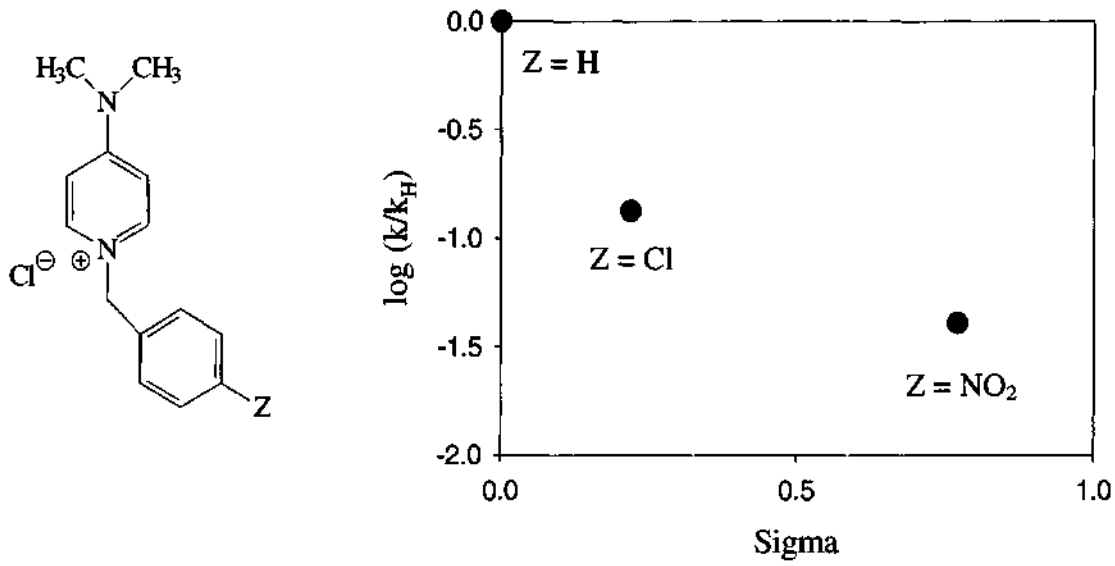

Figure 2-12. Hammett plot with substituted benzyl catalysts.

catalyst and, thus, a tighter ion pair. This supports the idea that a tighter ion pair would contain an anion that is less available for the nucleophilic attack depicted in the mechanism of the esterification reaction (Figure 2-10).

Conclusions

A hetereogeneous, series ethoxylation of terephthalic acid of the form diacid → monoester → diester can be run selectively to the monoester by supercritical fluid extraction of the desired monoester before the second acid group can be esterified. The tunable solubilizing power of supercritical dimethyl ether allows for the selective extraction of the monoester reaction intermediate from the catalyst bed and for a subsequent facile separation of the dimethyl ether and the monoester upon depressurization. Quaternary ammonium salt catalysts were designed to be stable under reaction conditions, as well as insoluble in the supercritical fluid, and to activate the esterification reaction to varying degrees depending on the structure of the catalyst.

The rate of the reaction increased with decreasing proximity of the anion to the cation in the series of quaternary ammonium salt catalysts studied. The availability of this anion decreased with inductively withdrawing groups on the benzyl ligand attached to the quaternized nitrogen. The availability of this anion was improved with an increase in the size of the anion, $I^- > Br^- > Cl^-$, as well as with electron-donating groups attached to the aromatic ring containing the cation.

References

Angus, S.; Armstrong, B.; deReuck, K.M. (Eds.) *International Thermodynamic Tables of the Fluid State – 3: Carbon Dioxide*; IUPAC, Pergamon Press: Oxford, 1976.

Brennecke, J. F.; Eckert, C. A. Phase Equilibria for Supercritical Fluid Process Design. *AIChE. J.* **1989**, *35*, 1409-1427.

Dehmlow, E. V.; Slopianka, M.; Heider, J. Phase Transfer Catalysis in Strongly Alkaline Media: Notes on the Extractability of Hydroxy Ions and on the Stability of Catalysts. *Tetrahedron Letters* **1977**, *27*, 2361-2364.

Dillow, A.K.; Hafner, K.P.; Yun, S.L.J.; Deng, F.; Kazarian, S.G.; Liotta, C.L.; Eckert, C.A. Cosolvent Tuning of Tautomeric Equilibrium in Supercritical Fluids. *AIChE J.* **1997**, *43*, 515-524.

Dobbs, J. M.; Johnston, K. P. Selectivities in Pure and Mixed Supercritical Fluid Solvents. *Ind. Eng. Chem. Res.* **1987**, *26*, 1476-1482.

Eckert, C. A.; Knutson, B. L. Molecular Charisma in Supercritical Fluids. *Fluid Phase Equilib* **1993**, *83*, 93-100.

Edwards, J. O.; Pearson, R. G. The Factors Determining Nucleophilic Reactivities. *J. Am. Chem. Soc.* **1962**, *84*, 16-24.

Ely, J.F.; Haynes, W.M.; Bain, B.C. Isochoric (p,Vm,T) Measurements on CO_2 and on ($0.982CO_2 + 0.018N_2$) from 250 to 330 K at Pressures to 35 MPa. *J. Chem. Thermodynamics* **1989**, *21*, 879-894.

Gurdial, G. S.; Foster, N. R. Solubility of o-Hydroxybenzoic Acid in in Supercritical Carbon Dioxide. *Ind. Eng. Chem. Res.* **1991**, *30*, 575-80.

Johnston, K.P.; Haynes, C. Extreme Solvent Effects on Reaction Rate Constants at Supercritical Fluid Conditions. *AIChEJ.* **1987**, *33*, 2017-2026.

Kim, S.; Johnston, K.P. Adjustment of the Selectivity of a Diels-Alder Reaction Network using Supercritical Fluids. *Chem. Eng. Commun.* **1988**, *63*, 49-59.

Kiran, E.; Saraf, V.P. Polymerization of Styrene in Supercritical *n*-Butane. *J. Supercrit. Fluids* **1990**, *3*, 198-204.

Knutson, B.L.; Dillow, A.K.; Liotta, C.L.; Eckert, C.A. Kinetics of a Diels-Alder Reaction in Supercritical Propane. In *Innovations in Supercritical Fluids:*

Science and Technology; Hutchenson, K.W.; Foster, N.R., (Eds.); ACS Symp. Ser. 608; American Chemical Society: Washington, DC, 1995.

Landini, D.; Maia, A.; Rampoldi, A. Stability of Quaternary Onium Salts under Phase Transfer Conditions in the Presence of Aqueous Alkaline Solutions. *J. Org. Chem.* **1986**, *51*, 3187-3191.

McHugh, M. A.; Krukonis, V. J. *Supercritical Fluid Extraction: Principles and Practice*, 2nd ed.; Butterworth-Heinemann: Boston, 1994.

Montanari, F.; Tundo, P. Hydroxymethyl Derivatives of 18-Crown-6 and [2.2.2] Cryptand: Versatile Intermediates for the Synthesis of Lipophilic and Polymer-bonded Macrocyclic Ligands. *J. Org. Chem.* **1982**, *47*, 1298-1302.

Pellerite, M. J.; Brauman, J. I. Intrinsic Barriers in Nucleophilic Displacements. A General Model for Intrinsic Nucleophilicity toward Methyl Centers. *J. Am. Chem. Soc.* **1983**, *105*, 2672-2680.

Starks, C.M.; Liotta, C.L.; Halpern, M. *Phase-Transfer Catalysis: Fundamentals, Applications, and Industrial Perspectives*; Chapman and Hall: New York, 1994.

Tsekhanskaya, Y.V.; Iomtev, M.B.; Mushkina, E.V. Solubility of Naphthalene in Ethylene and Carbon Dioxide Under Pressure. *Russ. J. Phys. Chem.* **1964**, *38*, 1173.

Tsekhanskaya, Y.V. Diffusion in the System of *p*-Nitrophenol - Water in the Critical Region . *Russ. J. Phys. Chem.* **1968**, *42*, 532.

Tsekhanskaya, Y.V. Diffusion of Naphthalene in Carbon Dioxide Near the Liquid - Gas Critical Point. *Russ. J. Phys. Chem.* **1971**, *45*, 744.

Winstein, S.; Savedoff, L. G.; Smith, S.; Stevens, I. D. R.; Gall, J. S. Ion Pairs, Nucleophilicity and Salt Effects in Bimolecular Nucleophilic Substitution. *Tetrahedron Lett.* **1960**, *9*, 24-30.

CHAPTER III

NEARCRITICAL WATER: A BENIGN MEDIUM FOR CATALYTIC HYDROLYSES

Introduction

Liquid water in the nearcritical region (250 – 300°C) offers opportunities both as a benign solvent and as a self-neutralizing catalyst. It has already been shown to have potential as a replacement for many toxic organic solvents, (Katritzky et al., 1996; An et al., 1997; Sealock et al., 1993) and this work demonstrates its ability to catalyze reactions that traditionally require the addition and eventual neutralization of acid or base.

Water under nearcritical conditions has properties similar to those of common polar organic solvents. As temperature is raised, the hydrogen bonding network in water weakens (Guissani and Guillot, 1993; Ryan et al., 1997). The dielectric constant decreases from 78 at 25°C to 20 at 300°C (Uematsu and Franck, 1980), and the density decreases to 0.8 g/mL at 300°C (Thomason and Modell, 1984) (Figure 3-1). While the relative permittivity is low enough for organics to be soluble in nearcritical water, it remains high enough to allow salt dissolution (Kuhlmann et al., 1994).

The ionization constant of water is maximized at 250°C (Marshall and Franck, 1981), where it is three orders of magnitude higher than that at room temperature (Figure

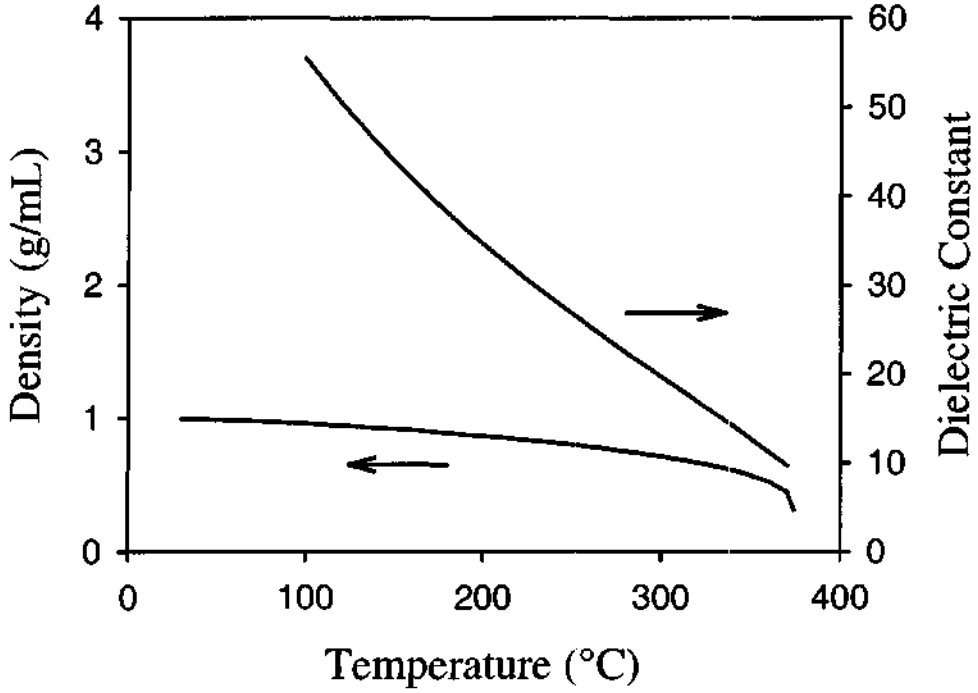

Figure 3-1. Density and dielectric constant of water as a function of temperature (Thomason and Modell, 1984; Uematsu and Franck, 1980).

3-2). Because nearcritical water is such a strong source of both hydronium cations and hydroxide anions, it can act as the catalyst in reactions that currently require additional acid or base (Katritzky et al., 1996; Chandler et al., 1997; Eckert et al., 1999); catalyst neutralization and subsequent salt disposal become obsolete. Friedel-Crafts acylations, which are currently run in an excess of a Lewis acid catalyst, require the disposal of several kilograms of salt for each kilogram of product (March, 1991). When run in nearcritical water (Eckert et al., 1999), there are no environmental or economic costs associated with catalyst synthesis, separation or disposal.

Many investigators have studied organic reactions in supercritical water (T_c = 374°C, P_c = 221 bar). Because both oxygen and organic compounds are soluble in supercritical water, it is an effective solvent for conversion of toxic waste into CO_2 and H_2O (Harradine et al., 1993; Li et al., 1993; Modell et al., 1992; Shanableh and Gloyna, 1991; Staszak et al., 1987). While the majority of studies of supercritical water have involved oxidative waste remediation, Deshpande et al. (1984) and Penninger (1989) have investigated it as an extraction solvent for fuels. Abraham and Klein (1987) have used model compounds to study mechanisms of reactions that occur during this extraction. Funazukuri et al. (1990) evaluated the liquefaction of lignin in supercritical water.

While supercritical water does offer promise as a reaction solvent, process design can be quite challenging. Oxygen or even traces of halogenated compounds in the water will cause stainless steel to corrode; expensive metallurgy is required. While the

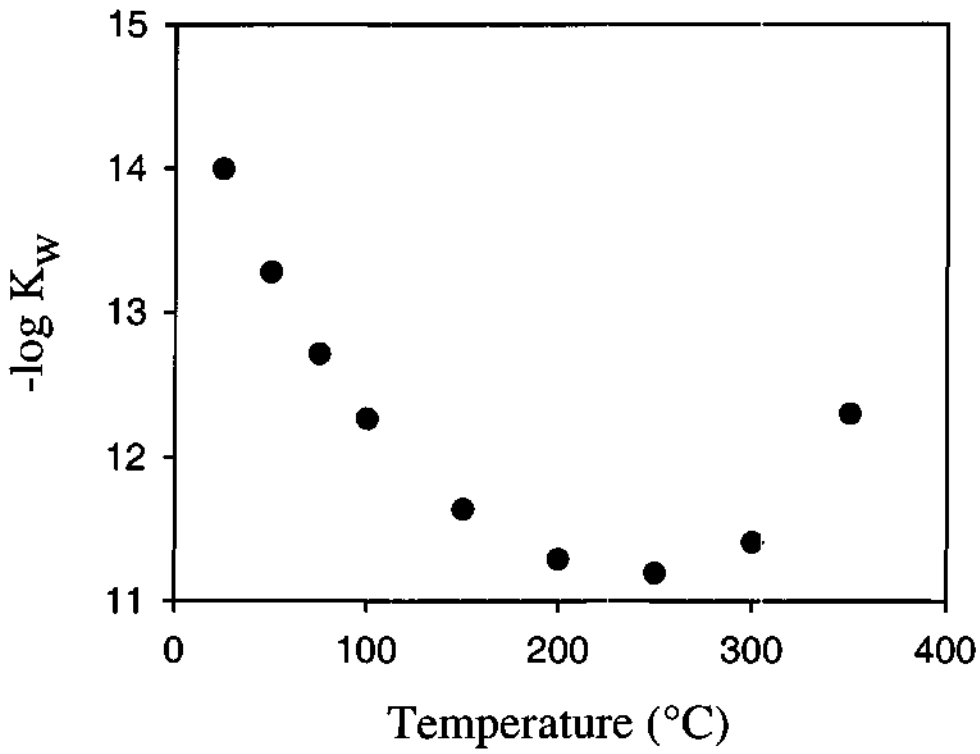

Figure 3-2. Dissociation constant of water as a function of temperature (Marshall and Franck, 1981).

insolubility of salts can enhance separations, it can complicate catalysis.

Nearcritical water offers many of the same advantages found in supercritical water, yet it is more likely to enable an economically viable process design. First, it is not corrosive. While it can solubilize organics, its dielectric constant is still high enough to support the dissolution of salts. The dissociation constant of water is orders of magnitude higher in the nearcritical region than it is at higher temperatures. Nearcritical water is not only a better solvent for catalyst salts, but it can also even eliminate the need for these salts by acting as an acid or base catalyst. In addition, its transport properties are similar to those of supercritical water (Figure 3-3).

Because nearcritical water offers so many advantages as a benign catalyst and solvent, we sought to elucidate its activity in acid- and/or base-catalyzed reactions, such as hydrolyses. We measured the effects of substituents on the hydrolyses of benzoate esters and anisoles using the Hammett equation (Hammett, 1970) (Equation 3-1), which

$$\log {k_X}/{k_H} = \sigma_X \rho, \qquad (3\text{-}1)$$

defines two key variables, σ_X and ρ. σ_X is the substituent constant, which measures how strongly electron donating or withdrawing a particular substituent is. Electron donating groups have negative substituent constants, and electron withdrawing groups have positive substituent constants. ρ is the reaction constant, which measures the sensitivity of a particular reaction to substituent effects. ρ is positive when electron

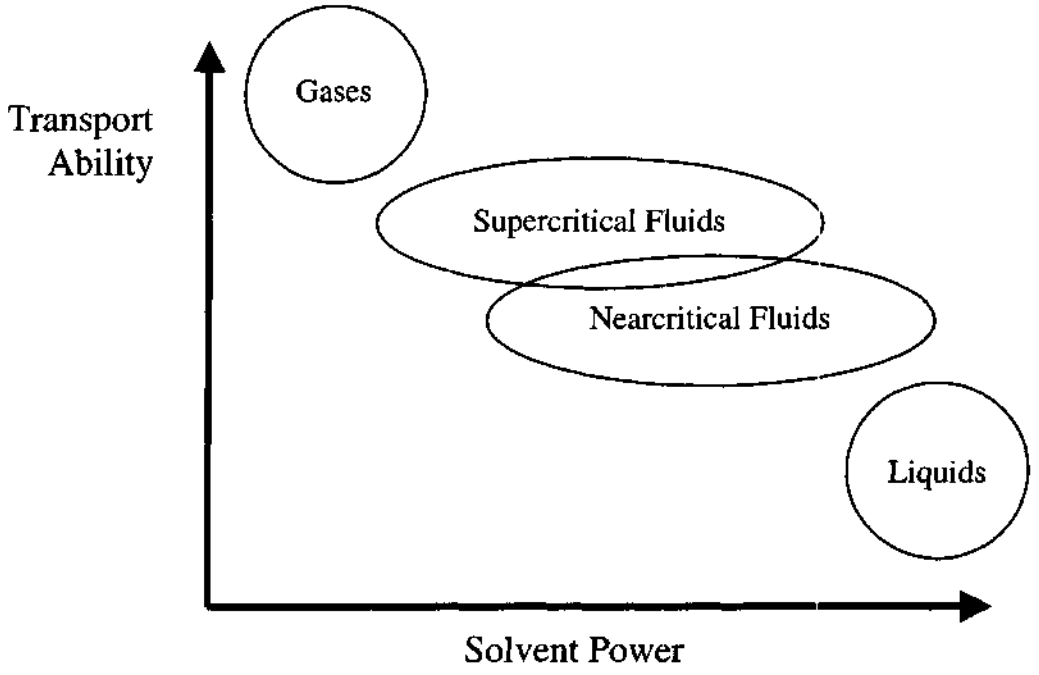

Figure 3-3. Solvent power and transport properties of nearcritical and supercritical fluids.

withdrawing groups accelerate reaction rates, negative when electron donating groups accelerate reaction rates, and zero when substituents do not affect reaction rates. k_X is the rate for the substituted reactant, and k_H is the rate for the non-substituted reactant. Ester hydrolyses run via a base-catalyzed mechanism are characterized by a positive reaction constant, while those run via an acid-catalyzed mechanism have a ρ of zero (Jaffe, 1953). Anisole hydrolyses which follow either a base-catalyzed or an S_N2 mechanism have a positive reaction constant, while those which follow an acid-catalyzed mechanism have a negative reaction constant.

Experimental Methods

Materials

Chemicals used in the experiments and calibrations were the following: acetone (Aldrich, HPLC grade, 99.9+%), anisole (Aldrich, 99.7%), benzoic acid (Aldrich, 99.5%), *p*-chlorobenzoic acid (Aldrich, 99%), *p*-chlorobenzoyl chloride (Aldrich, 99%), *p*-cresol (Aldrich, 99%), 3,5-dimethylanisole (Aldrich, 99+%), 3,5-dimethylphenol (Aldrich, 99+%), ethyl benzoate (TCI, 99.0+%), hydrochloric acid (Baker, 36.5 – 38.0%), isobutyl benzoate (TCI, 99.0+%), isobutyl *p*-hydroxybenzoate (TCI, 99.0+%), 2-methyl-1-propanol (Aldrich, anhydrous, 99.5%), *p*-methoxybiphenyl (Aldrich, 97%), *m*-methoxyphenol (Aldrich, 96%), methyl benzoate (TCI, 99.0+%), *p*-methylanisole (Aldrich, 99%), phenetole (Aldrich, 99%), phenol (Aldrich, 99+%), *p*-phenylphenol (Aldrich, 97%), potassium hydroxide (Baker, pellets), *n*-propyl benzoate (TCI, 99.0+%),

pyridine (Fisher Scientific, Certified ACS), resorcinol (Aldrich, 99+%), sodium hydroxide (Baker, pellets), *p*-trifluoromethylbenzoyl chloride (Aldrich, 97%), ααα-trifluoro-*p*-toluic acid (Aldrich, 98%) and water (Aldrich, HPLC grade). Isobutyl *p*-chlorobenzoate and isobutyl *p*-trifluoromethylbenzoate were synthesized as described below.

Benzoate Synthesis

Isobutyl *p*-chlorobenzoate and isobutyl *p*-trifluoromethyl benzoate were synthesized separately using *p*-chlorobenzoyl chloride and *p*-trifluoromethylbenzoyl chloride with the corresponding alcohol, 2-methyl-1-propanol. The alcohol (50mmol, 3.706g) was dissolved in 20 mL of dry pyridine (247 mmol, distilled over KOH), and the mixture was lowered into an ice bath. While stirring, the appropriate benzoyl chloride (50 mmol) was added slowly via syringe. Once addition was complete, the reaction mixture was heated to reflux overnight. The reaction mixture was cooled to room temperature, diluted with 150 mL of ethyl ether, washed with 2 x 75mL of DI H_2O, 2 x 50mL of saturated $NaHCO_3$, and 1 x 75mL of brine, dried over magnesium sulfate, and reduced via rotary evaporation. Both benzoate esters were purified by vacuum distillation, and purity, which was determined by gas chromatography, was found to be >98% in both cases. NMR spectra were taken with a Varian Gemini 300, and elemental analyses were performed by Atlantic Microlab, Inc., Norcross, GA.

Isobutyl *p*-chlorobenzoate: yield 91%; ^{1}H NMR ($CDCl_3$, 300 MHz): δ 7.97 (d, 2H), 7.38 (d, 2H), 4.06 (d, 2H), 2.07 (m, 1H), 0.98 (s, 6H); Calculated for $C_{11}H_{13}O_2Cl$: C, 62.12; H, 6.16; O, 15.05; Cl, 16.67. Found: C, 62.12; H, 6.15; O, 15.13; Cl, 16.60.

Isobutyl 4-(trifluoromethyl)benzoate: yield 96%; ^{1}H NMR ($CDCl_3$, 300MHz): δ 8.16 (d, 2H), 7.69 (d, 2H), 4.13 (d, 2H), 2.09 (m, 1H), 1.01 (s, 6H); Calculated for $C_{12}H_{13}O_2F_3$: C, 58.53; H, 5.32; O, 13.00; F, 23.15. Found: C, 58.80; H, 5.30; O, 12.72; F, 23.18.

Apparatus and Procedure

3.0 ml titanium reactors were loaded with benzoate ester or anisole and an excess of water (1:47 on a molar basis), where the excess of water makes the reverse reaction negligible. For all reactions, there was one liquid phase and one vapor phase present. The reactors were made on site and were sealed with titanium lids from High Pressure Products (model 15-7NMA). Reactors were placed in an aluminum heating block preheated to the desired temperature, between 250 and 300°C (Figure 3-4). Pairs of reactors were removed and quenched in room temperature water at various reaction times. Reactor heat-up was 99% complete after 7 minutes, and the reactors cooled to room temperature in 3 minutes (Figure 3-5). Reactor contents were diluted in acetone and analyzed using GC-FID and GC-MS.

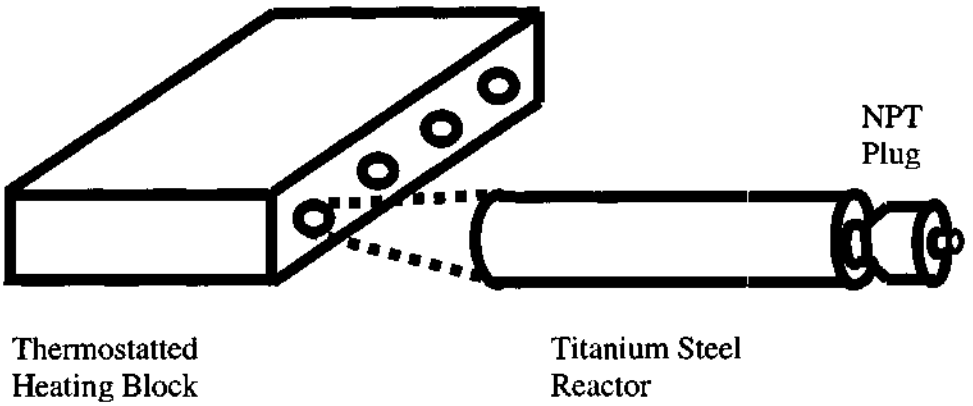

Figure 3-4. Experimental setup for batch reactions with nearcritical water.

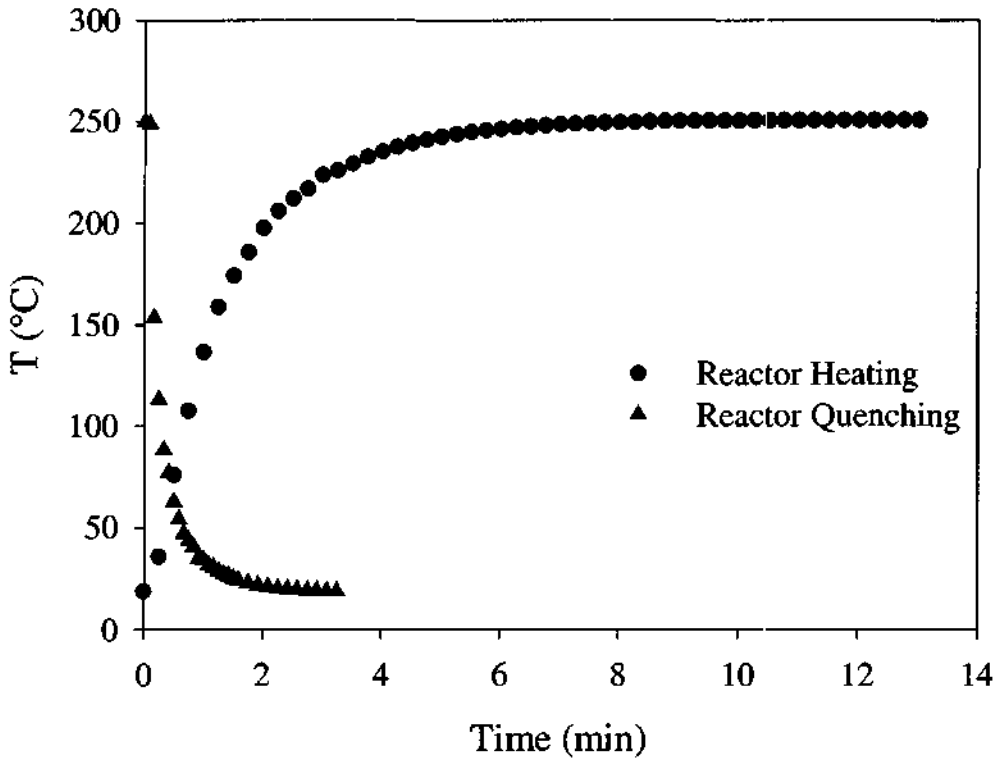

Figure 3-5. Time for a titanium reactor loaded with water (●) to heat to the desired 250°C and (▲) to cool to room temperature upon quenching.

Results and Discussion

Ester Hydrolysis

To elucidate the mechanism of ester hydrolysis in nearcritical water, we measured kinetics for several substituted benzoate esters (Figure 3-6). The main products formed from the hydrolyses of di-*n*-butyl phthalate (Penninger, 1988) and ethyl acetate (Broell et al., 1999) in nearcritical water are the corresponding acids and alcohols. The formation of thermolysis products, such as alkenes and carbon oxides, is considerably slower in nearcritical water than when performed neat. Because hydrolysis occurs so readily, there are no available solubility data for benzoate esters in nearcritical water, but extrapolation of low temperature data (Stephenson and Stuart, 1986) indicates that our dilute loading yielded a single liquid phase. Conversion versus time data yielded S-shaped curves (Figure 3-7), suggesting an autocatalytic mechanism. Because benzoic acid, whose pK_a

$$dx/dt = k[\text{ester}][H_2O][H^+], \quad (3\text{-}2)$$

is 5.4 at 250°C (Read, 1981; Kettler et al., 1995), is a product, autocatalysis implies that the reaction follows an acid-catalyzed mechanism. The rate equation for this reaction via an autocatalytic $A_{AC}2$ mechanism (Figure 3-8) is given in Equation 3-2 (Lesutis et al., 1999), where $k = K_1k_2$ (Lowry and Richardson, 1987) (Appendix B). K_1 is the equilibrium constant for the protonation of the ester, and k_2 is the rate constant for the addition of water to the protonated ester. The second step is rate-determining, and its

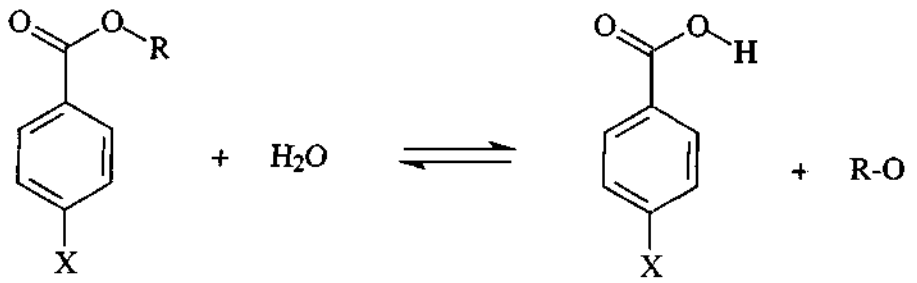

R = Me, Et, n-Pr, n-Bu, i-Bu

X = H, Cl, CF_3

Figure 3-6. Hydrolysis of substituted benzoate esters.

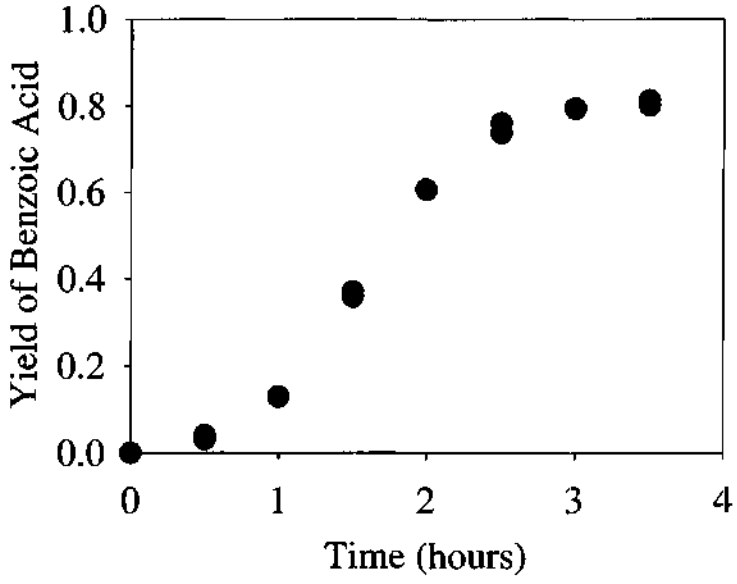

Figure 3-7. Yield of benzoic acid vs. time for the conversion of *n*-propyl benzoate at 250°C.

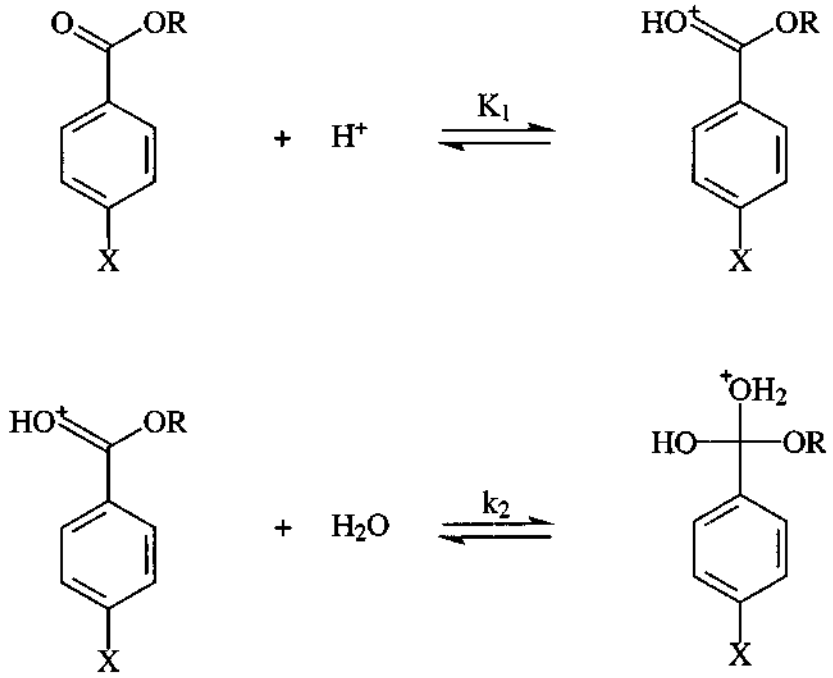

Figure 3-8. First steps of $A_{AC}2$ mechanism for acid-catalyzed ester hydrolysis.

product equilibrates rapidly to benzoic acid and the alcohol. The concentration of protons is determined from the dissociation constant of water and that of the applicable benzoic acid at 250°C. The dissociation constant of benzoic acid at 250°C is 3.7×10^{-6} M (Read, 1981; Kettler et al., 1995). The Hammett reaction constant ρ, for this dissociation, increases by only 2% from 25 to 250°C (Shock, 1995), and dissociation constants for substituted benzoic acids were calculated from the Hammett equation where ρ is 1.02. Numerical integration of Equation 3-2 gave k for each reaction. Table 3-1 reports these rate constants as products of k_2 and K_1*, where K_1* is the equilibrium constant for the protonation of the non-substituted ester. We assumed that the effect of substituents on the equilibrium constant for ester protonation is the same as the effect for acid dissociation.

Rates of hydrolysis of isobutyl benzoate were also measured at 260 and 300°C. Using dissociation constants of benzoic acid at these temperatures (Read, 1981; Shock, 1995), the activation energy was calculated to be 101 ± 13 kJ/mol, indicating that mass transfer limitations were negligible. This is also consistent with the activation energies obtained for the acid-catalyzed hydrolyses of substituted benzoate esters in low temperature aqueous solvents with a stoichiometric addition of acid (Timm and Hinshelwood, 1938).

As shown in Table 3-1, longer alkyl chains on the esters slow hydrolysis, and the branched butyl benzoate hydrolyzes more slowly than the linear butyl benzoate. As the carbonyl carbon becomes more sterically hindered, nucleophilic attack by water becomes more difficult, and the hydrolysis slows.

R	X	k_2K_1* ($L^2/mol^2/hr$)
Methyl	H	26.9 +/- 2.5
Ethyl	H	25.7 +/- 0.9
n-Propyl	H	10.4 +/- 0.5
n-Butyl	H	17.1 +/- 0.6
Isobutyl	H	6.7 +/- 0.3
Isobutyl	Cl	7.4 +/- 0.6
Isobutyl	CF_3	7.0 +/- 0.5

Table 3-1. Rate constants for the hydrolysis of benzoate esters at 250°C, where K_1* is the equilibrium constant for the protonation of nonsubstituted ester.

Rate constants for the hydrolyses of substituted benzoate esters provide further evidence that an acid-catalyzed mechanism predominates under nearcritical conditions. As shown in Table 3-1, substituents did not affect rates of hydrolysis under these conditions. In addition to the reactions reported in Table 3-1, the hydrolysis of isobutyl *p*-hydroxybenzoate was also attempted, but the hydroxyl group is strongly electron donating (σ = -0.38), and the ester decarboxylated. This negligible substituent effect is a well-documented characteristic of acid-catalyzed ester hydrolyses in aqueous solvents at a lower temperature. ρ for acid-catalyzed ester hydrolyses is zero, but ρ for base-catalyzed ester hydrolyses is 2.4 (Jaffe, 1953). The negligible substituent effect is consistent with the proposed $A_{AC}2$ mechanism because of competing substituent effects in the first two steps. It is evident that the acidity of nearcritical water is sufficient to initiate hydrolysis of the benzoate and formation of benzoic acid. Because the pK_a of benzoic acid is so low, an autocatalytic, acid-catalyzed mechanism was followed.

Anisole Hydrolysis

To measure the competitive catalytic activity of hydroxide and hydronium ions formed from the dissociation of water at elevated temperatures, we must measure kinetics for a non-autocatalytic reaction. The K_a of phenol is almost 6 orders of magnitude lower than that of benzoic acid at 25°C, so we next studied the hydrolysis of substituted anisoles (Figure 3-9). Anisole and water are completely miscible at 280°C (Lu et al.,

X = H, 4-methyl, 3,5-dimethyl, 4-phenyl, 3-hydroxy

Figure 3-9. Hydrolysis of substituted anisoles.

1999), so our reactors, which were at 300°C, contained only one liquid phase. Conversion versus time data did not yield S-shaped curves (Figure 3-10), indicating that the mechanism here was not autocatalytic.

Anisole can be hydrolyzed via three distinct pathways, and the sign of the Hammett reaction constant for each can be predicted from each mechanism (Figure 3-11). An acid-catalyzed reaction (Figure 3-11a) gives a negative ρ, and reactions run via base catalysis (Figure 3-11b) or S_N2 nucleophilic attack by water (Figure 3-11c) give a positive ρ. Hydrolyses run with electron donating groups, such as 3,5-dimethylanisole and 4-methylanisole, were slower than the nonsubstituted hydrolysis; hydrolyses run with electron withdrawing groups, such as 4-phenyl and 3-hydroxyl, were faster than the nonsubstituted hydrolysis. Because ρ is positive for this reaction, the acid-catalyzed mechanism must be subordinate to the others.

Additional evidence that the acid-catalyzed mechanism is negligible here is found in comparing the hydrolysis of anisole to that of phenetole. Because an ethyl group is more electron donating than a methyl group, the oxygen in phenetole should have a higher electron density. If the acid-catalyzed mechanism were predominant, phenetole would hydrolyze more rapidly than anisole. Because phenetole hydrolyzes more slowly than anisole (Figure 3-10), either the base-catalyzed or the S_N2 mechanism must predominate.

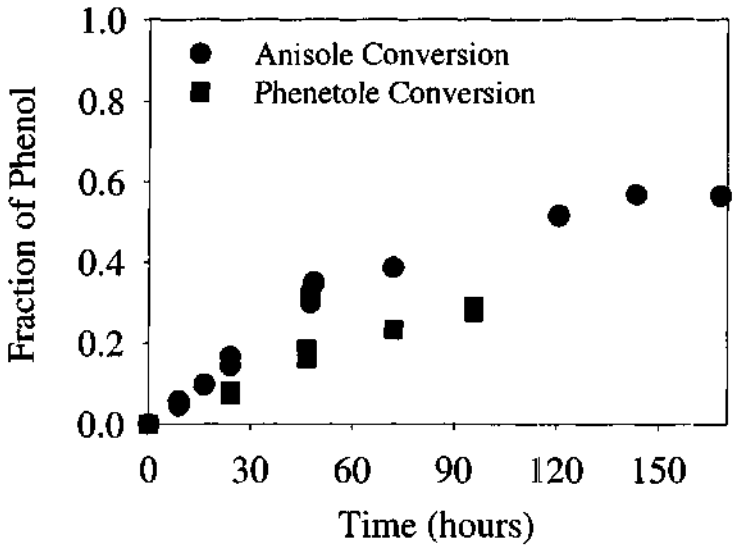

Figure 3-10. Comparison of anisole and phenetole hydrolyses at 300°C. Neither plot is S-shaped.

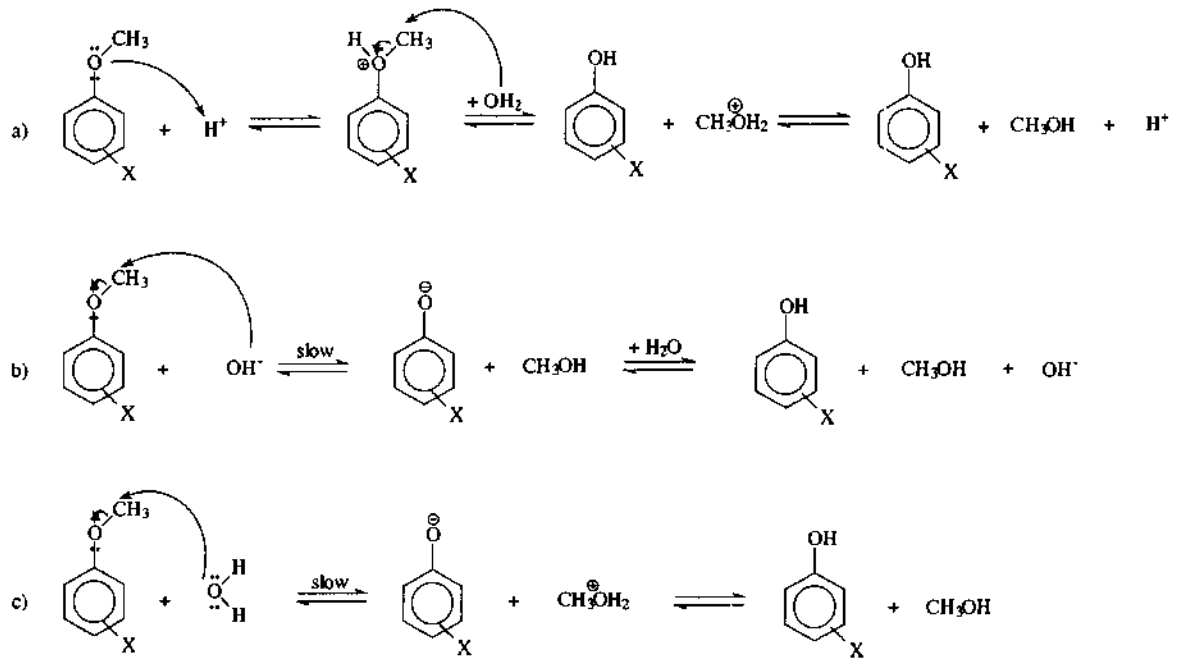

Figure 3-11. Mechanisms for anisole hydrolysis: a) acid-catalyzed, b) base-catalyzed and c) S_N2 attack by undissociated water.

Because the hydrolysis via the acid-catalyzed pathway is negligible, the reaction rate can be written as in Equation 3-3, where k_1 is the rate constant for the S_N2

$$dx/dt = k_1[\text{Anisole}][H_2O] + k_2[\text{Anisole}][OH^-] \qquad (3\text{-}3)$$

nucleophilic attack by water, and k_2 is the rate constant for the base-catalyzed reaction (Appendix B). To determine the relative importance of each of these mechanisms, anisole was hydrolyzed in water with 0.041M KOH. Because the reaction ran about 20 times faster with the KOH than it did under neutral conditions, the first term on the right side of Equation 3-3 was assumed to be negligible for this reaction. This set of data was analyzed using Equation 3-4, where the concentration of hydroxide was the sum of that

$$dx/dt = k_2[\text{Anisole}][OH^-] \quad (3\text{-}4)$$

formed from the dissociation of water and that formed from the dissociation of KOH. The KOH was assumed to dissociate completely under these conditions. The integrated rate expression for Equation 3-4 yielded a k_2 of 1.49 ± 0.14 L/mol/hr.

Once k_2 was known, hydrolyses run without any additional base could be analyzed with Equation 3-3. Calculated values of k_1 are given in Table 3-2, and a Hammett plot is shown in Figure 3-12. The Hammett reaction constant is 2.3 ± 0.3. Because the concentration of water is so much higher than the concentration of hydroxide formed from the dissociation of water, the base-catalyzed pathway is negligible here. S_N2 nucleophilic attack by water is the predominant mechanism for this reaction under these conditions.

Substituent	σ	$k_1 \times 10^4$ (L/mol/hr)
4-Methyl	-0.14	0.62 +/- 0.03
3,5-Dimethyl	-0.12	0.61 +/- 0.02
H	0	1.31 +/- 0.10
4-Phenyl	+0.05	2.04 +/- 0.15
3-Hydroxyl	+0.13	2.11 +/- 0.32

Table 3-2. Rate constants for S_N2 nucleophilic attack by water of substituted anisoles.

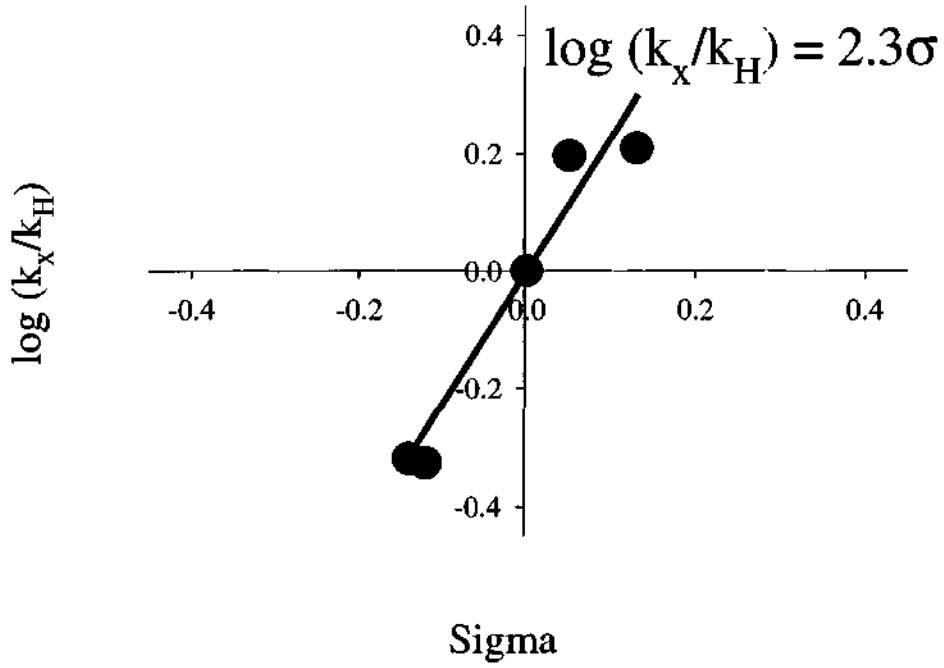

Figure 3-12. Hammett plot for anisole hydrolysis.

Conclusions

Substituted benzoic acid esters and substituted anisoles were successfully hydrolyzed in nearcritical water without the addition of any acid or base. For the esters, the protons formed from the dissociation of water were sufficient to initiate hydrolysis. Conversion versus time data yielded S-shaped plots, and the Hammett reaction constant was zero, indicating that the reaction was autocatalytic and followed an acid-catalyzed mechanism. The substituted phenols formed from the hydrolysis of anisoles are only very weakly acidic, precluding autocatalysis. Anisole hydrolysis in nearcritical water has a positive Hammett reaction constant, indicating that either the base-catalyzed mechanism or an S_N2 pathway with water, or perhaps both, predominates. Analysis of the rate of hydrolysis when base is added enables a comparison of the relative magnitudes of these two pathways. The S_N2 reaction is several orders of magnitude faster then the base-catalyzed reaction under these conditions. This work not only shows that nearcritical water can act both as a solvent and as a catalyst, but it also shows that it can catalyze different types of reactions. While the acidity and basicity of nearcritical water are high enough to initiate and catalyze reactions, it appears that water as a stoichiometric reactant takes part in the conversions in its undissociated form. Because of the versatility shown here, nearcritical water offers significant potential, both as a benign solvent and as a self-neutralizing catalyst, for a wide variety of reactions.

References

Abraham, M.A.,; Klein, M.T. Solvent Effects During the Reaction of Coal Model Compounds. In *Supercritical Fluids: Chemical and Engineering Principles and Applications*; Squires, T.G.; Paulaitis, M.E., Eds.; ACS Symp. Ser. 329; American Chemical Society: Washington, DC, 1987.

An, J.; Bagnell, L.; Cablewski, T.; Strauss, C.R.; Trainor, R.W. Applications of High-Temperature Aqueous Media for Synthetic Organic Reactions. *J. Org. Chem.* **1997**, *62*, 2505-2511.

Broell, D.; Kaul, C.; Kraemer, A.; Krammer, P.; Richter, T.; Jung, M.; Vogel, H.; Zehner, P. Chemistry in Supercritical Water. *Angew. Chem. Int. Ed.* **1999**, *38*, 2998-3014.

Chandler, K.; Deng, F.; Dillow, A.K.; Liotta, C.L.; Eckert, C.A. Alkylation Reactions in Near-Critical Water in the Absence of Acid Catalysts. *Ind. Eng. Chem. Res.* **1997**, *36*, 5175-5179.

Deshpande, G.V.; Holder, G.D.; Bishop, A.A.; Gopal, J.; Wender, I..; Extraction of Coal Using Supercritical Water. *Fuel* **1984**, *63*, 956-960.

Eckert, C.A.; Gläser, R.; Brown, J.S. Tuning of Chemical Reactions with Expanded Solvents. Proceedings of the 5th Conference of Supercritical Fluids and their Applications, Verona, Italy, 1999.

Funazukuri, T.; Wakao, N.; Smith, J.M. Liquefaction of Lignin Sulphonate with Subcritical and Supercritical Water. *Fuel* **1990**, *69*, 349-353.

Guissani, Y.; Guillot, B. A Computer Simulation Study of the Liquid-Vapor Coexistence Curve of Water. *J. Chem. Phys.* **1993**, *98*, 8221-8235.

Hammett, L.P. *Physical Organic Chemistry: Reaction Rates, Equilibria, and Mechanisms, 2nd Ed.*; McGraw-Hill: New York, 1970.

Harradine, D.M.; Buelow, S.J.; Dell'orco, P.C.; Dyer, R.B.; Foy, B.R.; Robinson, J.M.; Sanchez, J.A.; Spontarelli, T.; Wander, J.D. Oxidation Chemistry of Energetic Materials in Supercritical Water. *Haz. Waste Haz. Mat.* **1993**, *10*, 233-246.

Jaffe, H.H. A Reexamination of the Hammett Equation. *Chem. Rev.* **1953**, *53*, 191-261.

Katritzky, A.R.; Allin, S.M.; Siskin, M. Aquathermolysis: Reactions of Organic Compounds with Superheated Water. *Acc. Chem. Res.* **1996**, *29*, 399-406.

Kettler, R.M.; Wesolowski, D.J.; Palmer, D.A. Dissociation Quotient of Benzoic Acid in Aqueous Sodium Chloride Media to 250°C. *J. Solution Chem.* **1995**, *24*, 385-407.

Kuhlmann, B.; Arnett, E.M.; Siskin, M. Classical Organic Reactions in Pure Superheated Water. *J. Org. Chem.* **1994**, *59*, 3098-3101.

Lesutis, H.P.; Gläser, R.; Liotta, C.L.; Eckert, C.A. Acid/Base-Catalyzed Ester Hydrolysis in Near-Critical Water. *Chem Comm.* **1999**, *20*, 2063-2065.

Li, L.; Gloyna, E.F.; Sawicki, J.E. Treatability of DNT Wastewater by Supercritical Water Oxidation. *Water Env. Res.* **1993**, *65*, 250-257.

Lowry, T.H.; Richardson, K.S. *Mechanism and Theory in Organic Chemistry*, Harper and Row: New York, 1987, 717-723.

Lu, J.; Brown, J.S.; Liotta, C.L.; Eckert, C.A. Phase Equilibrium for Near-Critical Water. I. Solvatochromism Study. Proceedings of the Annual AIChE Meeting, Dallas, TX, 1999.

March, J. *Advanced Organic Chemistry: Reactions, Mechanisms, and Structure, 4th Ed.*; John Wiley and Sons: New York, 1991, 539 – 542.

Marshall, W.L.; Franck, E.U. Ion Product of Water Substance. 0 – 1000°C, 1 – 10,000 Bars. New International Formulation and Its Background. *J. Phys. Chem. Ref. Data* **1981**, *10*, 295-304.

Modell, M.; Larson, J.; Sobczynski, S.F. Supercritical Water Oxidation of Pulp Mill Sludges. *Tappi J.* **1992**, *75*, 195-202.

Penninger, J.M.L. Reactions of di-*N*-Butylphthalate in Water at Near-Critical Temperature and Pressure. *Fuel* **1988**, *67*, 490-496.

Penninger, J.M.L. Selectivity Effects in Aqueous Supercritical Fluid Extraction of Subbituminous Coal. *Fuel* **1989**, *68*, 983-989.

Read, A.J. Ionization Constants of Benzoic Acid from 25 to 250°C and to 2000 Bar. *J. Solution Chem.* **1981**, *10*, 437-450.

Ryan, E.T.; Xiang, T.; Johnston, K.P.; Fox, M.A. Absorption and Fluorescence Studies of Acridine in Subcritical and Supercritical Water. *J. Phys. Chem. A* **1997**, *101*, 1827-1835.

Sealock, Jr., L.J.; Elliot, D.C.; Baker, E.G.; Butner, R.S. Chemical Processing in High-Pressure Aqueous Environments. I. Historical Perspective and Continuing Developments. *Ind. Eng. Chem. Res.* **1993**, *32*, 1535-1541.

Shanableh, A.; Gloyna, E.F. Supercritical Water Oxidation – Wastewaters and Sludges. *Wat. Sci. Tech.* **1991**, *23*, 389-398.

Shock, E.L. Organic Acids in Hydrothermal Solutions: Standard Molal Thermodynamic Properties of Carboxylic Acids and Estimates of Dissociation Constants at High Temperatures and Pressures. *Amer. J. Science* **1995**, *295*, 496-580.

Staszak, C.N.; Malinowski, K.C.; Killilea, W.R. The Pilot-Scale Demonstration of the MODAR Oxidation Process for the Destruction of Hazardous Organic Waste Materials. *Environ. Prog.* **1987**, *6*, 39-43.

Stephenson, R.; Stuart, J. Mutual Binary Solubilities: Water – Alcohols and Water - Esters. *J. Chem. Eng. Data* **1986**, *31*, 56-70.

Thomason, T.B.; Modell, M. Supercritical Water Destruction of Aqueous Wastes. *Haz. Waste* **1984**, *1*, 453-467.

Timm, E.W.; Hinshelwood, C.N. The Activation Energy of Organic Reactions. Part III. The Kinetics of Acid Hydrolysis of Esters. *J. Chem. Soc.* **1938**, 862-869.

Uematsu, M.; Franck, E.U. Static Dielectric Constant of Water and Steam. *J. Chem. Phys. Ref. Data* **1980**, *9*, 1291-1306.

CHAPTER IV

NEARCRITICAL WATER: A BENIGN MEDIUM FOR ACID-CATALYZED REACTIONS

Introduction

Nearcritical water offers tremendous opportunities for novel reactions in an environmentally benign solvent. In the range of 250 – 300°C, it has a density and dielectric constant similar to those of ambient acetone (Thomason and Modell, 1984; Uematsu and Franck, 1980) (Figure 3-1), which permits the dissolution and reaction of both organic and ionic species (Kuhlmann et al., 1994). In addition, its ionization constant is three orders of magnitude greater than that of water at ambient temperature and pressure (Marshall and Franck, 1981) (Figure 3-2). This latter property facilitates promotion of acid-catalyzed and base-catalyzed reactions.

This chapter discusses work performed to study the applicability of nearcritical water as a solvent and catalyst for three industrially important reactions. First, it was investigated as a replacement solvent for the polymerizations of styrene and 1,3-pentadiene via cationic addition polymerization. It was also studied as a benign solvent and catalyst for acetylation reactions with cellulose acetate. Finally, the Beckmann rearrangement of cyclohexanone oxime to ε-caprolactam, a precursor of nylon 6, was studied in nearcritcal water.

Polymerization of Styrene and Piperylene in Nearcricical Water

Introduction

The polymerizations of styrene and 1,3-pentadiene (piperylene) in nearcritical water were studied (Figure 4-1). Polystyrene is commonly used in items ranging from packaging materials and insulation to machine housings, and the polymer resins formed from piperylene are commonly used in adhesives, paint, rubber, and coatings applications. Nearcritical water offers several advantages as an environmentally benign solvent for these polymerizations. First, the dissociation constant of nearcritical water is three orders of magnitude greater than that of water at ambient temperature and pressure (Marshall and Franck, 1981). Because nearcritical water is a good source of H_3O^+ ions, it is a good solvent for acid catalyzed reactions (Kuhlmann et al., 1994), such as cationic addition polymerizations.

In addition, the dielectric constant of water between 250 - 300°C is similar to that of acetone and a factor of four less than that of water at standard temperature and pressure (Uematsu and Franck, 1980). Because of this dramatic decrease in dielectric constant, hydrocarbons are slightly soluble in nearcritical water, and polar organics are completely miscible with it. Connally has found benzene to be 7 weight percent soluble in water at 260°C and toluene to be 7 percent soluble at 280°C (Connolly, 1966). Based on these data, it is expected that ethyl benzene is about 3 percent soluble in water at 275°C and perhaps 5 to 10 percent soluble at 300°C. Styrene should be slightly more

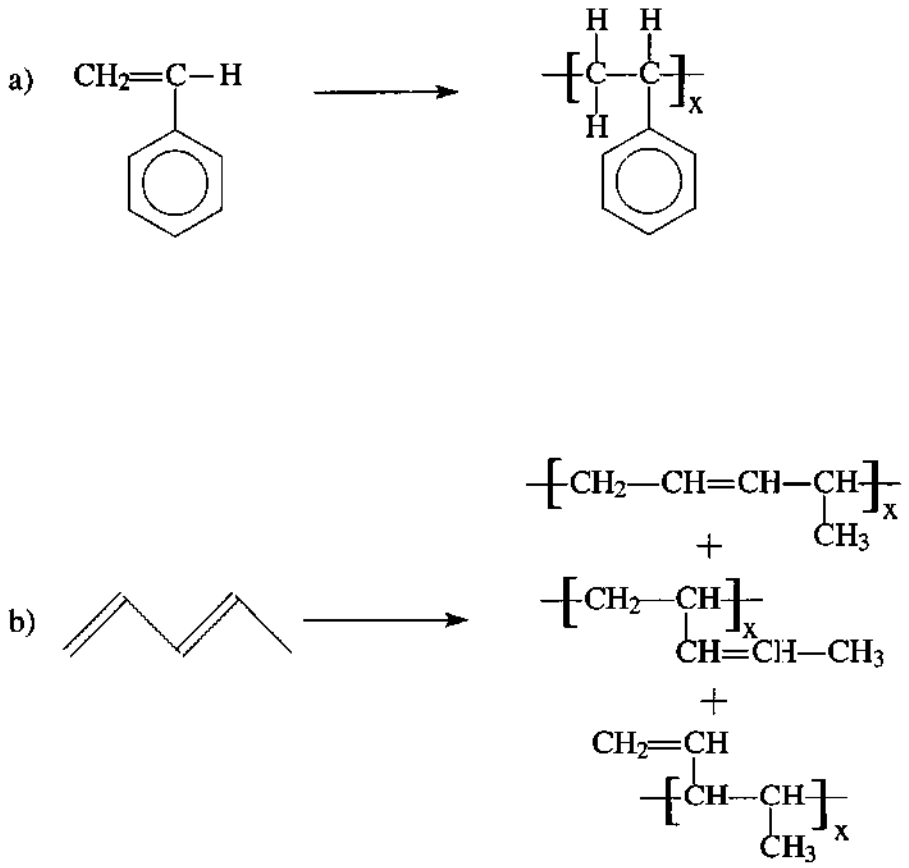

Figure 4-1. Polymerization of a) styrene and b) 1,3-pentadiene.

soluble than ethylbenzene. Connally has also measured pentane solubilities. He found pentane to be between 1 and 2 percent soluble in water at 300°C (Connolly, 1966); it is estimated that piperylene is between 2 and 5 percent soluble in water at this same temperature.

Both styrene and 1,3-pentadiene are commonly polymerized in a cationic polymerization in the presence of Lewis acid catalysts such as $AlCl_3$ or BF_3. These catalysts must eventually be neutralized by the addition of base, and the resulting salts leave the plant as a waste byproduct. Chandler et al. (1997) demonstrated that alkylation reactions, which are commonly catalyzed by these same Lewis acid catalysts, can be run in nearcritical water, without the addition of any acid. This work investigates the possibility of running polymerization reactions in nearcritical water and studies the effect of the addition of small amounts of acid on these reactions. In this work, average molecular weights, molecular weight distributions, and product yields were studied as functions of temperature, time, monomer concentration, and added acid concentration.

Materials

Chemicals used in the experiments were the following: glacial acetic acid (Baker), hexadecane (Aldrich, 99%), nitrogen (Air Products, UHP / Zero Grade), 1,3-pentadiene (Aldrich, 90%, mixture of isomers), styrene (Aldrich, 99+%), and water (Aldrich, HPLC grade).

Experimental Methods

3.0 ml stainless steel reactors were loaded with varying amounts of monomer, solvent, and glacial acetic acid. The monomer was either styrene or piperylene, and the solvent was either water or hexadecane. Solvent to monomer mass ratios of 10:1, 5:1, and 1:1 were used; additionally, some reactions were run without solvent present. Reactions were run with 0, 1, and 2 mass percent glacial acetic acid added. The reactors were made on site and were sealed with stainless steel lids and valves from High Pressure Products (models 15-11AF1 and 15-21AFANMD). Reactors were loaded in a nitrogen glove bag to prevent the inclusion of oxygen in the reactor headspace. The reactors were placed in a heating block and heated to a temperature between 250 -- 300°C. The reactors were overfilled and purged after heating to ensure that they were liquid-full (Figure 4-2). All reactions were run for between 2 and 5 hours. To quench the reaction, the reactors were removed from the heating block and placed in cool water. Product samples were sent to Hercules, Inc. for analysis by GPC and SEC.

Results and Discussion

Styrene was successfully polymerized in water for 3 1/2 to 5 hours at 275°C. Number-average molecular weights, $\overline{M_n}$, were of order 1000, and weight-average molecular weights, $\overline{M_w}$, were of order 40,000. Values for the third moment of the molecular weight distribution, $\overline{M_z}$, were of order 150,000.

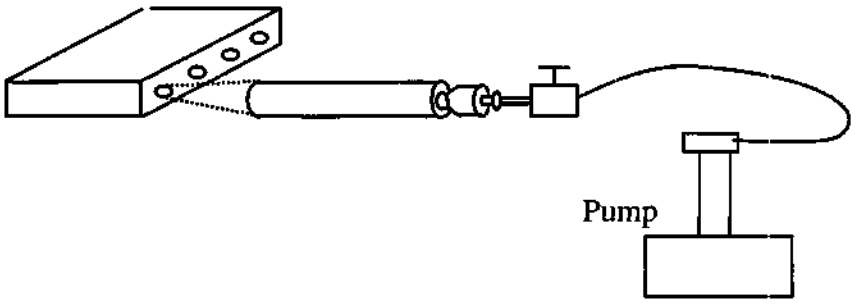

Figure 4-2. Apparatus for batch reactions with nearcritical water.

1,3-Pentadiene was successfully polymerized in water for 1 to 4 hours at temperatures ranging from 200 to 300°C (Table 4-1). Temperature and time of reaction greatly affected molecular weight distributions, indicating that the reaction is quite tunable. Trace amounts of product were obtained at 200°C and 250°C. The product had high average molecular weights and low polydispersity. For reactions at 300°C, average molecular weights were as follows: number-average molecular weights, $\overline{M_n}$, were of order 200, and weight-average molecular weights, $\overline{M_w}$, were of order 2000. Values for the third moment of the molecular weight distribution, $\overline{M_z}$, were of order 20,000.

2% added acid did not significantly alter product distributions in 2-hour runs. Comparing 4-hour runs, $\overline{M_n}$ increased with added acid, and $\overline{M_z}$ decreased with acid concentration. In both the reactions run with added acetic acid and those run without added acid, longer reaction times led to decreased $\overline{M_z}$. Reaction also occurred in the absence of water, suggesting an interesting thermal reaction. Because it appeared that temperature alone is sufficient to initiate polymerization, copolymerization in a nearcritical water solvent may be possible. Oxygen as an element in a monomer can inhibit traditional Lewis acid catalysis, precluding the incorporation of monomers like vinyl acetate and propyl vinyl ether into polymer resins. Thermal polymerization might be a means of incorporating these oxygen-containing monomers into polymer resins through copolymerization.

Rxn	Solvent	Solvent:C_5H_8 (by weight)	Wt% Acid	T (°C)	Rxn Time (hrs)	$\overline{M_n}$	$\overline{M_w}$	$\overline{M_z}$
1	Water	1:1	0	200	2	36900	47330	54310
						32330	43930	52130
2	Water	5:1	0	300	2	150	2520	19640
3	Water	5:1	1	300	2	160	2600	26260
						160	3240	24020
4	Water	5:1	2	300	2	160	2360	17400
						170	2400	20540
5	Water	5:1	0	300	4	180	2530	12840
6	Water	5:1	1	300	4	210	1650	10040
7	Water	5:1	2	300	4	240	1630	7940
8	Hexadecane	1:1	0	300	2	170	1890	14530
						170	1790	15050

Table 4-1. Molecular weight distributions for 1,3-pentadiene polymerization in nearcritical water and in hexadecane.

Conclusions

Styrene and 1,3-pentadiene were both successfully polymerized in nearcritical water without any added acid. Average molecular weights for the 1,3-pentadiene were tunable with temperature and time, and the addition of a couple mass percent acetic acid had only a slight effect on molecular weight distributions. 1,3-Pentadiene was also polymerized in the absence of water, suggesting thermal polymerization, which could be investigated as a means of incorporating oxygen-containing monomers into polymer resins.

Modification of Cellulose Acetate and Synthesis of Water Soluble Cellulose Acetate in Nearcritical Water

Introduction

In this work, nearcritical water was investigated as a solvent and catalyst for the redistribution of acetyl groups on cellulose acetate (Figure 4-3) and the production of water soluble cellulose acetate (Figure 4-4), where the degree of substitution is between 0.1 and 0.5. Cellulose acetate is currently produced by, first, completely acetylating cellulose using acetic acid with sulfuric acid as a catalyst. This completely acetylated cellulose acetate then reacts with magnesium acetate to reduce the degree of acetylation to 2.45. Downstream of the reaction, the acid catalyst must be neutralized with base, producing a salt byproduct.

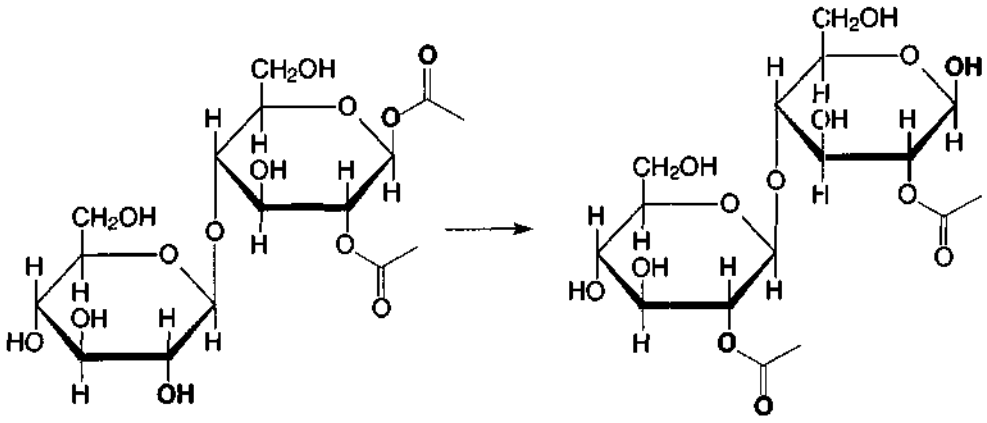

Figure 4-3. Redistribution of acetyl groups on cellulose acetate.

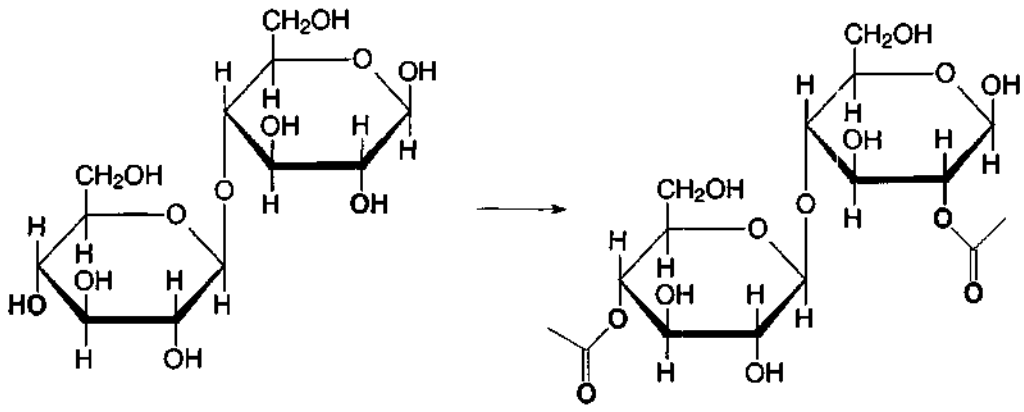

Figure 4-4. Production of water soluble cellulose acetate.

Because the ionization constant of water under nearcritical conditions is three orders of magnitude higher than that at standard temperature and pressure (Marshall and Franck, 1981), acylations that typically require the addition of an acid catalyst can be run in nearcritical water without any added acid (Eckert et al., 1999). The acid produced by the dissociation of water at elevated temperature neutralizes itself upon cooling; the cost and the waste associated with catalyst neutralization are eliminated. Here, the applicability of this technology to a commercial process is investigated. Both the rearrangement of cellulose acetate and the production of water soluble cellulose acetate in nearcritical water without added catalyst were evaluated.

Materials

Chemicals used in the experiments were the following: cellulose (Celanese Acetate), cellulose acetate flake (Celanese Acetate, average degree of substitution of 2.45), glacial acetic acid (Baker), nitrogen, (Air Products, UHP / Zero grade), and water (Aldrich, HPLC grade).

Experimental Methods

All reactions were run in 3.0 mL titanium autoclaves. Reactors were loaded in a nitrogen glove bag to preclude the presence of oxygen in the reactor headspace. This was done to limit the degradation of cellulose due to oxidation and to avoid other undesired side reactions due to free radicals introduced by oxygen. Reactors were placed in an aluminum heating block preheated to the desired temperature, between 100 and 250°C

(Figure 3-4). Pairs of reactors were removed and quenched in room temperature water at various times, between 10 and 60 minutes. Reactor heat-up was 99% complete after 7 minutes, and the reactors cooled to room temperature in 3 minutes (Figure 3-5). Samples were sent to Celanese Acetate for analysis by HPLC and FT-IR.

Results and Discussion

The redistribution of acetate groups in cellulose acetate subjected to nearcritical water was investigated (Figure 4-3). Reactors were loaded with 0.100 g of cellulose acetate, with a degree of substitution of 2.45, and 1.400 mL of H_2O. The reactions were run at the temperatures and times indicated in Table 4-2. The bulk acetyl value (AV) shifted very slightly, and HPLC chromatograms showed some signs of a broader distribution of acetyl groups. Visual inspection of the product, however, indicated that these changes were accompanied by product degradation.

Acetylation of cellulose with acetic acid in nearcritical water was also attempted (Figure 4-4), in an effort to produce water soluble cellulose acetate. In this product, the desired degree of substitution is between 0.1 and 0.5. Reactors were loaded with 0.100 g of cellulose and varying amounts of acetic acid and water. A series of reactions was run at 200°C, and these results are shown in Table 4-3. Time seemed to affect color more significantly than did acid content. Visual inspection of the product indicated that cellulose was decomposing with time at 200°C, so a series of reactions was run at 150°C. These results are shown in Table 4-4. There were fewer fibers in the liquid when the

Rxtr #	g cellulose acetate	ml H_2O	t(min)	T(°C)	bulk AV
1 & 2	0.100	1.400	10	150	55.78
3 & 4	0.100	1.400	30	150	55.49
5 & 6	0.100	1.400	60	150	55.52
1 & 2	0.100	1.400	10	100	55.83
3 & 4	0.100	1.400	30	100	55.55
5 & 6	0.100	1.400	60	100	55.55

Table 4-2. Bulk acetyl value (AV) of cellulose acetate after redistribution in nearcritical water.

Rxtr #	g cell	ml HOAc	ml H_2O	t(min)	solid	liquid
1 & 2	0.100	0.0107	1.489	10	matted; slight graying	clear; colorless; some fibers
3 & 4	0.100	0.0107	1.489	30	matted; off white some visible black specs	clear; slightly yellow; some fibers
5 & 6	0.100	0.0107	1.489	60	matted; off white some visible black specs	clear; yellow (more than 3&4, but less than 9&10); some fibers
7 & 8	0.100	0.107	1.393	10	matted; slight graying; some visible black specs	clear (like 1&2); colorless; some fibers
9 & 10	0.100	0.107	1.393	30	matted; off white fewer visible black specs	clear; yellow (more than 3&4); some fibers
11 & 12	0.100	0.107	1.393	60	matted; dark (gray /brownish)	cloudy (translucent); brownish/ yellow; some fibers

Table 4-3. Results of treatment of cellulose with acetic acid and water at 200°C.

Rxtr #	g cellulose	ml HOAc	ml H_2O	t(min)	solid	liquid
1 & 2	0.100	0.0107	1.489	10	matted; slightly off-white; few black specs	clear; colorless; a few fibers
3 & 4	0.100	0.0107	1.489	30	matted; a bit more color; some black specs	clear; colorless; a few fibers
5 & 6	0.100	0.0107	1.489	60	matted; slightly off-white; few black specs	clear; colorless; a few fibers
7 & 8	0.100	0.107	1.393	10	matted; slightly off-white; few black specs	clear; colorless; a few fibers
9 & 10	0.100	0.107	1.393	30	matted; slightly off-white; some black specs	clear; colorless; a few fibers
11 & 12	0.100	0.107	1.393	60	matted; slightly off-white; few black specs	clear; colorless; a few fibers

Table 4-4. Results of treatment of cellulose with acetic acid and water at 150°C.

reactions were run at the cooler temperature, and there was only a minimum appearance of color in both the solid and the liquid for these lower temperature runs. FT-IR scans, however, revealed no evidence of ester formation at either temperature.

Conclusions

The experimental results suggest some redistribution of the acetyl groups of cellulose acetate, but the amelioration of the unacceptable degradation of cellulose is necessary before this redistribution in nearcritical water will be a viable industrial option. Esterification reactions of cellulose were slower and in lower yield than expected, partly due to the rapid hydrolysis of ester linkages formed. Increasing the temperature to increase the rate resulted in unacceptable degradation. It is apparent that acceptable esterification rates will not be achieved in nearcritical water unless the residence time is very short or an additive is used that will inhibit degradation.

Beckmann Rearrangements in Nearcritical Water

Introduction

Cyclohexanone oxime is converted to ε-caprolactam on a commercial scale in a Beckmann rearrangement. This reaction is catalyzed by concentrated sulfuric acid and produces ammonium sulfate as a byproduct (Figure 4-5). Because over 4 million tons of ε-caprolactam, a precursor to nylon 6, are produced annually (Weissermel and Arpe,

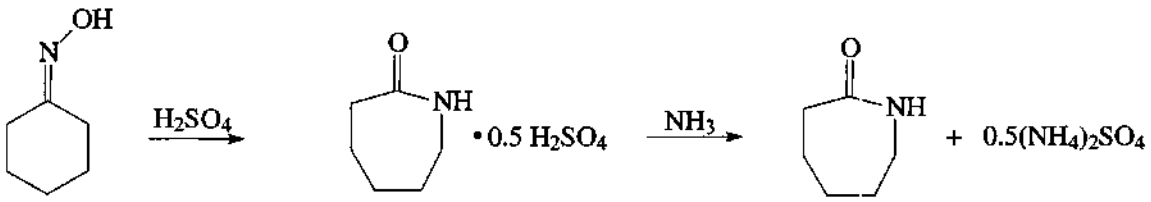

Figure 4-5. Commercial process for Beckmann rearrangement of cyclohexanone oxime to ε-caprolactam.

1997), the costs associated with this acid catalysis are significant. Looking for a less environmentally taxing synthesis scheme, Sato et al. (1998) and Ikushima et al. (1999) found that this rearrangement is promoted in supercritical water (T_c = 374°C, P_c = 221 bar), without any added catalyst. Unfortunately, supercritical water is quite corrosive; any process using this solvent demands exotic metallurgy, making capital costs prohibitively high.

In this work, kinetics of Beckmann rearrangements of cyclohexanone oximes in nearcritical water were measured. Because the ionization constant of water reaches a maximum at 250°C (Marshall and Franck, 1981), nearcritical water is a better source of protons than supercritical water is. Also, capital costs involved in a nearcritical water process would be much less than those in a supercritical water process because pressures are lower and standard metallurgy may be acceptable at the lower temperatures.

Materials

Chemicals used in the experiments and synthesis were the following: acetone (Aldrich, HPLC grade, 99.9+%), cyclohexanone oxime (Aldrich, 97%), hydroxylamine hydrochloride (Aldrich, 98%, A.C.S. reagent), sodium acetate trihydrate (Aldrich, 99+%, A.C.S. reagent), 3,3,5-trimethylcyclohexanone (Aldrich, 98%), and water (Aldrich, HPLC grade). 3,3,5-Trimethylcyclohexanone oxime was synthesized as described below (Hutchins et al., 1995; Hutchins et al., 1983; Harvill et al., 1950).

Experimental Methods

Synthesis of 3,3,5-Trimethylcyclohexanone Oxime

Hydroxylamine hydrochloride (129mmol 8.93g), sodium acetate trihydrate (129mmol 17.53g), and water (175mL) were heated to 60°C. 3,3,5-Trimethylcyclohexanone (65mmol 9.05g) in methanol (35mL) was then added. An additional 25mL of methanol was added until the solution became clear, and stirring was continued at 60°C overnight. The solution was cooled to room temperature, diluted with 200mL of water, and extracted with ethyl ether (3 x 200mL). The ether layers were combined and washed with saturated sodium bicarbonate (2 x 250mL) and brine (2 x 150mL). They were then dried over sodium sulfate and reduced via rotor evaporation. The white solid was recrystallized in a mixture of 75% water / 25% methanol to give 8.93g (89% yield) of white solid. mp 77-79°C (lit. mp 76-78°C (Hutchins et al., 1995); lit. mp 86-87°C (Hutchins et al., 1983); lit. mp 72-73°C (Harvill et al., 1950))

Kinetic Measurements

All reactions were run in 3.0 mL titanium reactors. Reactors were loaded with water and the appropriate oxime (47: 1 on a molar basis), sealed with a titanium plug, and placed in an aluminum heating block preheated to 250°C (Figure 3-4). Pairs of reactors were removed and quenched in room temperature water at various times, between 30 and 75 minutes. Reactor heat-up was 99% complete after 7 minutes, and the reactors cooled

to room temperature in 3 minutes (Figure 3-5). Samples were analyzed by GC-FID and GC-MS.

Results and Discussion

After 60 minutes at 250°C, roughly half of the cyclohexanone oxime had reacted, but only a few percent rearranged to the desired ε-caprolactam (Figure 4-6). Most of the product was cyclohexanone, resulting from the competitive hydrolysis reaction. Because the nitrile bond is polar, water can perform a nucleophilic attack on the protonated oxime, initiating hydrolysis (Figure 4-7).

Because of steric hindrance provided by the methyl groups, 3,3,5-trimethylcyclohexanone oxime was hypothesized to hydrolyze more slowly than nonsubstituted cyclohexanone oxime. The rate of the Beckmann rearrangement of these oximes in nearcritical water is limited by the rate of protonation of the oxime hydroxyl group (Figure 4-8), so the introduction of methyl groups, which are slightly electron donating, should not alter the rate of rearrangement. As shown in Figure 4-9, the hydrolysis reaction was inhibited by the methyl groups, but it remained significant. Hydrolysis occurs more rapidly than rearrangement, even for the sterically hindered oxime.

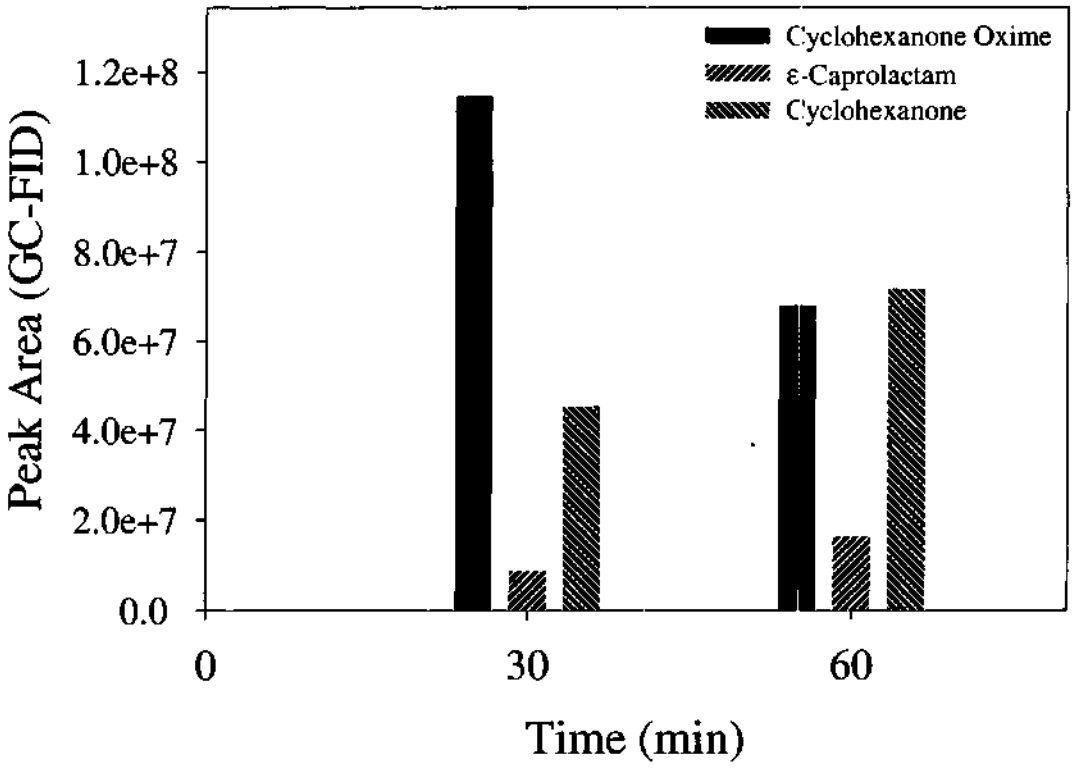

Figure 4-6. Selectivity to ε-caprolactam and cyclohexanone when cyclohexanone oxime is heated to 250°C in water.

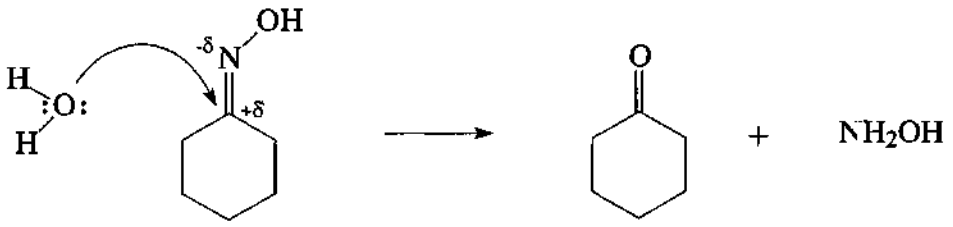

Figure 4-7. Nucleophilic attack on cyclohexanone oxime to initiate hydrolysis.

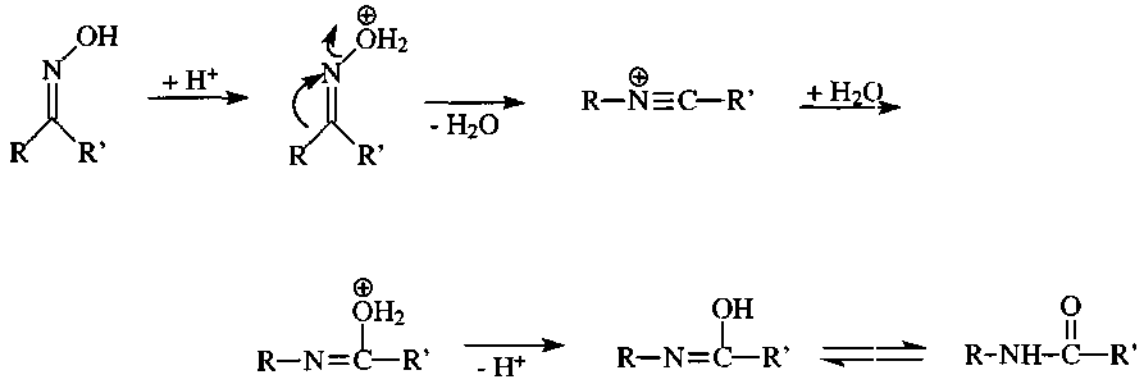

Figure 4-8. Mechanism for the Beckmann rearrangement.

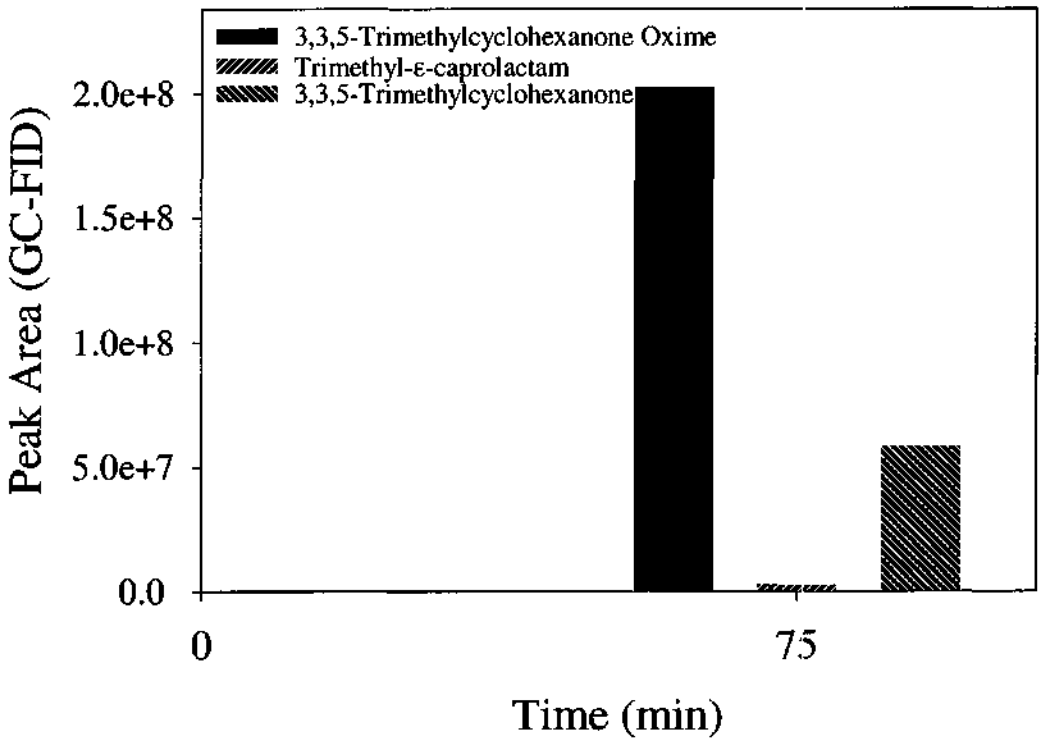

Figure 4-9. Selectivity to trimethyl-ε-caprolactam and 3,3,5-trimethylcyclohexanone when 3,3,5-trimethylcyclohexanone oxime is heated to 250°C in water.

Conclusions

While nearcritical water would provide an environmentally benign process for the Beckmann rearrangement of cyclohexanone oxime to ε-caprolactam, the rearrangement is precluded by the competing hydrolysis reaction. While steric hindrance provided by additional groups on the ring of cyclohexanone oxime do inhibit hydrolysis, it still proceeds much more rapidly than does the desired rearrangement.

References

Chandler, K.; Deng, F.; Dillow, A.K.; Liotta, C.L.; Eckert, C.A. Alkylation Reactions in Near-Critical Water in the Absence of Acid Catalysts. *Ind. Eng. Chem. Res.* **1997**, *36*, 5175-5179.

Connolly, J.F. Solubility of Hydrocarbons in Water Near the Critical Solution Temperatures. *J. Chem. Eng. Data* **1966**, *11*, 13-16.

Eckert, C.A.; Gläser, R.; Brown, J.S. Tuning of Chemical Reactions with Expanded Solvents. Proceedings of the 5th Conference of Supercritical Fluids and their Applications, Verona, Italy, 1999.

Harvill, E. K.; Roberts, C. W.; Herbst, R. M. The Synthesis of Alkylated Pentamethylenetetrazole Derivatives. *J. Org. Chem.* **1950**, *15*, 58-67.

Hutchins, R.O.; Adams, J.; Rutledge, M. C. Stereoselective Hydride Reductions of Cyclic N-Diphenylphosphinyl Imines. Highly Diastereoselective Syntheses of Protected Primary Amines. *J. Org. Chem.* **1995**, *60*, 7396-7405.

Hutchins, R.O.; Su, W.Y.; Sivakumar, R.; Cistone, F.; Stercho, Y. P. Stereoselective Reductions of Substituted Cyclohexyl and Cyclopentyl Carbon-Nitrogen π Systems with Hydride Reagents. *J. Org. Chem.* **1983**, *48*, 3412-3422.

Ikushima, Y.; Hatakeda, K.; Sato, O.; Yokoyama, T; Arai, M. Noncatalytic Organic Synthesis Using Supercritical Water: The Peculiarity Near the Critical Point. *Angew. Chem. Int. Ed.* **1999**, *38*, 2910-2914.

Kuhlmann, B.; Arnett, E.M.; Siskin, M. Classical Organic Reactions in Pure Superheated Water. *J. Org. Chem.* **1994**, *59*, 3098-3101.

Marshall, W.L.; Franck, E.U. Ion Product of Water Substance. 0 – 1000°C, 1 – 10,000 Bars. New International Formulation and Its Background. *J. Phys. Chem. Ref. Data* **1981**, *10*, 295–304.

Sato, O.; Ikushima, Y.; Yokoyama, T. Noncatalytic Beckmann Rearrangement of Cyclohexanone-Oxime in Supercritical Water. *J. Org. Chem.* **1998**, *63*, 9100-9102.

Thomason, T.B.; Modell, M. Supercritical Water Destruction of Aqueous Wastes. *Haz. Waste* **1984**, *1*, 453-467.

Uematsu, M.; Franck, E.U. Static Dielectric Constant of Water and Steam. *J. Phys. Chem. Ref. Data* **1980**, *9*, 1291-1306.

Weissermel, K.; Arpe, H.J. *Industrial Organic Chemistry, 3rd ed.*; Verlag Chemie: New York, 1997.

CHAPTER V

LOW TEMPERATURE PHASE-TRANSFER CATALYZED OXIDATION OF P-XYLENE

Introduction

Terephthalic acid (TA) is currently produced via the oxidation of *p*-xylene (*p*X) by air in the presence of a Co/Mn/Br catalyst in an acetic acid solvent (Fischer and Röhrscheid, 1996; Partenheimer, 1995; Weissermel and Arpe, 1997). The reaction is accomplished in three sequentially arranged vessels at 210 °C and 305 psig, 185 °C and 145 psig, and 240 °C and 450 psig, with typical yields around 98% (Weissermel and Arpe, 1997). The oxidation occurs stepwise, passing through the intermediates *p*-methylbenzyl alcohol (*p*MBA), *p*-tolualdehyde (*p*TAD), *p*-toluic acid (*p*TA), and *p*-carboxybenzaldehyde (*p*CBA) as shown in Figure 5-1.

While the oxidation of the first methyl group of *p*-xylene to form *p*-toluic acid is fast, the oxidation of the second methyl group to form terephthalic acid occurs comparatively slowly. Byproducts formed in the current process include the terephthalic acid isomers isophthalic acid and phthalic acid, as well as benzoic acid. Multi-ring compounds, such as dicarboxyl fluorenone, dicarboxyl anthraquinone, bibenzoic acid, and tricarboxy biphenyl, are formed from consecutive reactions of intermediate radicals and are also found in the product mixture.

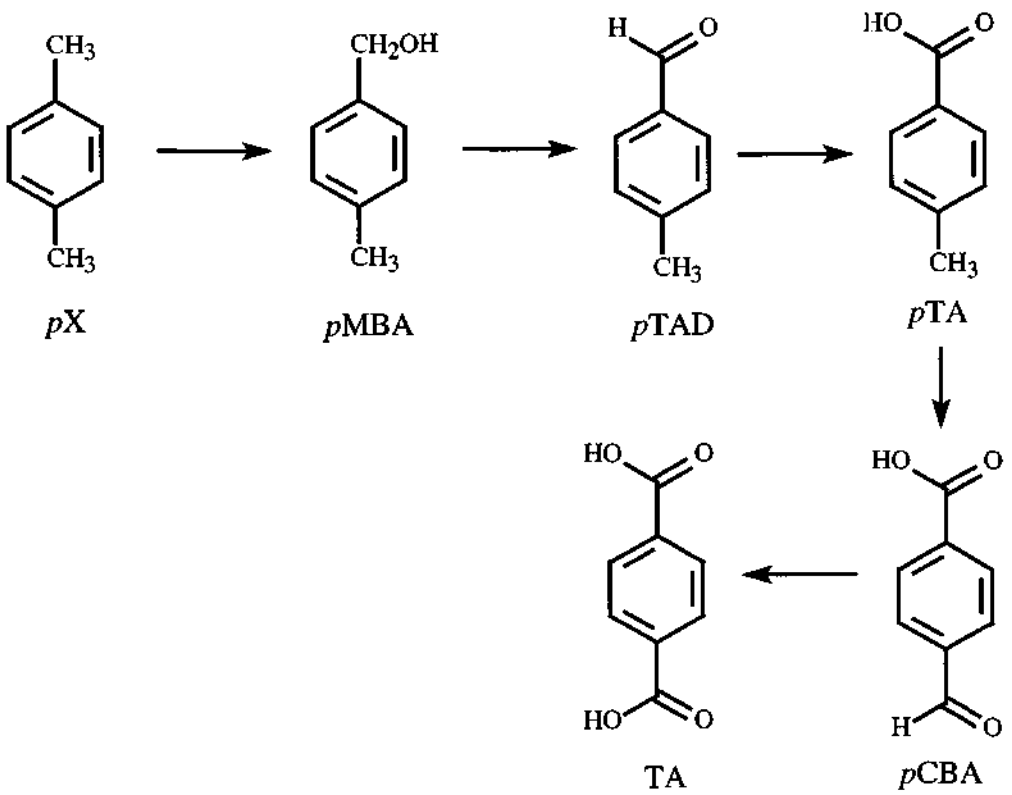

Figure 5-1. Key intermediates in the oxidation of *p*-xylene to terephthalic acid.

Four major problems of the current process are the loss of the acetic acid solvent due to oxidation, the corrosiveness of the process fluids, the formation of methyl bromide, and the incorporation of *p*CBA during precipitation of TA. To avoid the burning of acetic acid, it may be replaced by another solvent, or *p*-xylene may be oxidized without any solvent. In either case, the catalyst system must be adapted to the reaction environment, and both product separation and recovery must be re-optimized.

Among the possible substitutes for the acetic acid solvent, water is of particular interest. First, it is an environmentally benign alternative to acetic acid. In addition, the corrosiveness of the reaction mixture would be considerably reduced, and this, in turn, would reduce costs for expensive reactor metallurgy. Previous work on water as a solvent for the production of TA has been of limited success. Neither conversion and selectivity nor the run-time stability of the system have been found to be within an acceptable range for a commercial process. A patent assigned to Amoco in 1990 describes a two-stage process for *p*X oxidation with water as a solvent (Nowicki and Lowry, 1990). Although an appreciable yield of TA can be obtained, the low purity of the final product prohibits commercialization. Partenheimer's 1995 review covers additional investigations of liquid phase oxidations of aromatic hydrocarbons in water.

A phase-transfer catalyst could eliminate the need for a solvent in which both *p*-xylene and bromide ion catalyst are soluble. A phase-transfer catalytic process could run at a temperature and pressure much lower than those required in the acetic acid process. Aside from reducing losses of reactant and products due to burning and further alleviating the corrosiveness of the reaction mixture, methyl bromide formation might be

substantially diminished at lower temperature. In addition, the costly solvent purification in the acetic acid system would be avoided. With regard to purity, the TA product of a phase-transfer catalytic process would be intermediate between that of the current acetic acid process and that obtained by using only water as a solvent. Reduction of the color-forming impurities might be achieved by running a phase-transfer catalyzed *p*X oxidation as the first step of a two-step process. The second step would be carried out in acetic acid at higher temperature to finally convert the intermediate product into TA.

It has been shown previously that phase-transfer catalysts bring about the oxidation of *p*X in the presence of an aqueous phase containing cobalt(II) bromides (Hronec et al., 1985; Dakka et al., 1989). In these investigations, no reaction was observed when a cobalt salt was used in the absence of either the bromide or the phase-transfer catalyst. Later investigations have shown that the transition metal catalyst can be omitted, but that the bromide ion, which is a chain initiator, is necessary for successful oxidation of *p*X (Haruštiak et al., *React. Kinet. Catal. Lett.*, 1988). The transition metal catalyst is believed to decompose peroxides which form in the initiation step of the oxidation (Haruštiak et al., 1989). The selectivities for TA and other higher oxidized products over *p*TA is raised considerably by transition metal salts.

Although two investigations of the kinetics of phase-transfer catalytic oxidation of *p*X, in the presence and in the absence of transition metal salts, have been published (Haruštiak et al., 1989; Haruštiak et al., *J. Mol. Catal.*, 1988), data on product distribution with reaction time for systematically varied reactant concentrations, reaction conditions, and different phase-transfer catalytic systems are limited at this time. Also, the changes

of the reaction mixture with increasing conversion, in terms of polarity and phase distribution of the products between the organic and aqueous phase, have not been addressed. Little work has been reported to tailor the phase-transfer catalytic system to the specific reaction system.

Phase-Transfer Catalysis

There are thousands of known reactions which are thermodynamically feasible, but do not proceed to any measurable extent; they are limited by their kinetics. Many of these reactions fail to occur because the reactant molecules do not collide. If the reactant molecules are not both soluble either in a single phase or in the interfacial region between phases, then reaction will not proceed.

There are two common methods for encouraging two such reagents to come together; one can either use a polar aprotic solvent which can dissolve both reactant species, or one can use a phase-transfer catalyst (PTC). Many current processes that involve reagents which are not mutually soluble in a single phase utilize polar aprotic solvents, rather than PTCs. These solvents, which include dimethylsulfoxide, dimethylformamide, acetonitrile, and acetic acid, dissolve both salts and organic reagents (Starks et al., 1994). For the reaction to proceed to an adequate extent, large quantities of these economically costly and environmentally deleterious solvents must be used. An additional disadvantage to the use of these solvents is the difficulty and expense of their removal (Weber and Gokel, 1977).

Phase-transfer catalysis offers a viable alternative to the use of these harmful solvents. The role of a PTC can be explained with the reaction scheme shown in Figure 5-2 (Starks et al., 1994). The nucleophile (Nu) will react with the organic (R-X), but it must first contact the organic. Q^+ carries the nucleophile from the aqueous phase into the organic phase, and reaction proceeds. Q^+ then carries the leaving group (X) into the aqueous phase. Another substitution reaction occurs here, consuming the reactant salt (M-Nu) and regenerating the phase transfer catalyst (Q-Nu). This cycle can recur until either the M-Nu or the R-X is consumed.

While the concepts of PTC are quite general, most of its current applications involve anion transfer. Some common reactions made possible by PTC include S_N2 displacement reactions with alkyl halides and anions, alkylation reactions, elimination reactions to produce olefins and acetylenes, oxidation reactions, reduction reactions, polymerization reactions and modifications, and deuterium exchange reactions (Starks et al., 1994).

Several variables must be considered when designing any PTC reaction. First, the type of phase-transfer catalyst must be determined. The catalyst's partitioning and strength of anion binding are two important factors to consider. The amount of agitation required for adequate phase contacting is another important variable. The amount of water, as well as the temperature and pressure of reaction, must be optimized (Starks et al., 1994).

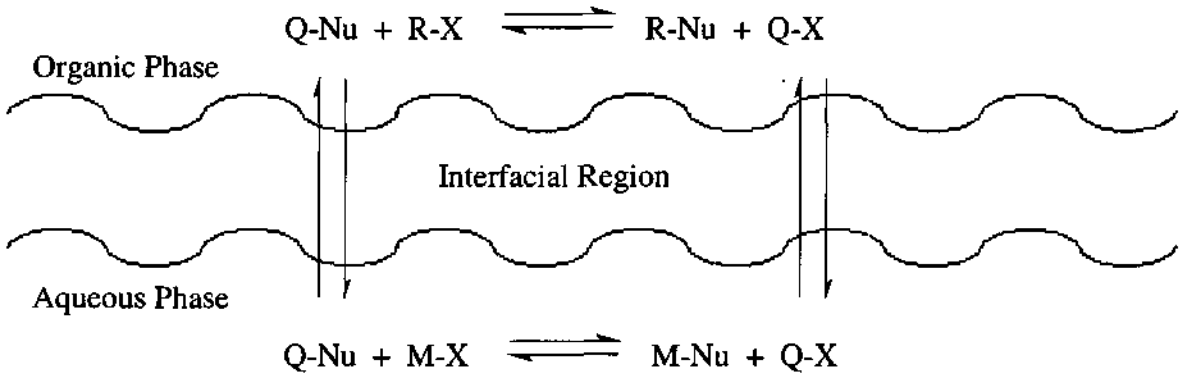

Figure 5-2. General PTC cycle.

Quaternary ammonium salts are popular phase transfer catalysts because a wide variety of them are readily available at low cost. They are easily separated from product mixtures, but they will degrade under basic conditions at temperatures above 120°C. Rates of degradation will increase as either agitation or basicity is increased (Starks et al., 1994).

Experimental Methods

Materials

Chemicals used in the experiments and calibrations were the following: air (Air Products, UHP / Zero grade), boron trichloride-methanol (Supelco, 12% w/w), *p*-carboxybenzaldehyde (Aldrich), cobalt(II) acetate tetrahydrate (Aldrich, 98+%), cobalt(II) bromide (Aldrich, 99%), cumene hydroperoxide (Aldrich, 80%), *o*-dichlorobenzene (Aldrich, 99%, HPLC grade), diethyl ether (Fluka, 99+%), 2,2-dimethoxypropane (Aldrich, 98%), dimethyl terephthalate (Aldrich, 99+%), glacial acetic acid (Baker), hydrogen bromide (Aldrich, 48 wt% in water), methanol (Aldrich, ACS HPLC Grade), *p*-methylbenzyl alcohol (Aldrich, 98%), nitrogen (Air Products, UHP / Zero grade), oxygen (Air Products, UHP / Zero grade), pentachlorobenzene (Aldrich, 98%), potassium bromide (Aldrich, 99+%), sodium chloride (Fisher, crytstalline, ACS), sodium hydroxide (Baker, pellets), sodium sulfate (Fisher, 99.5%), terephthalic acid (Aldrich, 98%), tetrabutylammonium bromide (Aldrich, 99%), tetraethylammonium bromide (Aldrich, 99%), tetrahexylammonium bromide (Aldrich, 99%), *p*-tolualdehyde

(Aldrich, 97%), *p*-toluic acid (Aldrich, 98%), tributylamine (Aldrich, 99+%), water (Aldrich, HPLC grade), and *p*-xylene (Aldrich, 99%). *N*-2-ethylhexylquinolinium bromide (EHQB) and *N*-2-ethylhexylnicotinium bromide (EHNB) were synthesized as described in Appendix C.

Experimental Procedure

p-Xylene was initially oxidized with molecular oxygen, using TBAB as the phase-transfer catalyst, in a 250 mL Büchi glass reactor. Temperature was controlled with a hot oil bath. Unfortunately, heat transfer and agitation were inadequate in the Büchi reactor. While the glass reactor was initially necessary for visual inspection of the reaction mixture, the mechanical stability of a glass reactor was insufficient; reactor replacement was costly and caused long experiment downtime. For safety reasons, we replaced the glass reactor with a less fragile metal reactor, and we began to oxidize the *p*X with air, rather than oxygen.

A 300 mL stirred tank reactor from PPI, Inc. (FC series, serial number 97U-0053) was used to carry out the remaining phase-transfer catalytic experiments. All wetted parts were Hastelloy C. The reactor was heated by an electrical heating jacket, and the temperature was controlled via a thermocouple inside the reactor. The reaction mixture was agitated by a DynaMag magnetic mixer, whose well could be equipped with different stir blade configurations. Optimal gas/liquid contacting was provided by a gaspersator.

For a typical run in batch mode, the reactor was charged with 120 mL of *p*X, 30 mL of H_2O, 1.540 g of KBr, 0.549 g of TBAB, and 5.20 g of pentachlorobenzene for an

internal standard. The reactor was then closed, flushed three times with nitrogen to remove included air, and heated to the desired reaction temperature under stirring at 900 rpm. For reactions run in the batch mode (Figure 5-3), nitrogen was added to 79% of the desired total pressure, and the nitrogen feed valve was then closed. A sample of the liquid reactant mixture was taken to ensure that no reaction occurred during heat-up, the agitation was increased to 1600 rpm, and oxygen was introduced to the reactor up to the desired total pressure to start the reaction. Oxygen flow was regulated with a back pressure regulator to maintain the desired nitrogen to oxygen ratio, as well as the specified total pressure.

Later reactions were run with continuously flowing air (Figure 5-4). For a typical semi-batch run, the reactor was charged with 60 mL of *p*X, 100 mL of *o*-dicholorbenzene (*o*DCB) as a diluent, 40 mL of H_2O, 2.077 g of KBr, 0.742 g of TBAB, and 1.80 g of pentachlorobenzene for an internal standard. The reactor was then closed, flushed three times with nitrogen to remove included air, and heated to the desired reaction temperature under stirring at 900 rpm. A liquid sample was taken immediately after heat-up to ensure that no reaction had occurred. After pressurizing the reactor vessel with air to the desired total pressure, the agitation was increased to 1600 rpm, and the air flow rate was set by an expansion valve downstream of the condenser and the phase separator. Samples are taken periodically from the liquid phase using a 6-port sample loop (Valco Instruments Co. model C6UWEHC), which was rinsed with methanol.

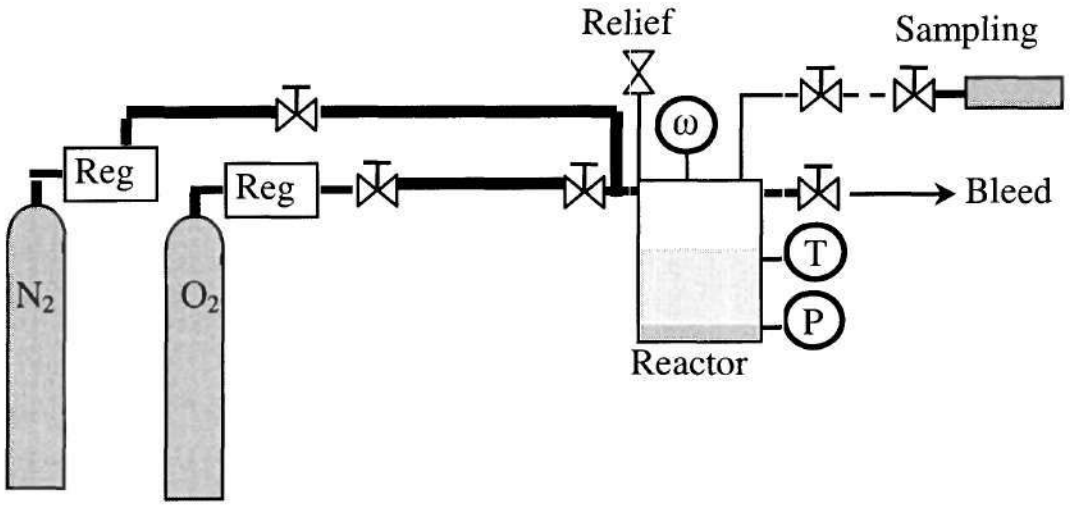

Figure 5-3. Experimental setup for batch PTC reactions.

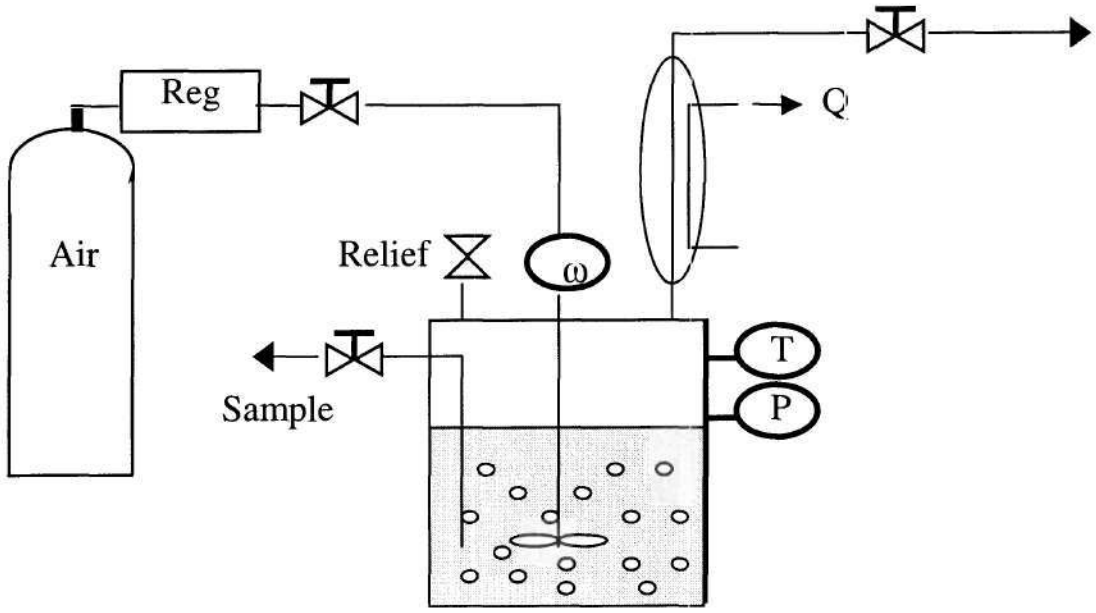

Figure 5-4. Experimental setup for semi-batch PTC reactions.

Product analysis of liquid phase samples was accomplished by gas chromotagraph (Hewlett-Packard model 6890) with both an MS detector and an FID. The MS was used for product identification, and the FID was used for quantification. The organic acids formed in the oxidation reaction were converted to their methyl esters using a BCl_3-methanol adduct (Ngan and Toofan, 1991). Because the amounts of *p*CBA and TA formed were so small, this esterification was not incorporated into the analysis of all samples. The mass balance of the samples relative to the internal standard was 100 ± 15%.

Gas phase samples were taken from the depressurized gas stream, which was passed through a constant volume glass cell with a septum and open/close valves on the inlet and the outlet. Samples from this cell were manually injected into a gas chromatograph (Hewlett Packard model 5890, series II), equipped with a thermal conductivity detector. A molecular sieve column (Hewlett Packard 12 FT, molecular sieve 5 A 60/80, model 19096A-012) was used for the separation of nitrogen and oxygen. A capillary column (Chrompack, PoraPLOT Q) was used for the separation of carbon oxides, volatile organics, and water.

Results and Discussion

Early experiments, run batch-wise with oxygen in the glass reactor, showed that the addition of cobalt(II)acetate tetrahydrate resulted in a significant rate increase. With no acetic acid present, the cobalt precipitated as a black solid during heat-up. The

addition of acetic acid increased catalyst solubility to limit its precipitation. When the cobalt(II)acetate tetrahydrate was added, the temperature of this exothermic reaction increased rapidly. Because temperature could not be controlled, the reaction was shut down prematurely. This reaction ran so quickly that conversion versus time data were not obtained, but the dramatic effect of cobalt addition was quite evident.

To ensure safety (see Appendix D) and slow the reaction for more accurate kinetic measurements, the oxidizing gas was changed from oxygen to synthetic air, using the apparatus shown in Figure 5-3. For additional safety, we replaced the glass reactor with a Hastelloy reactor rated to hold 6000 psig at 350°C.

Figure 5-5 shows results from a typical run in batch mode at 130°C with TBAB as the phase-transfer catalyst and overall reactant concentrations comparable to the ones used by Haruštiak et al. (*React. Kinet. Catal. Lett.*, 1988). The main product of the oxidation was *p*-tolualdehyde. It can be seen from the figure that, after a short initiation period of 30 min, the *p*X concentration in the organic phase rapidly decreased to 93 %, giving a conversion of 7 %, within 120 min. From then on, however, neither the *p*X concentration nor the concentration of any of the products changed during the following 12 hours. After 200 to 300 minutes, the oxygen flow into the reactor ceased. This is due to the formation of carbon dioxide by total oxidation of organic material. CO_2 was, in fact, detected in the gas phase of the reactor headspace via GC analysis. A conversion of *p*X to CO_2 less than 0.1 % would generate a partial pressure of CO_2 equal to the initial partial pressure of oxygen in the reactor. An accumulation of CO_2 would prevent oxygen

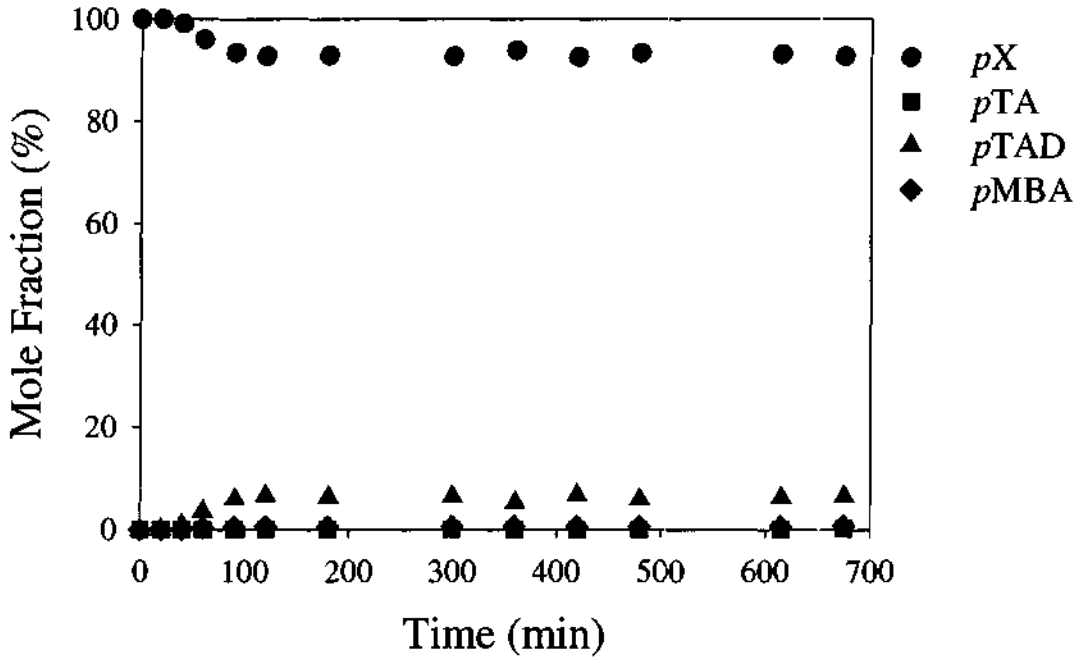

Figure 5-5. Product distribution as a function of reaction time for batch-wise *p*X oxidation at 130°C and 120 psig. Agitation was 1600 rpm. Reactor was loaded with 0.972 mol *p*X, 1.667 mol H_2O, 0.00170 mol TBAB, 0.0129 mol KBr, and 0.0208 mol pentachlorobenzene.

from flowing into the reactor, and the reaction would be starved. To test whether this formation of CO_2 was a limiting factor in achieving higher conversion, the reactor was loaded with half of the previous amounts of the reactants, leaving a larger headspace volume above the liquid reaction mixture. When liquid loading was halved, the reaction ran to 13% conversion of *p*X (Figure 5-6). The reaction ran longer because more CO_2 needed to be formed to before oxygen flow was halted.

To bypass the limitations due to the formation of CO_2, the reactor setup was altered to continuously flow air through the reactor headspace (Figure 5-4). The gas leaving the reactor was passed through a condenser, where the liquid and gas phases were separated in a static vessel. The liquid phase was recycled into the reactor, and the gas phase was expanded to atmospheric conditions, where its flow rate was measured and samples could be taken for analysis.

Typical results obtained with this setup are depicted in Figure 5-7. The reaction ran considerably longer than it did under batch conditions, and a higher conversion was reached. The reaction rate, as calculated from the linear section between 60 and 190 minutes, is about 1.5 times that of the batch system. After 230 minutes, the *p*X content in the mixtures seems to increase, but at this time the sampling was difficult because solid product precipitated in the tubing leading to the sample loop. As a possible consequence, more liquid than solid products appeared in the sample which could lead to a seemingly higher *p*X content in the product. Nevertheless, it can be seen that *p*TAD is an intermediate product which is further oxidized, mainly to *p*TA. The overall conversion

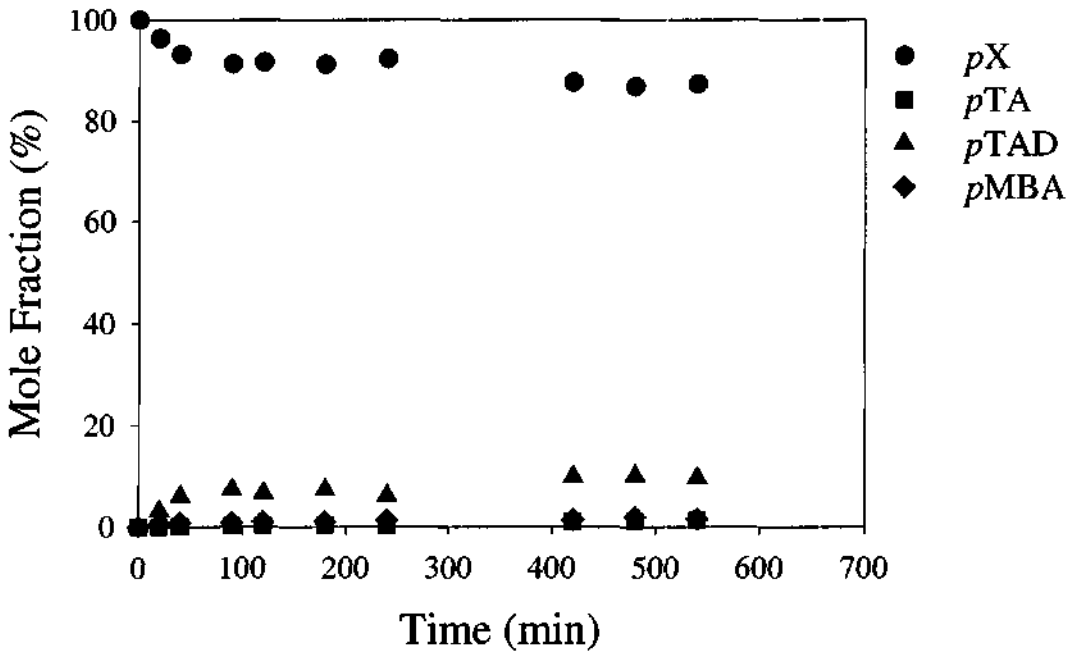

Figure 5-6. Product distribution as a function of reaction time for batch-wise *p*X oxidation at 130°C and 120 psig. Agitation was 1600 rpm. Reactor was loaded with 0.546 mol *p*X, 0.833 mol H_2O, 0.00085 mol TBAB, 0.00648 mol KBr, and 0.0104 mol pentachlorobenzene.

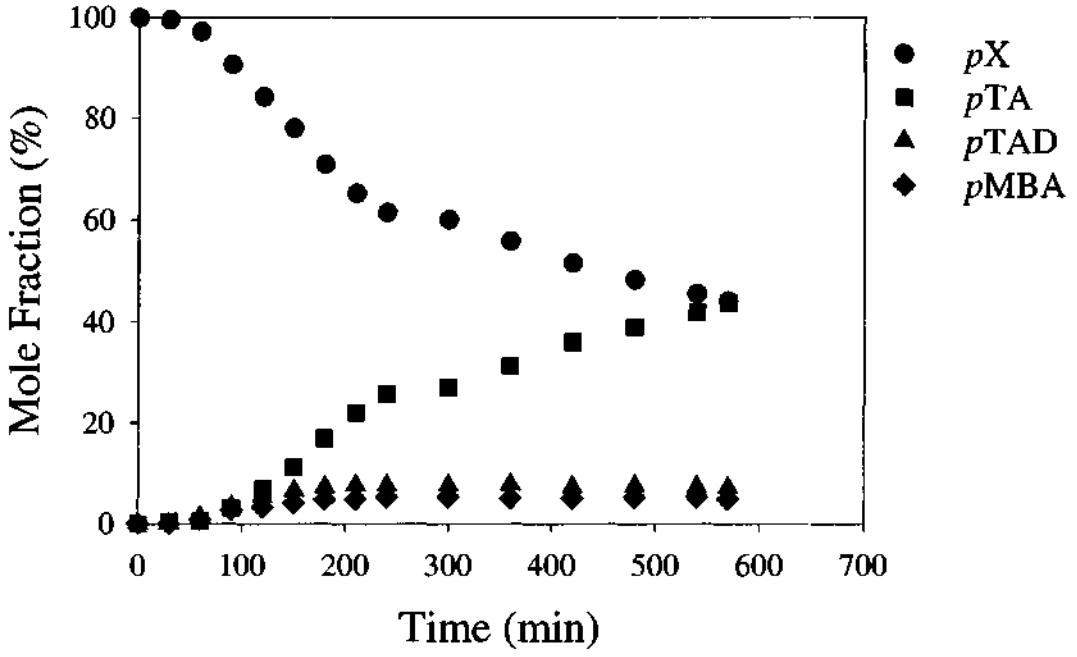

Figure 5-7. Product distribution as a function of reaction time for semi-batch *p*X oxidation at 130°C and 120 psig. Air flow rate was 0.38 L/min. Agitation was 1600 rpm. Reactor was loaded with 0.489 mol *p*X, 0.888 mol *o*DCB, 2.222 mol H_2O, 0.00230 mol TBAB, 0.0175 mol KBr, and 0.00720 mol pentachlorobenzene.

after 10 hours is at least 35 %, but might higher. Analysis of the contents of the reactor after stopping the reaction and cooling down to room temperature yielded the following product distribution (mole-%): 0.3 % *p*MBA, 19.9 % *p*TAD, 77.1 % *p*TA, 0.3 % *p*MBT, 0.7 % *p*CBA, and 1.7 % TA.

Several factors, including agitation rate, temperature, reactant loading, diluent concentration, and catalyst types and concentrations, were evaluated to determine their effects on reaction kinetics. Figure 5-8 shows that 1600 rpm was a sufficient agitation rate; increasing the stirring rate to 2200 rpm did not increase the reaction rate. Increasing the temperature of reaction by 10°C significantly increased the reaction rate (Figure 5-9). This is most likely because of both the positive activation energy for reaction and a change in phase equilibria with temperature.

A change in the ratio of the two liquid phases was accompanied by a change in reaction rate. An increase in the relative size of the aqueous phase caused an increase in reaction rate (Figure 5-10). It is well-documented, however, that an increasing aqueous phase should cause the rate to slow (Starks et al., 1994). It is possible that our measured rate increased because, in order to keep catalyst concentrations constant in the aqueous phase, the net amount of catalyst was increased.

o-Dichlorobenzene was commonly used as a diluent to prevent solid precipitation upon sampling. When there was no diluent present, there was no detectable initiation period. As the amount of diluent increased, the formation of *p*-xylene radicals became increasingly inhibited, and the initiation period increased (Figure 5-11).

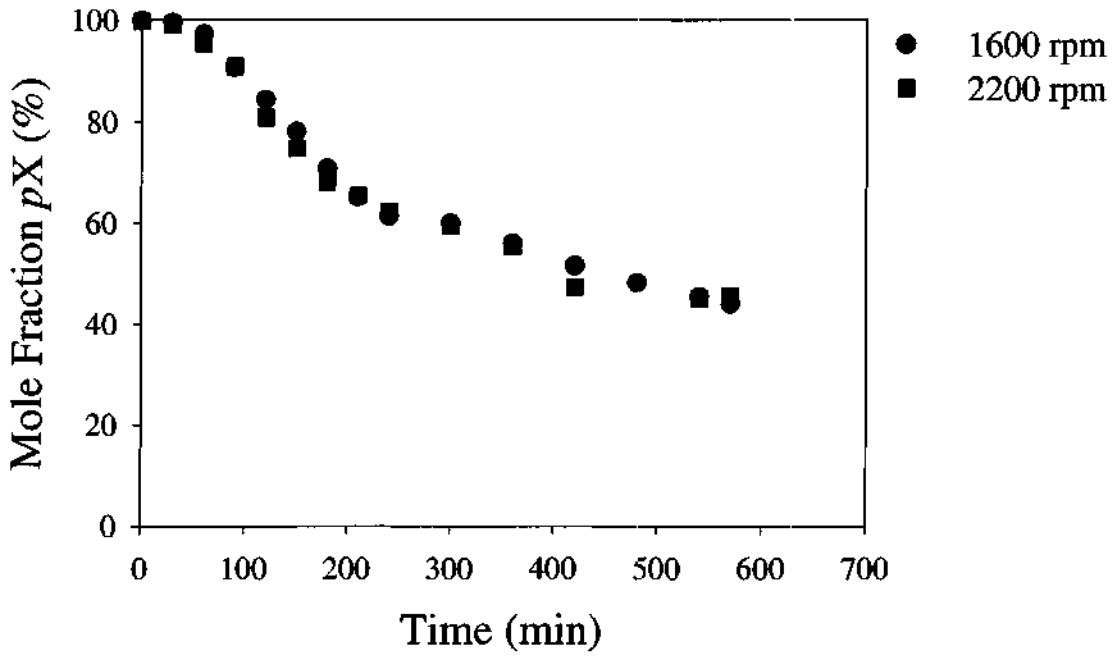

Figure 5-8. Mole fraction of *p*X in the product mixture as a function of reaction time at different agitation rates. Air flow rate was 0.38 L/min. Reactor was run at 130°C and 120 psig and was loaded with 0.489 mol *p*X, 0.888 mol *o*DCB, 2.222 mol H_2O, 0.00230 mol TBAB, 0.0175 mol KBr, and 0.00720 mol pentachlorobenzene: (●) 1600 rpm; (■) 2200 rpm.

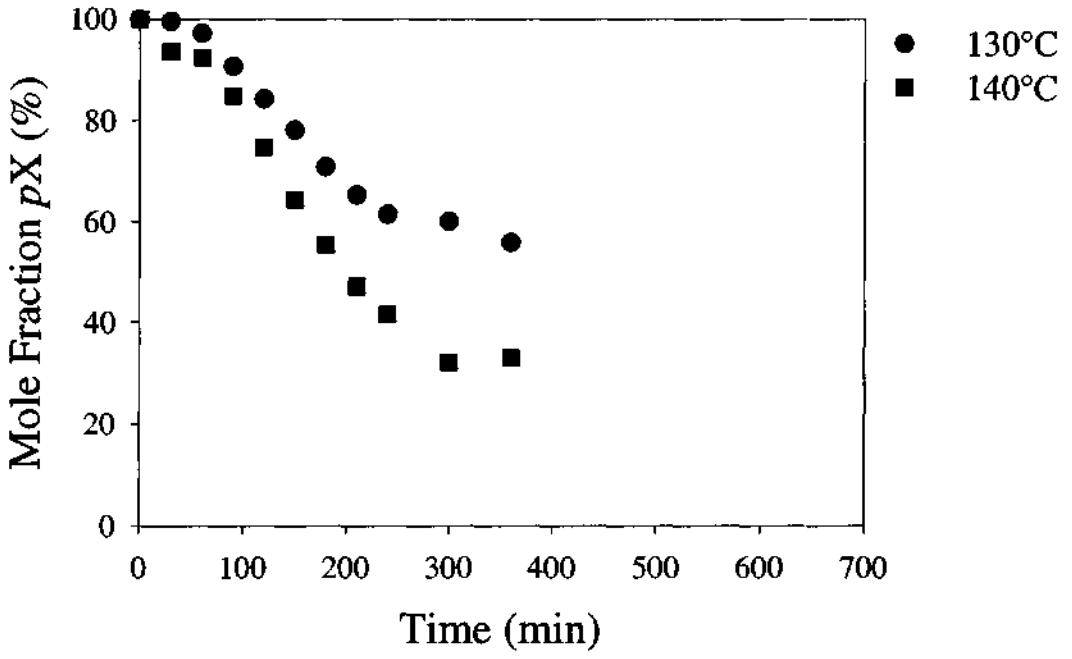

Figure 5-9. Mole fraction of *p*X in the product mixture as a function of reaction time at different temperatures. Air flow rate was 0.38 L/min. Reactor was run at 120 psig and agitated at 1600 rpm. It was loaded with 0.489 mol *p*X, 0.888 mol *o*DCB, 2.222 mol H_2O, 0.00230 mol TBAB, 0.0175 mol KBr, and 0.00720 mol pentachlorobenzene: (●) 130°C; (■) 140°C.

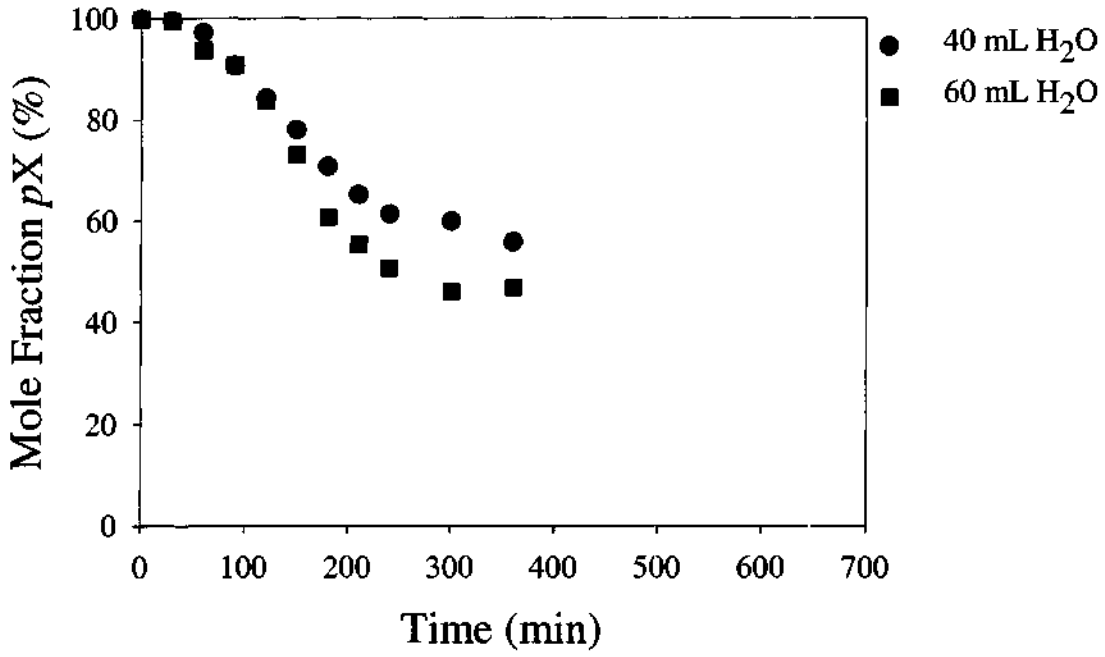

Figure 5-10. Mole fraction of *p*X in the product mixture as a function of reaction time with different organic phase : aqueous phase loadings. Air flow rate was 0.38 L/min. Reactor was run at 130°C and 120 psig and was agitated at 1600 rpm. It was loaded as follows: (●) 0.489 mol *p*X, 0.888 mol *o*DCB, 2.222 mol H_2O, 0.00230 mol TBAB, 0.0175 mol KBr, and 0.00720 mol pentachlorobenzene; (■) 0.428 mol *p*X, 0.777 mol *o*DCB, 3.333 mol H_2O, 0.00346 mol TBAB, 0.0262 mol KBr, and 0.00630 mol pentachlorobenzene.

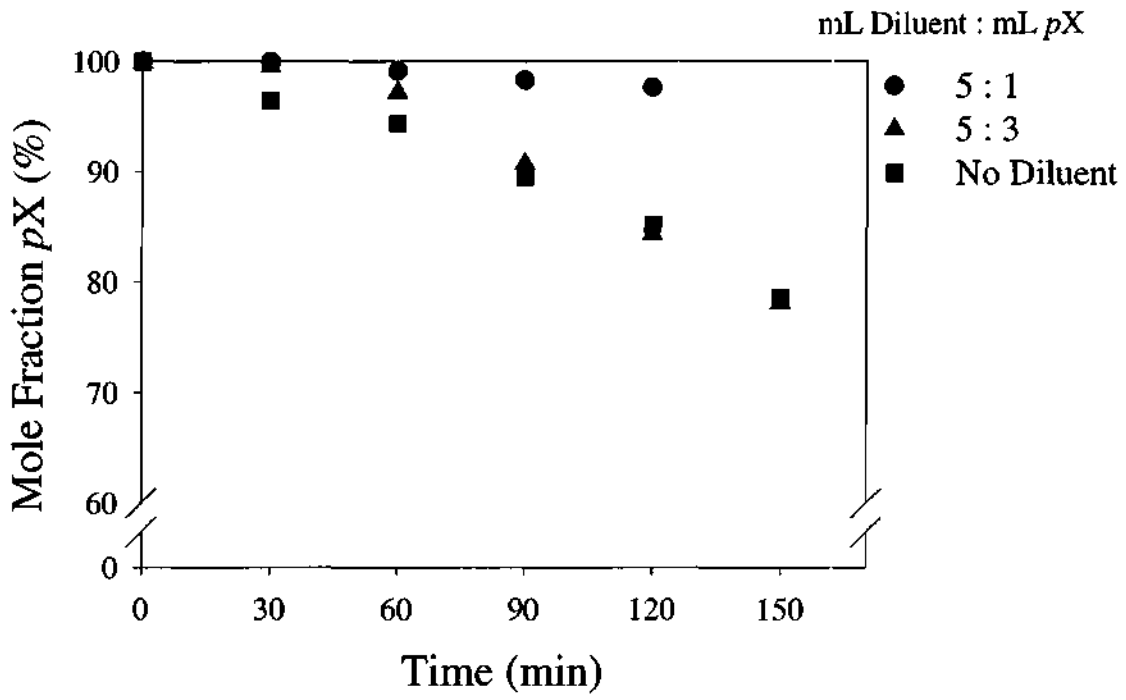

Figure 5-11. Mole fraction of *p*X in the product mixture as a function of reaction time with different diluent loadings. Air flow rate was 0.33 L/min. Reactor was run at 130°C and 120 psig and was agitated at 1600 rpm. It was loaded as follows: 2.222 mol H_2O, 0.00230 mol TBAB, 0.0175 mol KBr, 0.00720 mol pentachlorobenzene, and (●) 0.220 mol *p*X, 1.182 mol *o*DCB; (▲) 0.489 mol *p*X, 0.888 mol *o*DCB; (■) 1.305 mol *p*X.

As is predicted by the kinetic scheme outlined in Appendix E,

$$\text{rate} \propto [Q^+]^{1/2} [Br^-]^{1/2}.$$

Figure 5-12 shows the measured increase in rate with an increase in potassium bromide concentration. When the concentration of bromide anion was doubled, the rate, as measured by the linear part of the conversion versus time curve, increased by a factor of 1.36, which agrees with the predicted increase of $\sqrt{2}$. Figure 5-13 shows the measured increase in rate with an increase in tetrabutylammonium bromide concentration. When the concentration of phase-transfer catalyst was doubled, the rate increased by a factor of 1.42, again agreeing with the predicted increase of $\sqrt{2}$. The latter rate is slightly higher than the former because, when the concentration of TBAB is doubled, not only is the concentration of Q^+ doubled, but the concentration of Br^- increases by 12% under our conditions.

The type of phase-transfer catalyst also affected reaction rates. Figure 5-14 shows conversion of *p*X versus time for reactions run with tetraethylammonium bromide, tetrabutylammonium bromide, and tetrahexylammonium bromide. As expected, the tetraethylammonium bromide yielded very slow reaction. This quaternary ammonium salt is too hydrophilic; it does not partition adequately into the organic phase, and bromide transfer into this phase is limited. As the lengths of the alkyl chains increased, the partitioning into the organic phase also increased. The larger salts are better bromide

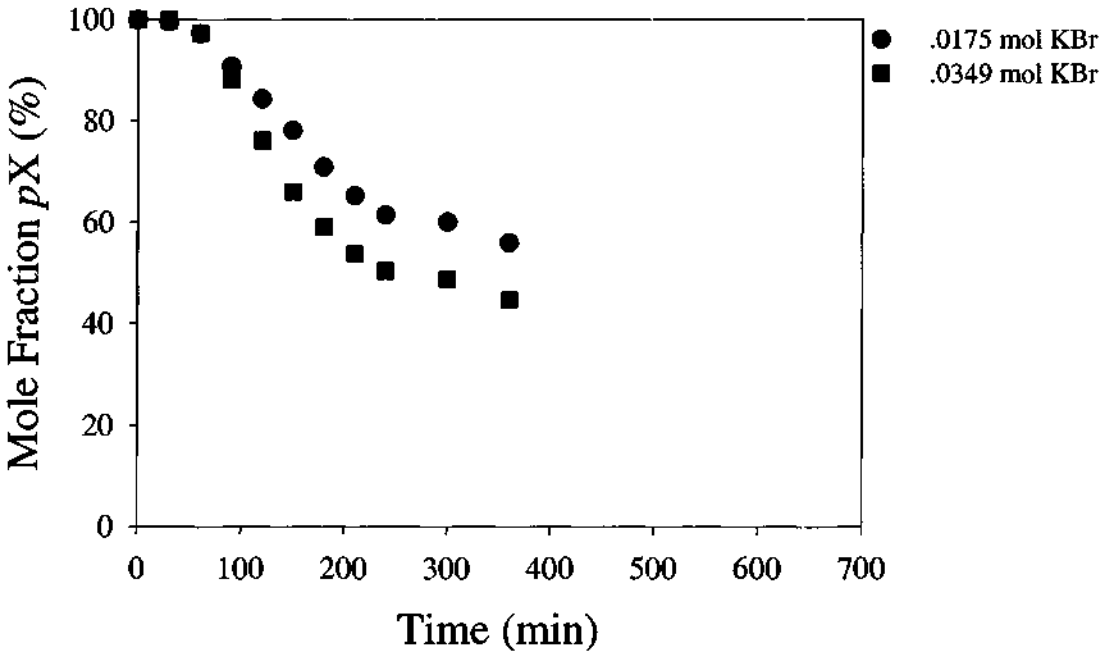

Figure 5-12. Mole fraction of pX in the product mixture as a function of reaction time with different KBr loadings. Air flow rate was 0.39 L/min. Reactor was run at 130°C and 120 psig and was agitated at 1600 rpm. It was loaded as follows: 0.489 mol *p*X, 0.888 mol *o*DCB, 2.222 mol H_2O, 0.00230 mol TBAB, 0.00720 mol pentachlorobenzene, and (●) 0.0175 mol KBr; (■) 0.0349 mol KBr.

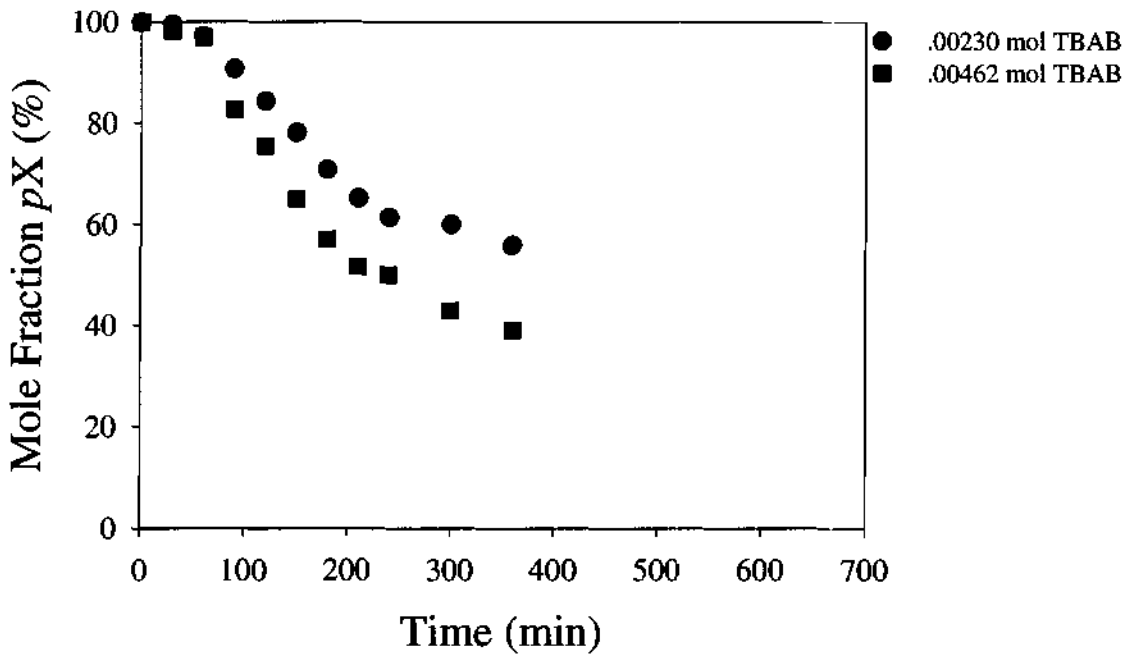

Figure 5-13. Mole fraction of *p*X in the product mixture as a function of reaction time with different TBAB loadings. Air flow rate was 0.38 L/min. Reactor was run at 130°C and 120 psig and was agitated at 1600 rpm. It was loaded as follows: 0.489 mol *p*X, 0.888 mol *o*DCB, 2.222 mol H_2O, 0.0175 mol KBr, 0.00720 mol pentachlorobenzene, and (●) 0.00230 mol TBAB; (■) 0.00462 mol TBAB.

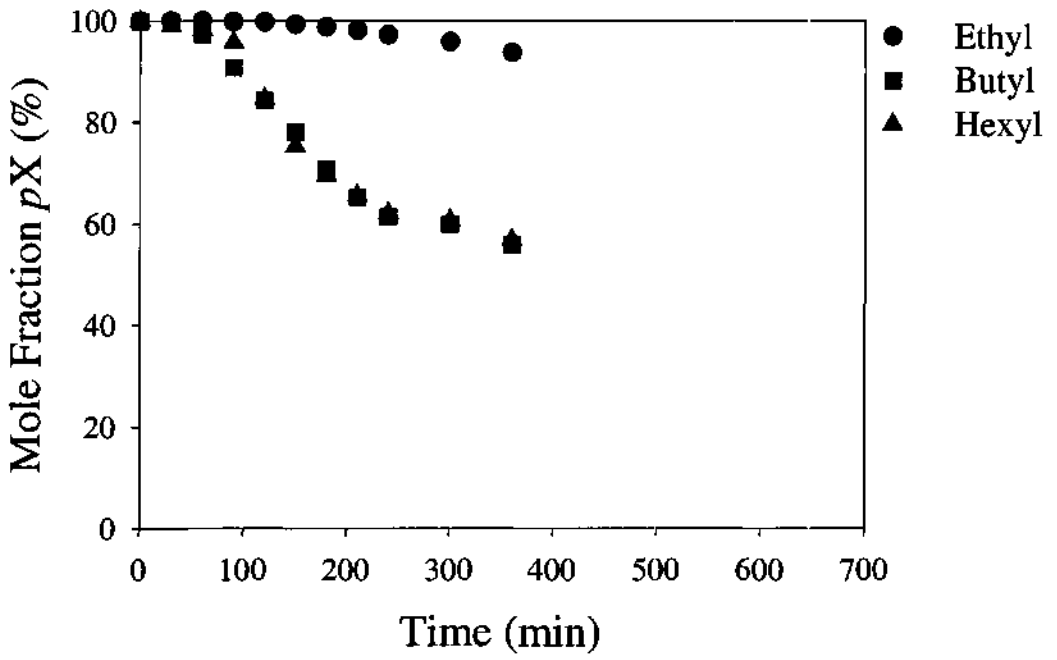

Figure 5-14. Mole fraction of *p*X in the product mixture as a function of reaction time with different tetraalkylammonium salts. Air flow rate was 0.38 L/min. Reactor was run at 130°C and 120 psig and was agitated at 1600 rpm. It was loaded as follows: 0.489 mol *p*X, 0.888 mol *o*DCB, 2.222 mol H_2O, 0.0175 mol KBr, 0.00720 mol pentachlorobenzene, and (●) .00230 mol tetraethylammonium bromide; (■) .00230 mol tetrabutylammonium bromide; (▲) .00230 mol tetrahexylammonium bromide.

shuttles. Because the rates are comparable for reactions run with the tetrahexyl catalyst and the tetrabutyl catalyst, the data shown in Figure 5-14 indicate that tetrabutylammonium bromide is sufficiently organophilic.

Because tetraalkylammonium salts are known to be of limited thermal stability at elevated temperature (Starks, et al., 1994), we designed several thermally stable phase-transfer catalysts (see Appendix C). Commercially available quaternary ammonium salts can decompose via two distinct mechanisms. They can undergo internal displacement to yield a trialkylamine and a displacement product, or, in a basic environment, they can undergo Hoffman elimination to yield a trialkylamine and an olefin (Starks et al., 1994; Dehmlow et al., 1977; Montanari and Tundo, 1982; Landini et al., 1986). Fortunately, both modes of decomposition involve attack on a β hydrogen. By designing catalysts with either no β hydrogen or sterically hindered β hydrogens, this decomposition can be prevented.

We synthesized and evaluated two thermally stable phase-transfer catalysts, *N*-2-ethylhexylquinolinium bromide (EHQB) and *N*-2-ethylhexylnicotinium bromide (EHNB). As is evident from Figure 5-15, both of these catalysts have only one β hydrogen, and this hydrogen is sterically protected in both cases. Unfortunately, neither catalyst encouraged oxidation (Figures 5-16 and 5-17). No detectable reaction occurred with either catalyst, while reaction did occur, although slowly, when no phase-transfer catalyst was present. Upon further evaluation of these catalysts, they were found to

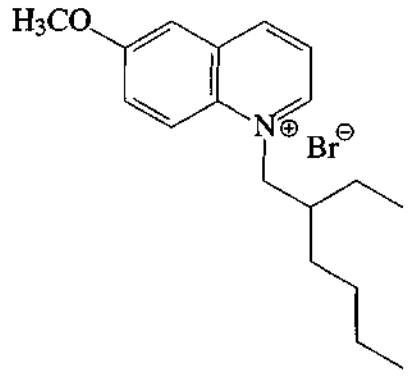

EHQB

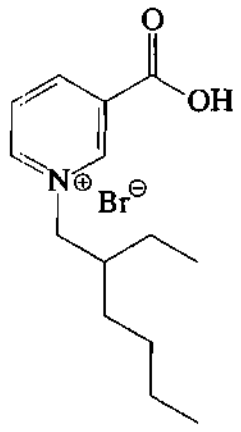

EHNB

Figure 5-15. Thermodynamically stable PTCs.

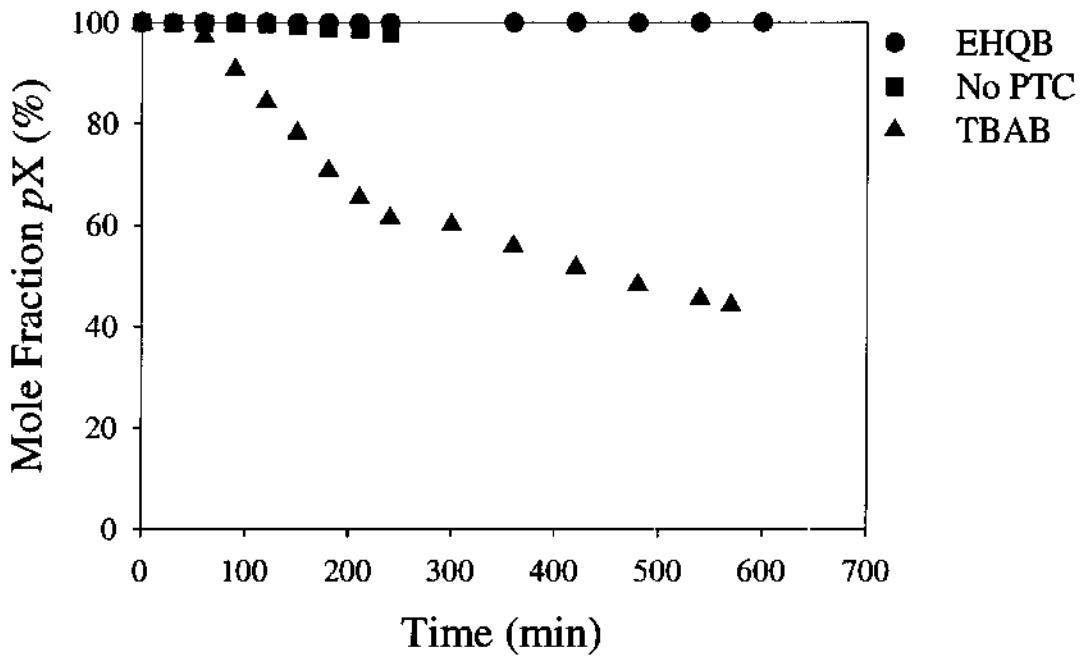

Figure 5-16. Mole fraction of *p*X in the product mixture as a function of reaction time with different PTCs. Air flow rate was 0.38 L/min. Reactor was run at 130°C and 120 psig and was agitated at 1600 rpm. It was loaded as follows: 0.489 mol *p*X, 0.888 mol *o*DCB, 2.222 mol H_2O, 0.0175 mol KBr, 0.00720 mol pentachlorobenzene, and (●) .00230 mol *N*-2-ethylhexylquinolinium bromide; (■) no PTC; (▲) .00230 mol tetrahexylammonium bromide.

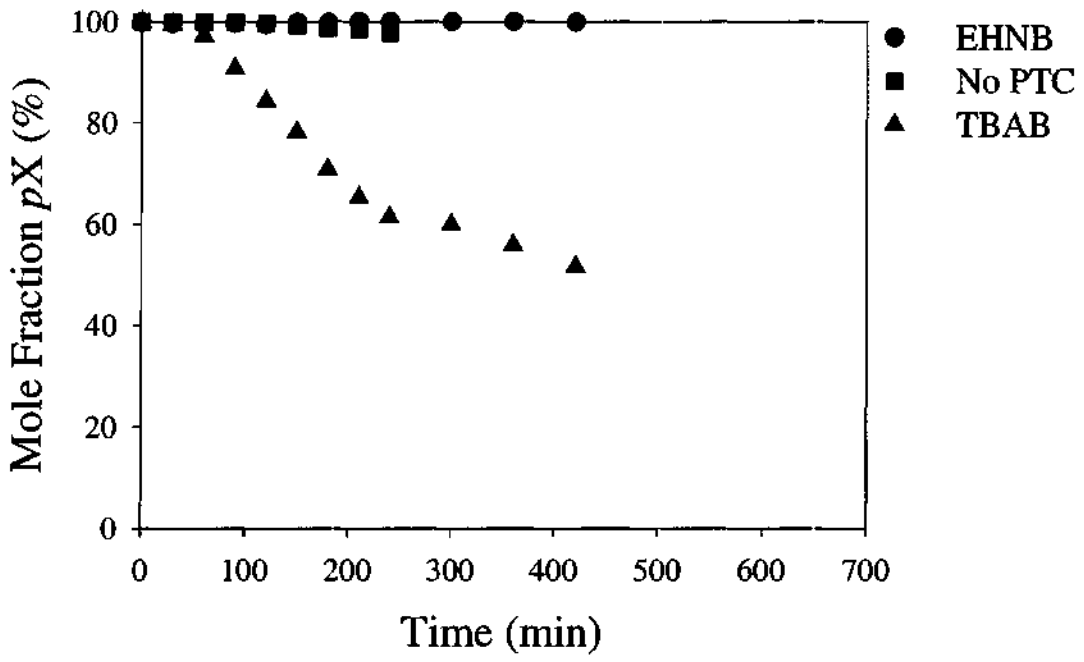

Figure 5-17. Mole fraction of *p*X in the product mixture as a function of reaction time with different PTCs. Air flow rate was 0.38 L/min. Reactor was run at 130°C and 120 psig and was agitated at 1600 rpm. It was loaded as follows: 0.489 mol *p*X, 0.888 mol *o*DCB, 2.222 mol H_2O, 0.0175 mol KBr, 0.00720 mol pentachlorobenzene, and (●) .00230 mol inner salt of *N*-2-ethylhexylnicotinium bromide and .00230 mol HBr; (■) no PTC; (▲) .00230 mol tetrahexylammonium bromide.

contain no bromide ion. We postulate that, because bromide is a better leaving group than mesylate, the anion exchange did not occur. Further work would be required to assess the possibility of oxidizing *p*X with either EHQB or EHNB.

Because an earlier batch reaction run with pure oxygen indicated that cobalt(II)acetate tetrahydrate would dramatically increase oxidation rates, several experiments were run with added cobalt. When running semi-batch with air, rate enhancements due to cobalt(II)acetate tetrahydrate were negligible (Figure 5-18). When $CoBr_2$ was added, the rate increased slightly, but this is likely due to the increase in the bromide concentration, rather than the addition of cobalt.

While the reaction proceeded further in the semi-batch system than it did batchwise, conversions still leveled off before equilibrium was reached. Initially, this was believed to be due to catalyst decomposition. Reactions were run where, after the one-hour heat-up period, the reactor was maintained at temperature for three additional hours before air was introduced and oxidation commenced. The additional time at elevated temperature did not affect the reaction (Figure 5-19), which indicated that catalyst decomposition was not the sole cause of the leveling off. Additionally, reactions were run where the reactor was loaded with the composition attained after 300 minutes of reaction under standard conditions. These reactions proceeded as the standard reactions did when concentrations were the same (Figure 5-20). The time spent at 130°C was not causing the slowing in conversion; instead, the compounds present in the reactor were the culprit. In an attempt to boost the free radical concentration, cumene hydroperoxide was

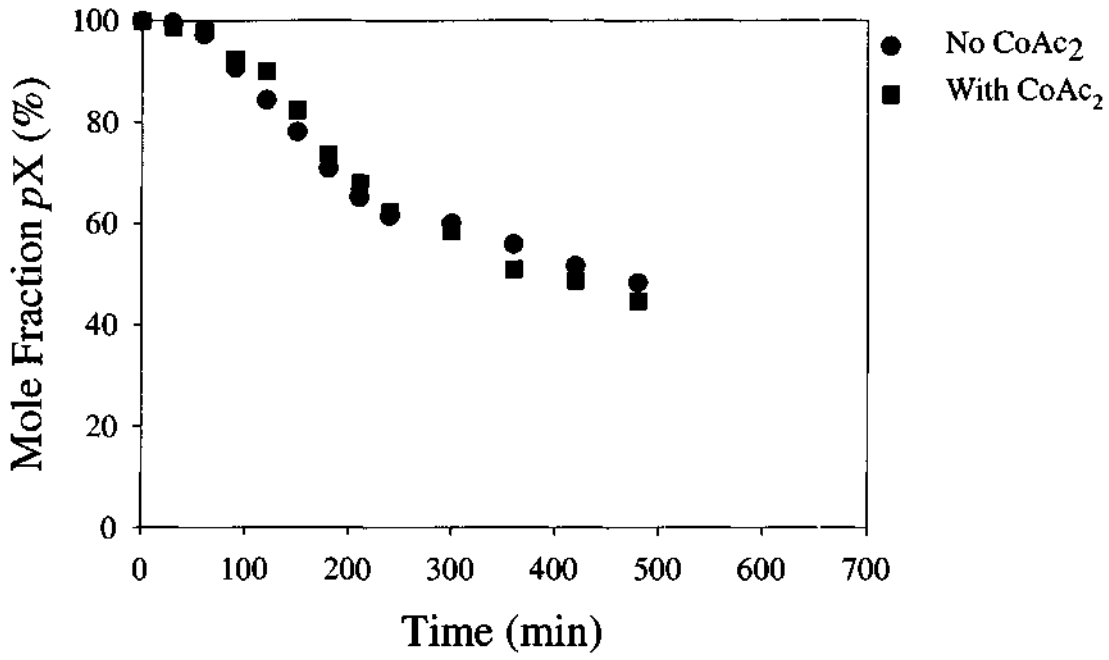

Figure 5-18. Mole fraction of *p*X in the product mixture as a function of reaction time with and without added cobalt. Air flow rate was 0.38 L/min. Reactor was run at 130°C and 120 psig and was agitated at 1600 rpm. It was loaded as follows: 0.489 mol *p*X, 0.888 mol *o*DCB, 2.222 mol H_2O, .00230 mol TBAB, 0.0175 mol KBr, 0.00720 mol pentachlorobenzene, and (●) no cobalt; (■) .00230 mol cobalt(II) acetate tetrahydrate and 0.9 ml acetic acid.

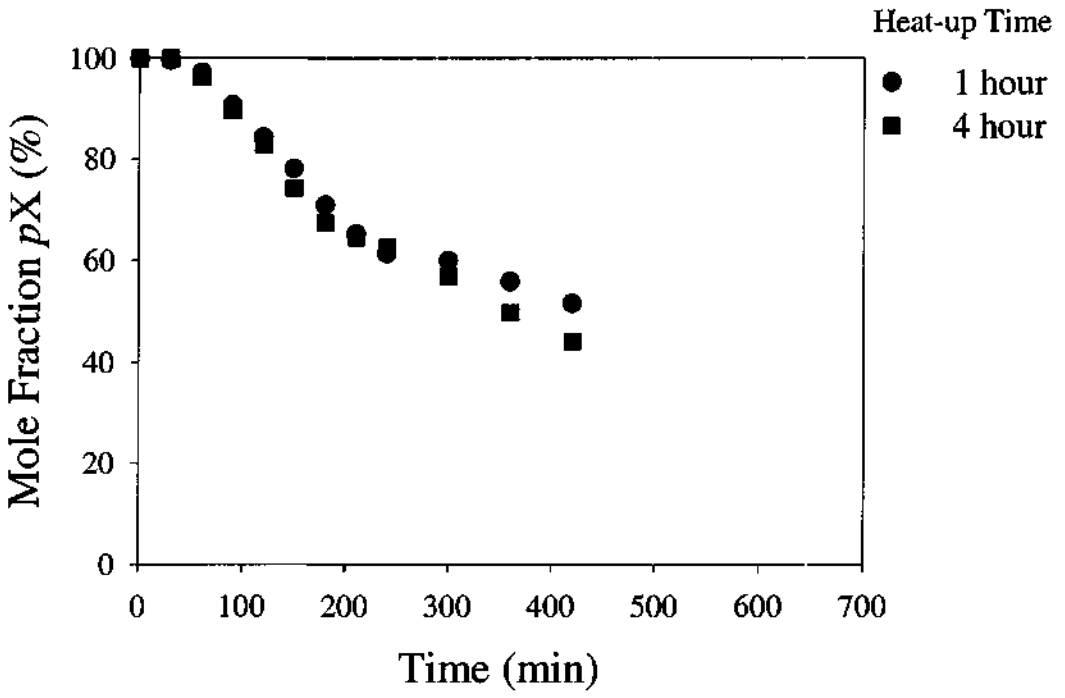

Figure 5-19. Mole fraction of *p*X in the product mixture as a function of reaction time at different temperatures. Air flow rate was 0.38 L/min. Reactor was run at 130°C and 120 psig, and it was agitated at 1600 rpm. It was loaded with 0.489 mol *p*X, 0.888 mol *o*DCB, 2.222 mol H_2O, 0.00230 mol TBAB, 0.0175 mol KBr, and 0.00720 mol pentachlorobenzene. Time to heat-up before introduction of air was: (●) 1 hour; (■) 4 hours.

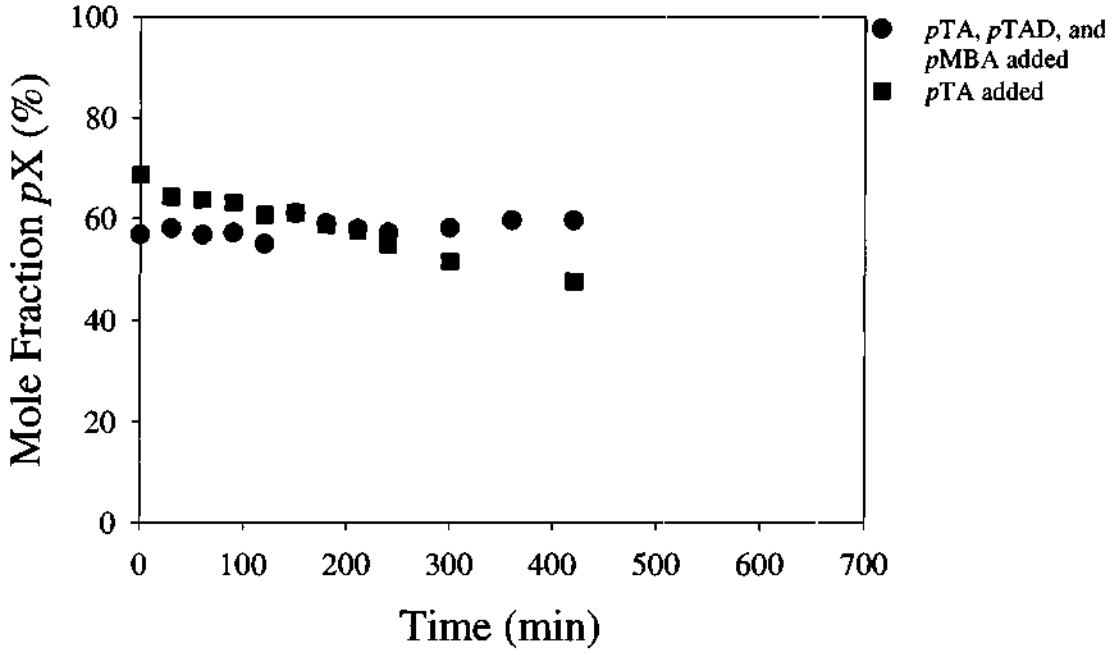

Figure 5-20. Mole fraction of *p*X in the product mixture as a function of reaction time with different reactor loadings. Air flow rate was 0.38 L/min. Reactor was run at 130°C and 120 psig, and it was agitated at 1600 rpm. It was loaded with 0.294 mol *p*X, 0.888 mol *o*DCB, 2.222 mol H_2O, 0.00230 mol TBAB, 0.0175 mol KBr, 0.00720 mol pentachlorobenzene, and (●) 0.132 mol *p*TA, 0.0376 mol *p*TAD, 0.0248 mol *p*MBA; (■) 0.196 mol *p*TA.

added to a reactor loaded with the composition attained after 300 minutes of reaction under standard conditions. The rate of pX oxidation did not change significantly (Figure 5-21). An additional experiment was performed, where the reactor was loaded with *p*X, *p*TA, water, TBAB, and KBr. Again, the reaction proceeded only very slowly (Figure 5-20). It was hypothesized that our product, *p*TA, was inhibiting the reaction. One experiment was run with added NaOH, attempting to extract the *p*TA out of the organic phase. The NaOH lengthened the observable initiation period, and it did not appear to prevent the levelling off (Figure 5-22).

Binuclear products, such as anthraquinone-2,6-dicarboxylic acid, anthraquinone-2,7-dicarboxylic acid, fluorenone-3,6-dicarboxylic acid, fluorenone-2,6-dicarboxylic acid, and fluorenone-2,7-dicarboxylic acid are known to be formed during the oxidation of *p*X. These products are colored, and their inclusion decreases the quality of TA. We developed synthesis procedures for these compounds, which are given in Appendix C.

Conclusions

The phase-transfer catalyzed oxidation of *p*-xylene occurs with tetraalkylammonium salt catalysts in the absence of transition metal compounds. Without further optimization of reaction conditions and reactant concentrations, conversion levels achieved 40% in 10 hours at 130°C and 120 psig. Reaction rates and conversions could be increased by increasing temperature, concentration of phase-transfer catalyst, or concentration of bromide catalyst. The structure of the phase-transfer

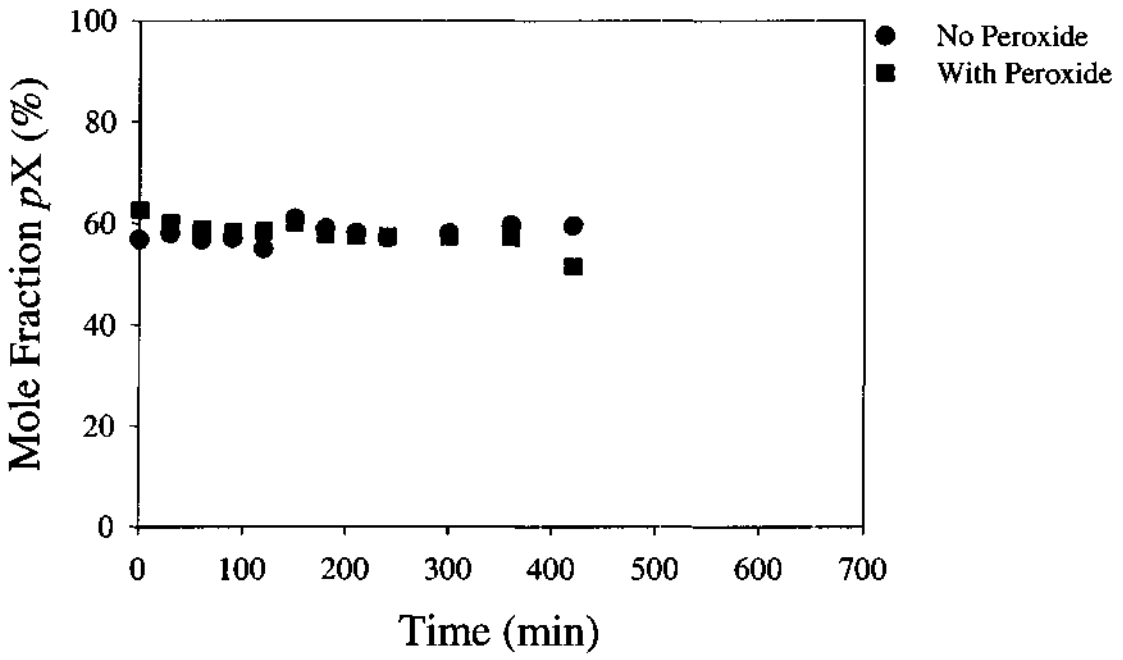

Figure 5-21. Mole fraction of *p*X in the product mixture as a function of reaction time with different reactor loadings. Air flow rate was 0.38 L/min. Reactor was run at 130°C and 120 psig, and it was agitated at 1600 rpm. It was loaded with 0.294 mol *p*X, 0.132 mol *p*TA, 0.0376 mol *p*TAD, 0.0248 mol *p*MBA, 0.888 mol *o*DCB, 2.222 mol H_2O, 0.00230 mol TBAB, 0.0175 mol KBr, 0.00720 mol pentachlorobenzene, and (●) no peroxide; (■) 0.0832 mol cumene hydroperoxide.

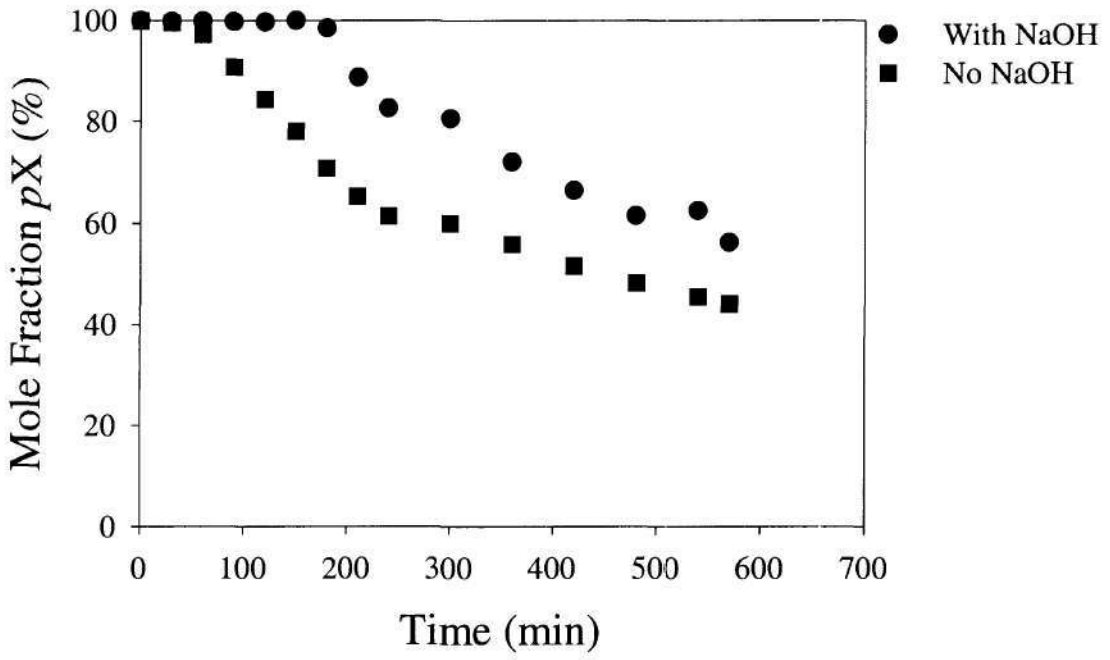

Figure 5-22. Mole fraction of *p*X in the product mixture as a function of reaction time at different temperatures. Air flow rate was 0.38 L/min. Reactor was run at 130°C and 120 psig, and it was agitated at 1600 rpm. It was loaded with 0.489 mol *p*X, 0.888 mol *o*DCB, 2.222 mol H_2O, 0.00230 mol TBAB, 0.0175 mol KBr, 0.00720 mol pentachlorobenzene, and (●) 0.00224 mol NaOH; (■) no base.

catalyst also affected reaction rates, with more organophilic PTCs yielding faster reactions. Some novel, thermally stable PTCs were designed, but their synthesis was flawed. These salts still offer promise for the low temperature, phase-transfer catalyzed oxidation of *p*-xylene, where water is the only solvent.

References

Dakka, J.; El Garbia, B.; Zoran, A.; Sasson, Y. US Patent 4, 853, 479; August 01, 1989; assigned to Gadot Petrochemical Industries, Ltd. and Yissum R&D Company of the Hebrew University of Jerusalem.

Dehmlow, E. V.; Slopianka, M.; Heider, J. Phase Transfer Catalysis in Strongly Alkaline Media: Notes on the Extractability of Hydroxy Ions and on the Stability of Catalysts. *Tetrahedron Letters* **1977**, *27*, 2361-2364.

Fischer, R.W.; Röhrscheid, F. Oxidation of Alkyl-Substituted Aromatic Compounds with Air. In *Applied Homogeneous Catalysis with Organometallic Compounds*; Cornils, B.; Herrmann, W.A., (Eds.); vol. 1, pp. 439-464, Verlag Chemie, Weinheim: New York, 1996.

Haruštiak, M.; Hronec, M.; Ilavský, J. Phase-Transfer Oxidations of Hydrocarbons by Molecular Oxygen in the Absence of Metals. *React. Kinet. Catal. Lett.* **1988**, *37*, 215-220.

Haruštiak, M.; Hronec, M.; Ilavský, J. Kinetics and Mechanism of Phase-Transfer Catalyzed Oxidation of p-Xylene by Molecular Oxygen. *J. Mol. Catal.* **1988**, *48*, 335-342.

Haruštiak, M.; Hronec, M.; Ilavský, J. Kinetics and Mechnism of Cobalt Bromide Catalyzed Oxidation of p-Xylene in the Presence of Phase-Transfer Catalysts. *J. Mol. Catal.* **1989**, *53*, 209-217.

Haruštiak, M.; Hronec, M.; Ilavský, J. The Use of Phase-Transfer Catalysis for the Initiation of p-Xylene Oxidation. *React. Kinet. Catal. Lett.* **1985**, *27*, 231-233.

Landini, D.; Maia, A.; Rampoldi, A. Stability of Quaternary Onium Salts under Phase Transfer Conditions in the Presence of Aqueous Alkaline Solutions. *J. Org. Chem.* **1986**, *51*, 3187-3191.

Montanari, F.; Tundo, P. Hydroxymethyl Derivatives of 18-Crown-6 and [2.2.2] Cryptand: Versatile Intermediates for the Synthesis of Lipophilic and Polymer-bonded Macrocyclic Ligands. *J. Org. Chem.* **1982**, *47*, 1298-1302.

Ngan, F.; Toofan, M. Modification of Preparation of Diazomethane for Methyl Esterification of Environmental Samples Analysis by Gas Chromatography. *J. Chrom. Sci.* **1991**, *29*, 8-10.

Nowicki, N.R.; Lowry, Jr., J.D. US Patent 4, 892, 970; January 09, 1990; assigned to Amoco Corporation, Chicago, Ill.

Partenheimer, W. Methodology and Scope of Metal Bromide Autoxidation of Hydrocarbons. *Catal. Today* **1995,** *23*, 69-158.

Starks, C.M.; Liotta, C.L.; Halpern, M. *Phase-Transfer Catalysis: Fundamentals, Applications, and Industrial Perspectives*; Chapman & Hall: New York, 1994.

Weber, W. and Gokel, G. *Phase Transfer Catalysis in Organic Synthesis*; Springer-Verlag: Berlin, 1977.

Weissermel, K.; Arpe, H.J. *Industrial Organic Chemistry, 3rd ed.*; Verlag Chemie: New York, 1997.

CHAPTER VI

RECOMMENDATIONS

The investigations in this thesis indicate that alternative reaction systems, which include supercritical and nearcritical fluid solvents and phase-transfer catalysts, offer enormous potential for running commercial reactions in a more sustainable fashion. Supercritical dimethyl ether was used to produce and isolate an intermediate in a series reaction. Nearcritical water was used as a solvent that, because of its high dissociation constant, simultaneously acts as a catalyst. Reactions catalyzed by nearcritical water do not require catalyst neutralization and subsequent salt disposal, and separations for reactions run in nearcritical water can be achieved simply by cooling the product mixture. Phase-transfer catalysis with water as the solvent was also investigated as an alternative reaction system for an oxidation reaction. Because the work presented in this thesis appears so promising, further work is suggested for the reactions studied herein. Also, several new avenues of investigation, which appear promising in light of the previously described work, are suggested.

Reactions in Nearcritical Water

Thermal Copolymerization in Nearcritical Water

As exhibited in Chapter IV, polymerization of 1,3-pentadiene occurred in the absence of water at 300°C. It appears that temperature alone is sufficient to initiate polymerization, suggesting the possibility of running copolymerizations in a nearcritical water solvent. Oxygen as an element in a monomer can inhibit traditional Lewis acid catalysis, precluding the incorporation of monomers like vinyl acetate and propyl vinyl ether into polymer resins.

It is proposed that thermal polymerization be investigated as a means of incorporating these oxygen-containing monomers into polymer resins through copolymerization. Nearcritical water would be a benign solvent for these copolymerizations, and solvent separation would be easily accomplished by simply cooling the reaction mixture.

Reaction kinetics could be measured using a series of batch reactors loaded into an aluminum heating block, as in the experiments outlined in Chapter IV. Oxygen content of the copolymer could be measured by IR, and molecular weight distributions could be determined by GPC and SEC.

Hydrolysis of Halogenated Aromatics in Nearcritical Water

The hydrolyses of substituted benzoic acid esters and anisoles outlined in Chapter III confirm that nearcritical water is capable of catalyzing these reactions which typically

require additional acid or base. The dissociation constant of water between 250 and 300°C is high enough to initiate these reactions. It is hypothesized that halogenated aromatics, such as PCBs, can also be hydrolyzed in nearcritical water (Figure 6-1).

Because of the carcinogenic properties of chlorinated aromatics, a safe and cost-effective method for their destruction is imperative. Incineration has been used for the destruction of chlorinated hydrocarbons, but the gaseous byproducts render this method unacceptable. Recently, several investigators have focused on supercritical water oxidation (SCWO) as a means of halogenated waste elimination. Houser and Liu (1996) measured the product distributions for the oxidations of 1-chloro-3-phenylpropane, 2-chlorotoluene, and 4-chlorophenol in supercritical water. Marrone et al. (1998a; 1998b) studied the hydrolysis of methylene chloride to formaldehyde and hydrochloric acid in nearcritical water; subsequent oxidation of formaldehyde in supercritical water led to the complete oxidation to carbon dioxide and hydrogen. Bunte et al. (1994) investigated the simultaneous hydrolysis and oxidation of hexachlorocyclohexane in aqueous NaOH solutions, both above and below the critical temperature of water. They found that, for reactions run in the nearcritical region, 50% of the Cl-content was ionic after 2 hours. Their results were the same for reactions run with both 1:1 and 1:2 hexachlorocyclohexane to NaOH. Catalyst-free reactions were not reported.

Reaction conditions are quite corrosive in supercritical water, and reactors must be able to withstand extreme temperatures and pressures. Capital costs are high because exotic metallurgy is required and the reactors must hold high pressures. While

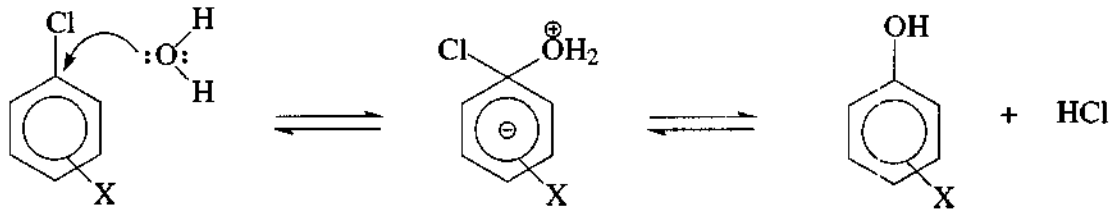

Figure 6-1. Hydrolysis of substituted chlorobenzenes in nearcritical water.

nearcritical water with halogenated organics is also quite corrosive, the necessary temperature and pressure ratings are much lower than those required for a supercritical water system. The capital costs for a reactor are significantly lower, making it a more likely replacement solvent for commercial processes. In addition to the nearcritical hydrolyses reported by Marrone et al. (1998a; 1998b), Jeffers et al. (1989) and Jeffers and Wolfe (1996) have measured kinetics of hydrolyses of several halogenated alkanes in water from 0 to 180°C. While there is a significant body of work encompassing the destruction of chlorinated waste in hot water, there are no kinetic measurements for the hydrolysis of halogenated aromatics in nearcritical water. A kinetic study of the hydrolysis of a series of halogenated aromatics is proposed. Reactions could be run batchwise in titanium tube reactors, and analysis could be done with GC-FID and GC-MS. Hammett analysis would permit the extraction of many hydrolysis rate constants from only a few measured data sets. It is predicted that highly chlorinated aromatics will hydrolyze quickly because electron withdrawing groups should activate the aromatic ring (Figure 6-1).

Hydrolysis of Polyacrylonitrile in Nearcritical Water

The polarity of the nitrile groups of polyacrylonitrile (PAN) holds these chains in a lattice (Figure 6-2), giving this polymer the ability to form strong fibers. Because this carbon-nitrogen association is so strong, the polymer does not act as a thermoplastic; the polymer degrades before these interactions are broken. The partial hydrolysis of these

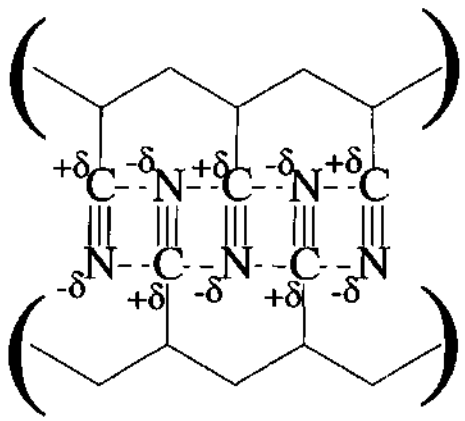

Figure 6-2. Intermolecular chain association in polyacrylonitrile.

nitrile groups could result in a polymer with properties intermediate between those of PAN and polyacrylic acid, a common absorbent. These properties would likely be tunable with the degree of hydrolysis.

Previous work done by this group indicates that nicotinonitrile hydrolyzes rapidly to nicotinic acid in nearcritical water at 250°C (Hallett, personal communication). The success of this hydrolysis indicates that PAN should also hydrolyze in nearcritical water. It is suggested that the kinetics of this hydrolysis be studied by loading several series of titanium reactors with PAN and water and then placing them in an aluminum heating block for varying time periods. Analysis for oxygen content of the product could be accomplished with IR spectroscopy.

Oxidation of *p*-Xylene in Nearcritical Water

As explained in Chapter V, the oxidation of *p*-xylene to terephthalic acid (Figure 5-1) is currently carried out in acetic acid at elevated temperature and pressure. This harsh solvent is required to solubilize both the organic reactant and the catalyst salt. While the dielectric constant of nearcritical water is low enough for organics and oxygen to be quite soluble, it remains high enough to allow salt dissolution (Uematsu and Franck, 1980; Kuhlmann et al., 1994). This oxidation could be run homogeneously in water between 250 and 300°C. Solvent separation would be achieved by simply cooling the reaction mixture.

The kinetics of this oxidation could be measured in a semi-batch reactor, where oxygen flows through the reactor. These reactions must be run dilute in *p*-xylene to

prevent oxygen transfer from limiting the reaction rate, as well as to ensure that there is a single liquid phase. *p*-Xylene is 0.3% soluble in water at 250°C (Pryor and Jentoft, 1961). Analysis could be done by a combination of GC-FID and GC-MS.

Phase-Transfer Catalyzed Oxidation of *p*-Xylene

While degradation of tetraalkylammonium salts was not evident in the phase-transfer catalytic oxidation experiments reported in Chapter V, it is a well-documented phenomenon (Landini et al., 1986; Starks et al., 1994); it would likely prove important in a commercial process, where catalyst charging results in significant down-time. These phase-transfer catalysts can degrade via either in an internal nucleophilic displacement reaction or a Hofmann elimination reaction (Figure 6-3). At moderate temperatures, and especially in a basic environment, Hofmann elimination is a much more significant source of catalyst decomposition (Starks et al., 1994). Because Hofmann elimination is initiated by the deprotonation of an α-carbon, more thermally stable catalysts can be designed by either introducing steric hindrance to these protons or by reducing the number of α-CH bonds.

Two thermally stable phase-transfer catalysts were designed for the low-temperature oxidation of *p*-xylene, *N*-2-ethylhexylquinolinium bromide (EHQB) and *N*-2-ethylhexylnicotinium bromide (EHNB). Each of these catalysts contains only one β-hydrogen (Figure 6-4), making Hofmann degradation quite slow. The synthesis of these catalysts was attempted, as described in Appendix C. Reactions run with the products of

a) $R_4N + A^- \longrightarrow R_3N + R{-}A$

b) 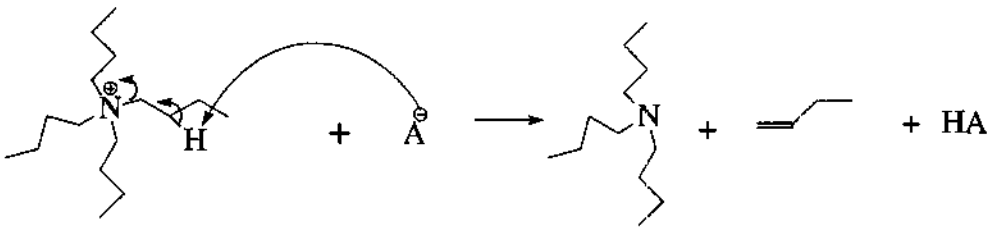

Figure 6-3. a) Internal nucleophilic displacement and b) Hofmann elimination mechanisms for the degradation of tetraalkylammonium salts.

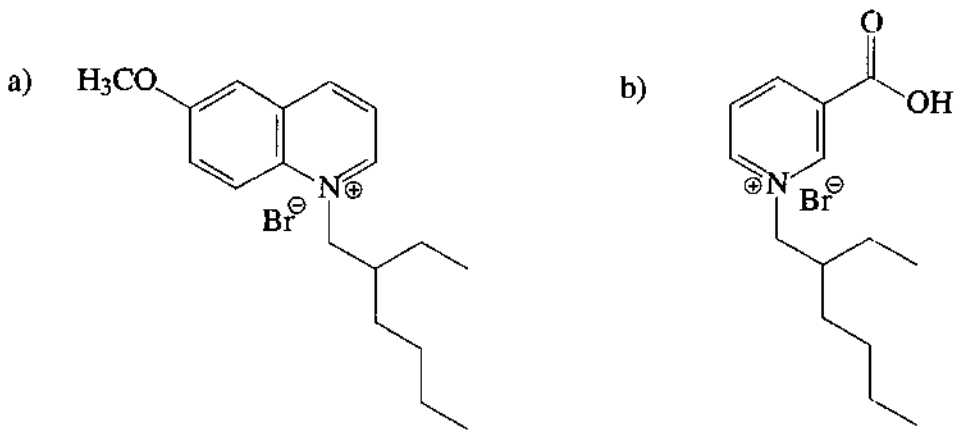

Figure 6-4. Thermally stable phase-transfer catalysts:
a) *N*-2-ethylhexylquinolinium bromide (EHQB) and
b) *N*-2-ethylhexylnicotinium bromide (EHNB).

these syntheses actually ran more slowly than reactions run without any phase-transfer catalyst. Further analysis of the EHQB indicated that there was not any bromide ion on our product. It is hypothesized that, because mesylate is such a poor leaving group, the anion exchange never occurred. While simply washing the mesylate salt with NaBr did not produce the desired exchange, this exchange could likely be accomplished with an ion exchange resin. *N*-Butylpyridinium tosylate has been converted to *N*-butylpyridinium chloride by running the tosylate salt through an ion exchange column (BioRad, AG1-X8 Resin Chloride form, 100 – 200 mesh). Exchange was confirmed with a positive flame test (Culp and Griffith, personal communication).

It is recommended that the catalyst synthesis procedures be amended to include running the previously synthesized salts through an ion exchange resin, so that the desired bromide catalysts are produced. These catalysts are predicted to effectively transfer bromide ion into the organic phase, where oxidation of *p*-xylene can occur. If the kinetics with these salts are favorable, the thermal stability of these catalysts could make the phase-transfer catalytic process an economically viable, more environmentally benign process for the synthesis of terephthalic acid.

References

Bunte, G.; Eisenreich, N.; Hirth, T.; Krause, H. Hydrolysis and Oxidation of Hexachlorocyclohexane in Sub- and Supercritical Water. *Proceedings. International Symposium on Supercritical Fluids.* **1994**, 201 – 206.

Culp, C.; Griffith, K. Personal Communication, 1999.

Hallett, J. Personal Communication, 2000.

Houser, T.J.; Liu, X. Reactions of 1-Chloro-3-phenylpropane, 2-Chlorotoluene, and 4-Chlorophenol in Supercritical Water. *J. Supercric. Fluids.* **1996**, *9*, 167–171.

Jeffers, P.M.; Ward, L.M.; Woytowitch, L.M.; Wolfe, N.L. Homogeneous Hydrolysis Rate Constants for Selected Chlorinated Methanes, Ethanes, Ethenes, and Propanes. *Environ. Sci. Technol.* **1989**, *23*, 965-969.

Jeffers, P.M.; Wolfe, N.L. Homogeneous Hydrolysis Rate Constants – Part II: Additions, Corrections and Halogen Effects. *Environ. Toxicol. Chem.* **1996**, *15*, 1066-1070.

Kuhlmann, B.; Arnett, E.M.; Siskin, M. Classical Organic Reactions in Pure Superheated Water. *J. Org. Chem.* **1994**, *59*, 3098-3101.

Landini, D.; Maia, A.; Rampoldi, A. Stability of Quaternary Onium Salts under Phase-Transfer Conditions in the Presence of Aqueous Alkaline Solution. *J. Org. Chem.* **1986**, *51*, 3187-3191.

Marrone, P.A.; Gschwend, P.M.; Swallow, K.C.; Peters, W.A.; Tester, J.W. Product Distribution and Reaction Pathways for Methylene Chloride Hydrolysis and Oxidation under Hydrothermal Conditions. *J. Supercrit. Fluids.* **1998**, *12*, 239–254.

Marrone, P.A.; Arias, T.A.; Peters, W.A.; Tester, J.W. Solvation Effects on Kinetics of Methylene Chloride Reactions in Sub- and Supercritical Water: Theory, Experiment, and Ab Initio Calculations. *J. Phys. Chem. A* **1998**, *102*, 7013 - 7028.

Pryor, W.A.; Jentoft, R.E. Solubility of *m*- and *p*-Xylene in Water and in Aqueous Ammonia from 0°C to 300°C. *J. Chem Eng. Data* **1961**, *6*, 36-37.

Starks, C.M.; Liotta, C.L.; Halpern, M. *Phase-Transfer Catalysis: Fundamentals, Applications, and Industrial Perspectives*; Chapman & Hall: New York, 1994.

Uematsu, M.; Franck, E.U. Static Dielectric Constant of Water and Steam. *J. Phys. Chem. Ref. Data* **1980**, *9*, 1291-1306.

APPENDIX A

SYNTHESIS OF NOVEL, THERMALLY STABLE QUATERNARY AMMONIUM SALT CATALYSTS FOR MHET SYNTHESIS

Eleven quaternary ammonium salt catalysts were synthesized, characterized and tested, along with some commercially available compounds. All starting materials were purchased from Aldrich Chemical Company, unless otherwise noted. NMR spectra were taken with a Varian Gemini 300, IR spectra were taken with a Nicolet 520 FT-IR spectrometer, and CHN elemental analyses were sent to Atlantic Microlab, Inc., Norcross, GA.

N-(2-Ethylhexyl)-4-(dimethylamino)pyridinium chloride (EHPC)

A mixture of 4.0952 g of 2-ethylhexyl mesylate, 1.8682 g of 4-(diethylamino)pyridine, and 25 ml of dry toluene was flushed with argon, brought to reflux, and allowed to stir for 3 hours. The solution was allowed to cool to room temperature, and the solvent was removed via rotary evaporation. The resulting residue was dissolved in 50 ml of methylene chloride and washed with 50 ml of saturated sodium chloride three times for 3 minutes each. The aqueous layers were combined and extracted with 50 ml of methylene chloride. The organic layers were combined and dried over magnesium sulfate. The solvent was again removed with rotary evaporation, and the resulting residue was recrystallized from methylene chloride/diethyl ether to give 3.54

g of white crystals (88%) with a melting point of 191-192°C. Calculated for $C_{15}H_{27}N_2Cl$: C, 66.5197; H, 10.0476; N, 10.3430. Found: C, 61.29; H, 9.59; N, 9.57. ^1H NMR ($CDCl_3$, 300 MHz): δ 0.85 (m, 6H), 1.21 (m, 8H), 1.80 (m, 1H), 3.25 (s, 6H), 4.12 (d, 2H), 7.10 (d, 2H, aromatic), 8.38 (d, 2H, aromatic).

N-(2-Ethylhexyl)-4-(dimethylamino)pyridinium bromide (EHPB)

The same procedure was used as for the chloride analog, except the crude product was washed with saturated sodium bromide, as opposed to sodium chloride, and gave 83%. Calculated for $C_{15}H_{27}N_2Br$: C, 57.1416; H, 8.6310; N, 8.8848. Found: C, 56.99; H, 8.65; N, 8.75. ^1H NMR ($CDCl_3$, 300 MHz): δ 0.88 (m, 6H), 1.28 (m, 8H), 1.85 (m, 1H), 4.19 (d, 2H), 7.10 (d, 2H, aromatic), 8.39 (d, 2H, aromatic).

N-(2-Ethylhexyl)-4-(dimethylamino)pyridinium iodide (EHPI)

The same procedure was used as for the chloride analog, except the crude product was washed with saturated sodium iodide, as opposed to sodium chloride, and gave yellow crystals (71%). ^1H NMR ($CDCl_3$, 300 MHz): δ 0.88 (m, 6H), 1.28 (m, 8H), 1.85 (m, 1H), 4.15 (d, 2H), 7.08 (d, 2H, aromatic), 8.30 (d, 2H, aromatic).

N-(2-Ethylhexyl)-4-(dimethylamino)pyridinium thiocyanate (EHPT)

The same procedure was used as for the chloride analog, except the crude product was washed with saturated sodium thiocyanate, as opposed to sodium chloride, and gave

a viscous orange oil (96%). ^{1}H NMR ($CDCl_3$, 300 MHz): δ 0.88 (m, 6H), 1.28 (m, 8H), 1.85 (m, 1H), 4.15 (d, 2H), 7.08 (d, 2H, aromatic), 8.20 (d, 2H, aromatic).

N-Benzyl-(*N*,*N*-dimethylamino)pyridinium chloride (BPC)

A mixture of 4.9227 g of (*N*,*N*-dimethylamino)pyridine. 4.63 ml of benzyl chloride, and approximately 10 ml toluene was added to a clean, dry 25 ml round-bottom flask fitted with a stir bar, a condenser, and a drying tube. The reaction flask was then lowered into an oil bath at 80°C and stirred. The solution was initially completely miscible and then became a white solid after 5 minutes. The reaction was allowed to proceed overnight and was then cooled to room temperature. The toluene was removed via rotary evaporation, and the resulting solid was recrystallized in ethanol/ether to give 7.9804 g (79.8%). Calculated for $C_{14}H_{17}N_2Cl$: C, 67.5983; H, 6.8880; N, 11.2615. Found: C, 66.34; H, 7.01; N, 11.06. ^{1}H NMR (D_2O, 300 MHz): δ 2.95 (s, 6H), 5.10 (s, 2H), 6.62 (d, 2H), 7.22 (m, 5H), 7.85 (d, 2H). Melting point: 257-258°C.

N-*p*-Chlorobenzyl-(*N*,*N*-dimethylamino)pyridinium chloride (CBPC)

A mixture of 1.1313 g of *p*-chlorobenzyl chloride, 0.8623 g of (*N*,*N*-dimethylamino)-pyridine, and approximately 10 ml of toluene was added to a clean, dry 50 ml round-bottom flask equipped with a stir bar, a condenser, and a drying tube. The reaction apparatus was then lowered into an oil bath at 110°C. The solution immediately became miscible, and, after 5 minutes, a thick white precipitate formed. The reaction was allowed to continue overnight, and, after 12 hours, was cooled to room temperature. The

solvent was removed via rotary evaporation. The resulting solid was recrystallized from ethanol/diethyl ether to give 1.790 g (89.5%). Calculated for $C_{14}H_{16}N_2Cl_2$: C, 59.3765; H, 5.6944; N, 9.8917. Found: C, 57.63; H, 5.88; N, 9.59. ^{1}H NMR (D_2O, 300 MHz): δ 3.02 (s, 6H), 5.15 (s, 2H), 6.71 (d, 2H), 7.18 (d, 2H), 7.30 (d, 2H), 7.90 (d, 2H). Melting point: 208-210°C.

N-*p*-Nitrobenzyl-(*N*,*N*-dimethylamino)pyridinium chloride (NBPC)

To a 50 ml round bottom flask equipped with a stir bar, a condenser, and a drying tube was added 2.923 g of *p*-nitrobenzyl chloride, 2.078 g of (*N*,*N*-dimethyamino)pyridine, and approximately 10 ml of toluene. The reaction flask was lowered into an oil bath at 80°C and stirred. After about 10 minutes, a white precipitate formed. After four hours, the reaction flask was cooled to room temperature, and the solvent was removed via rotary evaporation. The resulting solid was recrystallized from methanol/2-propanol to give 4.055 g (81.1%) of pale yellow crystals. ^{1}H NMR ($CDCl_3$, 300 MHz): δ 3.20 (s, 6H), 6.05 (s, 2H), 6.88 (d, 2H), 7.92 (d, 2H), 8.15 (d, 2H), 9.02 (d, 2H). Melting point: 239°C (decomposition).

N-*p*-Nitrobenzyl-(*N*,*N*-dimethylamino)pyridinium bromide (NBPB)

To a clean dry 100 ml round-bottom flask fitted with a stir bar, a condenser, and a drying tube was added 1.4065 g of *p*-nitrobenzyl bromide, 0.7233 g of (*N*,*N*-dimethylamino)pyridine, and 40 ml of toluene. This mixture was heated to 93°C and stirred overnight (avoided refluxing due to violent degradation of *p*-nitrobenzyl bromide).

Toluene was removed via rotary evaporation, and the resulting solid was recrystallized from ethanol/ether to give 1.79 g (89.5%) of pale yellow crystals. Calculated for $C_{14}H_{16}N_3O_2Br$: C, 49.720; H, 4.768; N, 12.425. Found: C, 49.67; H, 4.75; N, 12.37. ^1H NMR (D_2O, 300 MHz): δ 3.25 (s, 6H), 6.02 (s, 2H), 6.76 (d, 2H), 7.80(d, 2H), 8.22 (d, 2H), 8.80 (d, 2H). Melting point: 283°C (decomposition).

N-*p*-Methoxybenzyl-(*N*,*N*-dimethylamino)pyridinium chloride (MBPC)

To a clean dry 50 ml round-bottom flask equipped with a stir bar, a condenser, and a drying tube was added 0.8768 g of (*N*,*N*-dimethylamino)pyridine and 0.97 ml of *p*-methoxybenzyl chloride. The reaction flask was then lowered into an oil bath at 100°C and stirred for 30 minutes. A white precipitate formed after 5 minutes. The crude solid was recrystallized from ethanol/ether to give 1.7181 g (86%) of white crystals. Calculated for $C_{15}H_{19}N_2OCl$: C, 64.2557; H, 6.8299; N, 9.9910. Found: C, 61.75; H, 6.97; N, 9.59. ^1H NMR ($CDCl_3$, 300 MHz): δ 3.21(s, 6H), 3.78 (s, 3H), 5.57 (s, 2H), 6.90(m, 4H), 7.50(d, 2H), 8.71 (d, 2H). Melting point: 166-167°C.

Xylylbis[*N*,*N*-[(*N*,*N*-dimethylamino)pyridinium]] dichloride (XPDC)

To a clean, dry 25 ml round-bottom flask fitted with a stir bar, a condenser, and a drying tube was added 1.7265 g of (*N*,*N*-dimethylamino)pyridine, 1.1776 g of dichloroxylene, and about 10 ml of toluene. The reaction flask was then lowered into an oil bath at about 100°C and stirred overnight. The reaction flask was then cooled, and the solvent was removed via rotary evaporation. The resulting solid was then recrystallized

from ethanol/ether to give 1.80 g of white crystals (64%). Calculated for $C_{22}H_{28}N_4Cl_2$: C, 63.0054; H, 6.7290; N, 13.3589. Found: C, 61.69; H, 6.79; N, 13.03. ^{1}H NMR (D_2O, 300 MHz): δ 3.00 (s, 6H), 5.16 (s, 2H), 6.66(d, 4H), 7.22(m, 4H), 8.85 (d, 4H). Melting point: 310°C (decomposition).

Bis(tetrabutyl)ammonium terephthalate ($TBTA_t$)

To a clean, dry 500 ml round-bottom flask equipped with a stir bar, a Dean-Starke adapter, a condenser, a drying tube, and a nitrogen inlet was added 10.0 ml of a 40 wt% aqueous solution of tetrabutylammonium hydroxide, 1.2801 g of terephthalic acid, 100 ml of ethanol, and 150 ml of benzene. The apparatus was lowered into an oil bath and heated to reflux for 6 hours. The azeotrope distilled at 64.9°C, and water was removed overnight. The reaction flask was cooled to room temperature, and the solvent was removed via rotary evaporation. A sample of the crude product was shown to be very soluble in water, and an NMR was taken which showed the absence of terephthalic acid. The wax-like solid was recrystallized from ethanol/ether to give 3.9104 g of white crystals (78%). Calculated for $C_{40}H_{76}N_2O_4$: C, 740219; H, 11.8019; N, 4.3161. Found: C, 69.16; H, 11.74; N, 4.02. ^{1}H NMR ($CDCl_3$, 300 MHz): δ 0.92(t, 24H), 1.30-1.50 (mm, 32H), 3.10 (t, 16H), 8.00 (m, 4H). Melting point: 135-137°C.

APPENDIX B

KINETIC ANALYSIS OF ESTER AND ANISOLE HYDROLYSES

Kinetic Analysis of Ester Hydrolysis

The reaction scheme assumed for the hydrolysis of benzoate esters is given in Figure B-1. If x is the molar extent of the first reaction, y is the molar extent of the second reaction, and z is the molar extent of the third reaction, the rate equation for this hydrolysis via an autocatalytic $A_{AC}2$ mechanism (Figure B-2) is

$$dx/dt = k[\text{Ester}][H_2O][H^+]. \qquad \text{(B-1)}$$

Writing Equation B-1 in terms of molar extents of reaction gives

$$dx/dt = k[E_o - x][W_o - x - z][y + z], \qquad \text{(B-2)}$$

where E_o is the initial concentration of ester and W_o is the initial concentration of water. Rearranging Equation B-2 and integrating gives

$$\int_0^x dx/\{[E_o - x][W_o - x - z][y + z]\} = k\int_0^t dt. \qquad \text{(B-3)}$$

K_c, the equilibrium constant for the acid dissociation at 250°C, was found in the literature and is defined in Equation B-4. K_w, the dissociation constant for water at 250°C, was also found in the literature and is defined in Equation B-5.

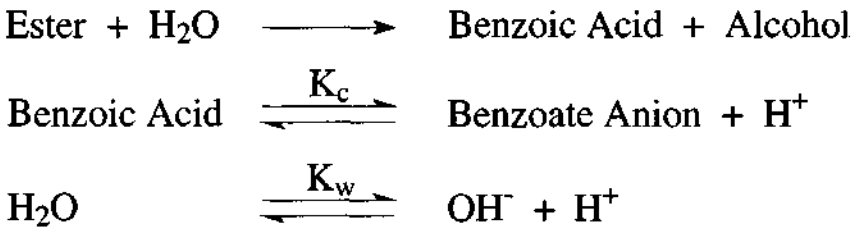

Figure B-1. Reaction scheme for hydrolysis of benzoic acid esters.

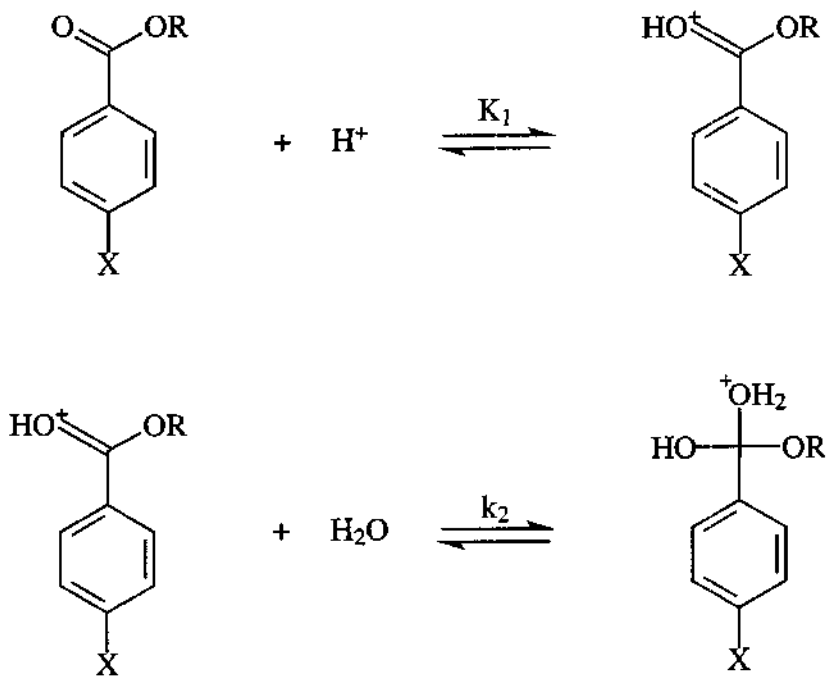

Figure B-2. First steps of $A_{AC}2$ mechanism for acid-catalyzed ester hydrolysis.

$$K_c = \frac{[\text{Benzoate Anion}][H^+]}{[\text{Benzoic Acid}]} = \frac{(y)(y+z)}{(x-y)} \qquad \text{(B-4)}$$

$$K_w = \frac{[OH^-][H^+]}{[H_2O]} = \frac{(y)(y+z)}{(Wo-x-z)} \qquad \text{(B-5)}$$

The integral on the left side of Equation B-3 was evaluated numerically for each measured conversion, using known values for E_o, W_o, K_c, and K_w. In a plot of this integral versus time (Figure B-3), the slope gives the rate constant, k, in $L^2/mol^2/hr$. k is the product of K_1, the equilibrium constant for the protonation of the ester, and k_2, the rate constant for the rate-limiting addition of water to the protonated ester. We assumed that the effect of substituents on the equilibrium constant for ester protonation is the same as that for acid dissoication. Rate constants were reported as products of K_1*, the equilibrium constant for the protonation of non-substituted ester, and k_2.

Kinetic Analysis of Anisole Hydrolysis

After the rigorous data analysis performed for the hydrolysis of esters, two assumptions were made for the analysis of anisole hydrolyses. First, the dissociation of water was assumed to have a negligible effect on the concentration of water. Second, because conversion versus time data did not yield S-shaped curves, the dissociation of phenol was hypothesized to have a negligible effect on the proton concentration. One run was analyzed where the only assumption was that the water concentration was constant. For this run, the rate constant obtained when the dissociation of phenol was included in the calculation of the proton concentration was the same as that obtained when the proton

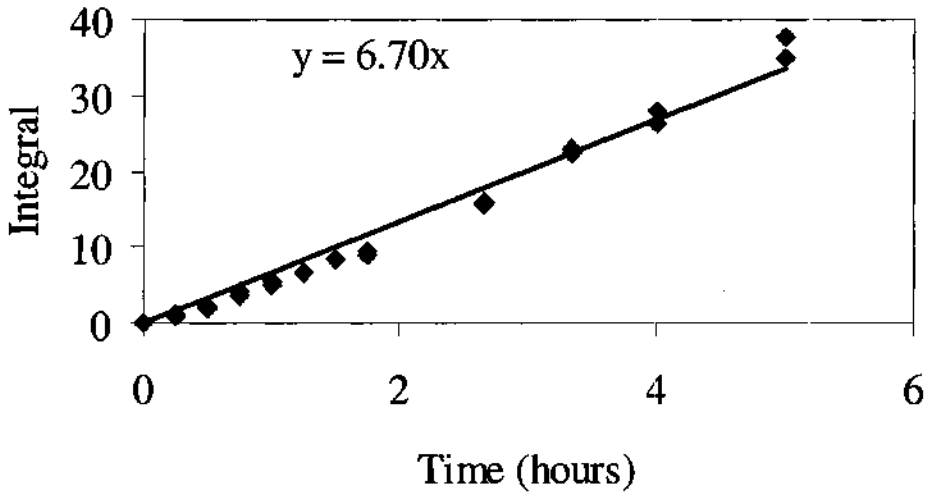

Figure B-3. Numerical integration of conversion versus time data yields the rate constant for the hydrolysis of isobutyl benzoate at 250°C in $L^2/mol^2/hr$.

concentration was calculated only from the dissociation of water. This result confirmed the hypothesis that the dissociation of phenol had a negligible effect on the proton concentration for these hydrolyses.

As explained in Chapter 3, hydrolyses of substituted anisoles and the hydrolysis of phenetole indicate that the acid-catalyzed pathway is negligible in the hydrolysis of anisole in nearcritical water. The reaction rate can be written as in Equation B-6 (Figure

$$dx/dt = k_1[\text{Anisole}][H_2O] + k_2[\text{Anisole}][OH^-] \qquad \text{(B-6)}$$

3-11), where k_1 is the rate constant for the S_N2 nucleophilic attack by water, and k_2 is the rate constant for the base-catalyzed reaction. To determine the relative importance of each of these mechanisms, anisole was hydrolyzed in water with 0.041M KOH. Because the reaction ran about 20 times faster with the KOH than it did under neutral conditions, the first term on the right side of Equation B-6 was assumed to be negligible for this

$$dx/dt = k_2[\text{Anisole}][OH^-] \quad \text{(B-7)}$$

reaction. This set of data was analyzed using Equation B-7, where the concentration of hydroxide was the sum of that formed from the dissociation of water and that formed from the dissociation of KOH. The KOH was assumed to dissociate completely under these conditions. The integrated rate expression for Equation 3-4 yielded a k_2 of 1.49 ± 0.14 L/mol/hr.

Once k_2 was known, hydrolyses run without any additional base could be analyzed with Equation B-8, where x represents the molar extent of reaction and A_o represents the initial concentration of anisole.

$$dx/dt = k_1[A_o - x][H_2O] + k_2[A_o - x]\{\frac{[H_2O]K_w}{[H^+]}\} \quad \text{(B-8)}$$

Rearranging and integrating Equation B-8 gives Equation B-9. The slope of a plot of

$$\ln\frac{(A_o - x)}{A_o} = -(k_1 + \frac{(k_2)(K_w)}{[H^+]})[H_2O]t \quad \text{(B-9)}$$

$\ln (A_o - x) / A_o$ versus time yields k_1 (Figure B-4).

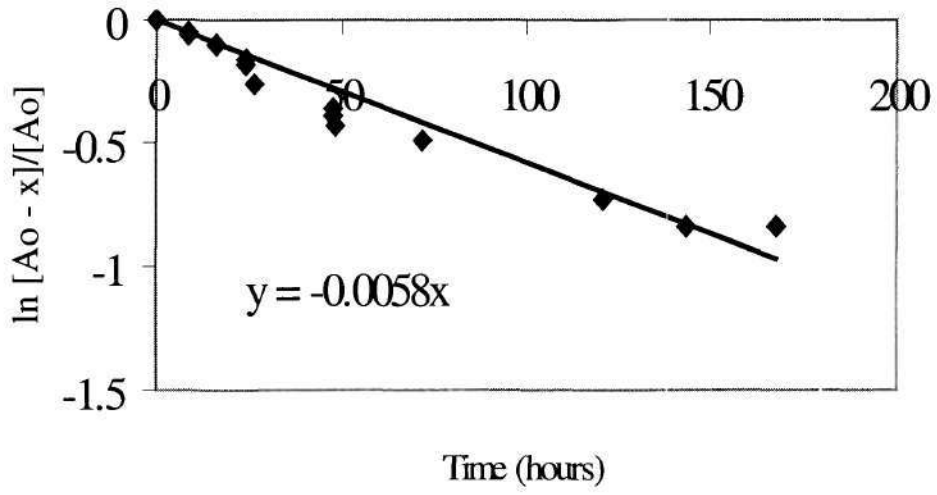

Figure B-4. Pseudo-first order kinetics yields the rate constant for the hydrolysis of anisole at 300°C in L/mol/hr.

APPENDIX C

SYNTHESIS OF BINUCLEAR, AROMATIC BYPRODUCTS AND NOVEL, THERMALLY STABLE QUATERNARY AMMONIUM SALT CATALYSTS FOR PTC OXIDATION OF P-XYLENE

Synthesis of Binuclear, Aromatic Byproducts

The following binuclear byproducts are expected to be formed during the oxidation of *p*X to *p*TA and TA. These products are colored, and would therefore decrease the quality of TA. Procedures are provided to synthesize these compounds.

Synthesis of Anthraquinone-2,7-Dicarboxylic Acid

Anthraquinone-2,7-dicarboxylic acid, a gray solid, was synthesized as shown in Figure C-1. To a 1000 mL steel autoclave, 85.0 g (0.23 mol) of *p*-benzoquinone, 159.8 g (0.69 mol) of isoprene, 13.1 g (0.07 mol) of hydroquinone, and 136 ml of absolute ethanol were added. The reactor was closed and heated to 130°C for 6 hrs. After cooling to room temperature, the formed crystals were filtered off and washed with cool ethanol and petroleum ether. The solvent was evaporated from the filtrate until crystallization of the 2,7-dimethylanthraquinone began. 93.3 g of crystals (2,7-isomer) was obtained (Yield: 83%).

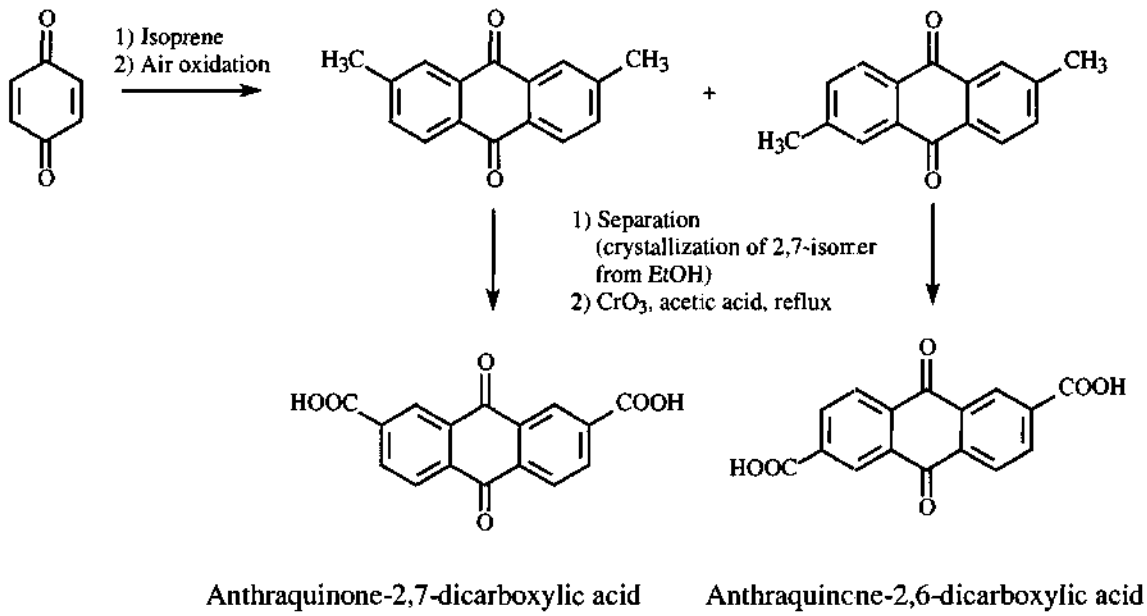

Anthraquinone-2,7-dicarboxylic acid Anthraquinone-2,6-dicarboxylic acid

Figure C-1. Synthesis of anthraquinone-2,7-dicarboxylic acid and anthraquinone-2,6-dicarboxylic acid.

A 500 ml three-necked flask was charged with 2.36 g (0.01 mol) of 2,7-dimethylanthraquinone and 150 ml of acetic acid. The flask was cooled in an ice bath, and 2 ml of concentrated sulfuric acid, 10 ml of acetic anhydride, and 10 g (0.1mol) of CrO_3 were added very slowly. The mixture was stirred at 20°C for 1 hour, at room temperature (below 35°C) for an additional 2 hours, and finally the mixture was heated to 130°C for 3 hrs. The mixture was allowed to cool down under stirring overnight. The contents of the flask were poured into 100 ml of cold water, and the crude solid was filtered, dissolved in 1M NaOH solution, filtered from solid impurities, and precipitated with concentrated aqueous HCl. This purification method was repeated three times. 2.8 g of pure anthraquinone-2,7-dicarboxylic acid was obtained as pale green crystals (Yield: 95%).

Synthesis of Anthraquinone-2,6-Dicarboxylic Acid

Anthraquinone-2,6-dicarboxylic acid, a pale green solid, was synthesized as explained in the procedure given above (Figure C-1).

Synthesis of Fluorenone-3,6-Dicarboxylic Acid

Fluorenone-3,6-dicarboxylic acid, a pale green solid, was synthesized as shown in Figure C-2. 1 g of 4,4'-dimethylbenzil was ground very well with 1 g of anhydrous $AlCl_3$, and the mixture was placed in a test tube with $CaCl_2$. The mixture was then heated in an oil bath to 120°C for 2 hrs. The resulting dark melt was decomposed

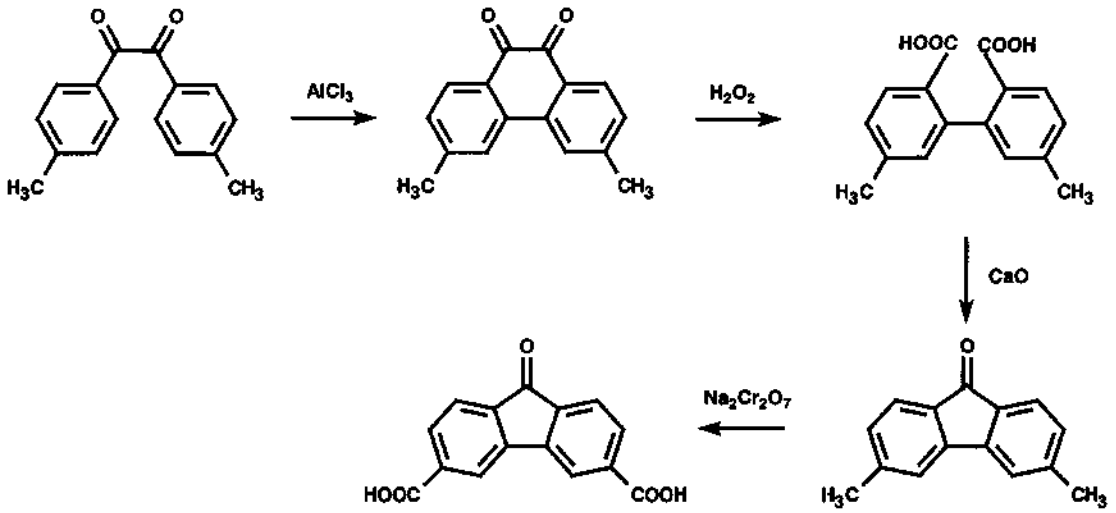

Figure C-2. Synthesis of fluorenone-3,6-dicarboxylic acid.

with diluted HCl and extracted with acetic acid. The acetic acid solution was diluted with water, upon which a precipitate formed which was extracted with cold Et_2O. The evaporation residue of the ether extract was extracted at 50-60°C with technical hydrogen sulfite solution, to which alcohol was added (1/6 of its volume). A brown precipitate was obtained by addition of aqueous HCl to the sulfite solution, which was recrystallized from ethanol. 3,6-dimethylphenanthren-9,10-dione was obtained as orange needles (0.1 g; m.p. = 219-220°C).

4 g of 3,6-dimethylphenanthren-9,10-dione was refluxed in 30 ml of acetic acid, and it was heated gradually with 24ml of perhydroxyl. The reaction went to completion after 3.5 hrs. The next day, 2.2 g of 5,5'dimethyl-dibenzoic acid crystallized as yellow, shiny leaflets (m.p. = 268 – 270°C). The acid was recrystallized from a large amount of water.

2 g of 5,5'dimethyl-dibenzoic acid was mixed with 4.8 g of lime (CaO), and the mixture was transferred into a thick-walled, open-ended glass ampule, which was annealed while CO_2 was passed over. A red oil, which solidified immediately, was obtained. The oil was washed with its ether solution and a NaOH solution, and the evaporation residue was recrystallized twice with petroleum ether. Gold shiny leaflets of 3,6-dimethylfluorenone were obtained (m.p. = 116 – 117°C).

Finally, 3,6-dimethylfluorenone was oxidized to fluorenone-3,6-dicarboxylic acid with sodium dichromate in an aqueous solution while being heating to 250°C.

Synthesis of Fluorenone-2,7-Dicarboxylic Acid

Fluorenone-2,7-dicarboxylic acid, a pale yellow solid, was synthesized as shown in Figure C-3. Aluminum chloride (44 g), suspended in dry 1,2-dichloroethane (50 ml), was stirred and treated dropwise at 0°C with acetic anhydride (17.5 g). The resulting solution was then added, while being stirred at 0°C, to a solution of fluorene (12.5 g) in 1,2-dichloroethane (70 ml). When the addition was complete, half of the solvent was distilled out, and the residue was poured into aqueous 2M HCl. The resulting solid was collected by filtration, washed with hot water, dried, and recrystallized from acetone. 2,7-diacetylfluorene was obtained as pale green needle-like crystals (16.2 g) (Yield: 86.2 %).

2,7-Diacetylfluorene (7.0 g, 0.028 mol) was added to a solution of sodium hydroxide (1.5 g) in 4.5% aqueous sodium hypochlorite (350 ml) with stirring. The mixture was heated to 80°C for 5 hrs. It was then cooled and filtered. The solid was treated with hot water (100 ml) and filtered to remove unreacted 2,7-diacetylfluorene. The filtrate was washed twice with dichloromethane and then acidified with concentrated hydrochloric acid. The resulting pale yellow precipitate was filtered, washed with water, and dried to give 4.2 g of pure fluorenone-2,7-dicarboxylic acid (m.p. > 300°C, decomp; Yield 56 %).

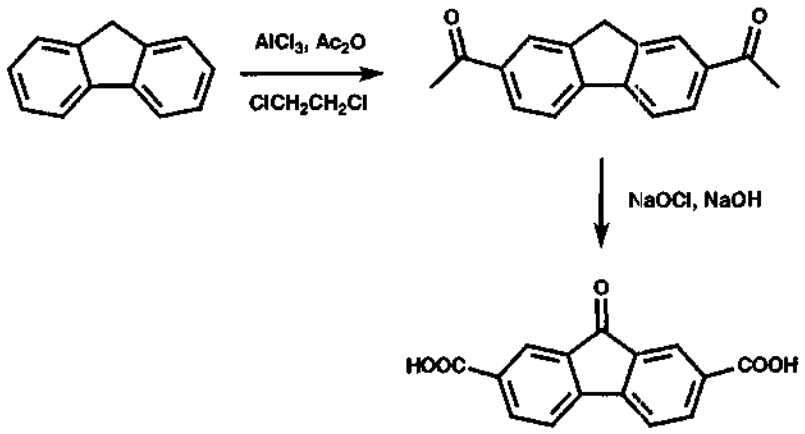

Figure C-3. Synthesis of fluorenone-2,7-dicarboxylic acid.

Synthesis of Novel, Thermally Stable PTCs

One major problem with traditional phase-transfer catalysis is the degradation of the catalyst due to internal nucleophilic displacements and/or Hofmann elimination (Landini et al., 1986; Starks et al., 1994). The latter is especially significant at elevated temperature and under basic conditions. Tetraalkylammonium compounds, such as TBAB, are well known to degrade to a considerable extent when exposed to higher temperature for a longer time. In the design of new catalysts, it is of major importance to avoid basic conditions and to reduce the number of α-CH bonds which would favor Hofmann degradation. At the same time, the catalyst must distribute between both the aqueous and the organic phase.

Synthesis of *N*-2-Ethylhexylquinolinium Bromide

N-2-Ethylhexylquinolinium bromide (EHQB) was synthesized by converting 6-methoxyquinoline with 2-ethylhexylmesylate and, in a second step, exchanging mesylate for bromide ion (Figure C-4). To a clean dry 25 mL three neck round-bottom flask was added 2.707 g (0.013 mol) of 2-ethylhexyl mesylate and 5 mL of freshly dried toluene. The flask was fitted with a magnetic stirrer, a gas inlet, a condenser, and a drying tube. The reaction setup was flushed with argon, and 1.83 mL (0.013 mol) of 6-methoxyquinoline (98 %) was added via a syringe. The flask was then lowered into an oil bath, and the solution was brought to reflux. After 17 hours, an aliquot was removed and analyzed via NMR to show approximately 5 % product formation. The reaction was

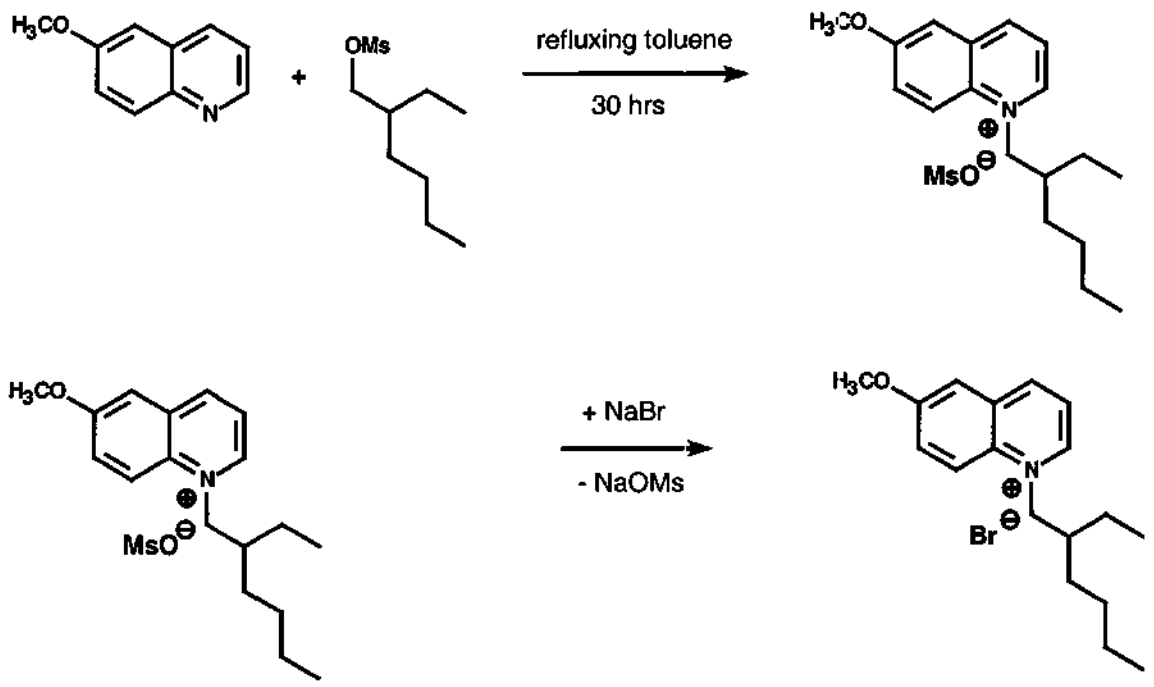

Figure C-4. Synthesis of *N*-2-ethylhexylquinolinium bromide.

allowed to reflux for an additional 20 hours. The solution was allowed to cool, and solvent was removed via rotary evaporation. The resulting solid was dissolved in methylene chloride and washed with saturated NaBr (3 x 3 minutes each). The aqueous layers were combined and washed with methylene chloride, and the organic layers were combined and dried over magnesium sulfate. The solid was filtered off, and the solvent was removed. The resulting crude solid was recrystallized from methylene chloride/diethyl ether to give 2.16 g of a white solid with a melting point of 116-117°C (Yield: 54%).

Subsequent analysis has indicated that this procedure did not synthesize the desired EHQB. A flame test for bromide was negative, suggesting that the anion exchange did not take place.

Synthesis of *N*-2-Ethylhexylnicotinium Bromide

N-2-Ethylhexylnicotinate, the precursor to *N*-2-ethylhexylnicotinium bromide (EHNB), was synthesized as shown in Figure C-5. To a 25 mL vial was added 5.3481 g of methyl nicotinate and 8.1281g of 2-ethylhexylmesylate. The two components were heated slightly to facilitate dissolution. Once completely miscible, approximately 8 mL of the mixture was loaded into a variable volume inner vessel (Figure C-6). A syringe, which acted as the inner reaction cell, was then loaded into the high pressure vessel, which was subsequently filled with toluene as pressurizing fluid. After pumping toluene through the vessel to displace any air that was present, the reaction apparatus was heated

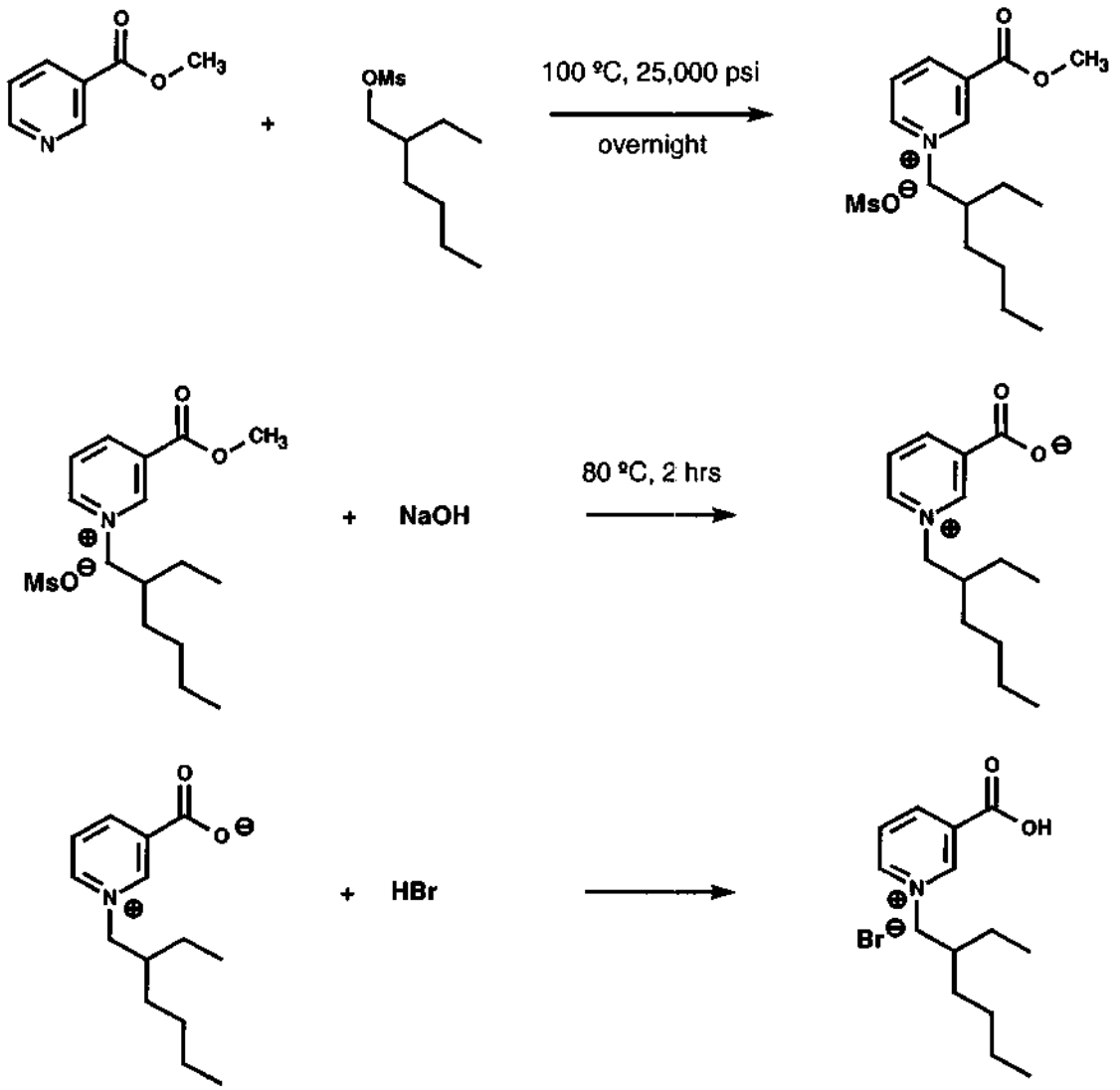

Figure C-5. Synthesis of *N*-2-ethylhexylnicotinium bromide.

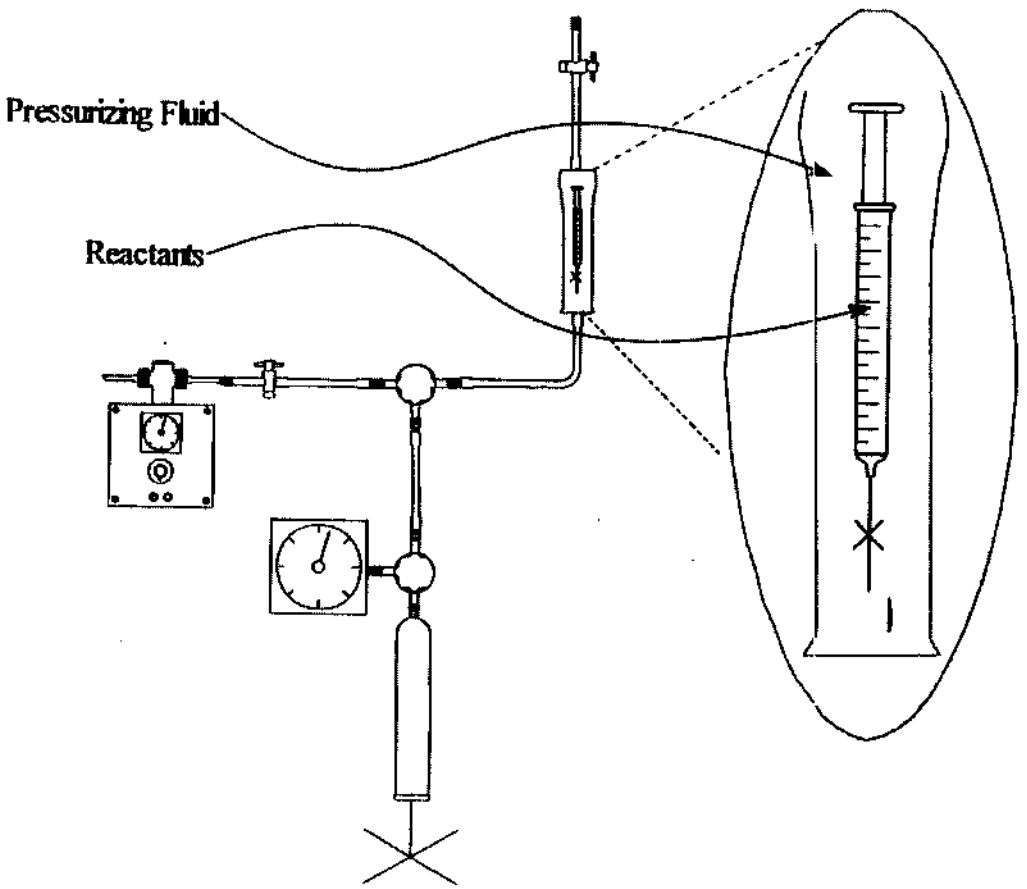

Figure C-6. Schematic representation of the high pressure, variable volume reactor used for the synthesis of phase-transfer catalysts.

to 100°C with heating tape. The reactor was then sealed off and pressurized with additional toluene to approximately 24,000 psi and held at this pressure for 20 hrs. The reaction was stopped by depressurizing and cooling to room temperature.

The contents of the inner vessel were dissolved in methylene chloride and transferred to a round-bottom flask, where the solvent was removed via rotary evaporation to give 13.485 g of crude solid. 39 mL of 1M NaOH and a stir bar were added to the crude product, and the flask was fitted with a reflux condenser. The resulting solution was heated to ~ 80°C and stirred for 2 hours. The solution was cooled to room temperature, and 10 % HCl was added dropwise until neutral to pH paper. The mixture was then diluted with 100 mL each of ethanol and benzene. The flask was fitted with a Dean-Starke adapter, a nitrogen inlet, a condenser, and a drying tube. The mixture was heated to reflux in an oil bath, and water was removed at the water/ethanol/benzene azeotrope (b.p. = 64.9°C). The solvent was then removed via rotary evaporation to give 12.921 g of crude inner salt. NMR of the inner salt showed pure product and absence of the mesylate group. The product proved to be extremely hygroscopic, and therefore was not purified further.

The hydrobromide of the inner salt product was the desired PTC. It was prepared immediately before the phase-transfer catalyzed *p*X oxidation reaction by adding HBr to an aqueous solution of the inner salt. Because the presence of the nicotinate and HBR in the reaction mixture actually inhibited reaction (Figure 5-17) and because mesylate is a poor leaving group, it is hypothesized that this procedure did not synthesize EHNB.

References

Landini, D.; Maia, A.; Rampoldi, A. Stability of Quaternary Onium Salts under Phase Transfer Conditions in the Presence of Aqueous Alkaline Solutions. *J. Org. Chem.* **1986**, *51*, 3187-3191.

Starks, C.M.; Liotta, C.L.; Halpern, M. *Phase-Transfer Catalysis: Fundamentals, Applications, and Industrial Perspectives*; Chapman & Hall: New York, 1994.

APPENDIX D

ESTIMATION OF THE FLAMMABLE REGION FOR PHASE-TRANSFER CATALYTIC P-XYLENE OXIDATION

To ensure safe operation of the reactor under reaction conditions, an estimation of the flammable region of *p*X vapor in the presence of oxygen and nitrogen was carried out. This estimation was performed according to general recommendations given in the literature (Clark and Sylvester, 1996; Britton, 1996). For our reaction conditions (130°C, 120 psig) and reactant concentrations, the following assumptions were made:

- The Upper Flammability Limit (UFL) and the Lower Flammability Limit (LFL) are independent of pressure and temperature. UFL and LFL are available from the Material Safety Data Sheets by Sigma Aldrich Corporation for air at ambient pressure and temperature.
- The Minimum Oxygen Concentration (MOC) is estimated by 10.5 x LFL (Clark and Sylvester, 1996), according to the total oxidation of *p*-xylene,

$$C_8H_{10} + 10.5\ O_2 \longrightarrow 8\ CO_2 + 5\ H_2O.$$

  This equation has an error of ± 2 % for hydrocarbon fuels (Britton, 1996).
- Water vapor and nitrogen in the gas phase are inert diluents.
- Conversion of *p*X by the oxidation reaction yields only involatile products.

- The effects of salts in the aqueous phase (ca. 1 mol %) and the internal standard added to the organic phase (ca. 2 mol %) are negligible.

The resulting flammability envelope is depicted in Figure D-1. When air is used as the oxidizing agent, the flammable region will be reached at 55% conversion. Oxygen concentrations in the gas phase greater than 21%, which yield higher reaction rates, will shift the operating conditions closer to the flammable region and are, therefore, not desirable. If higher conversion levels are to be reached, air must be diluted by nitrogen to run at a lower oxygen concentration.

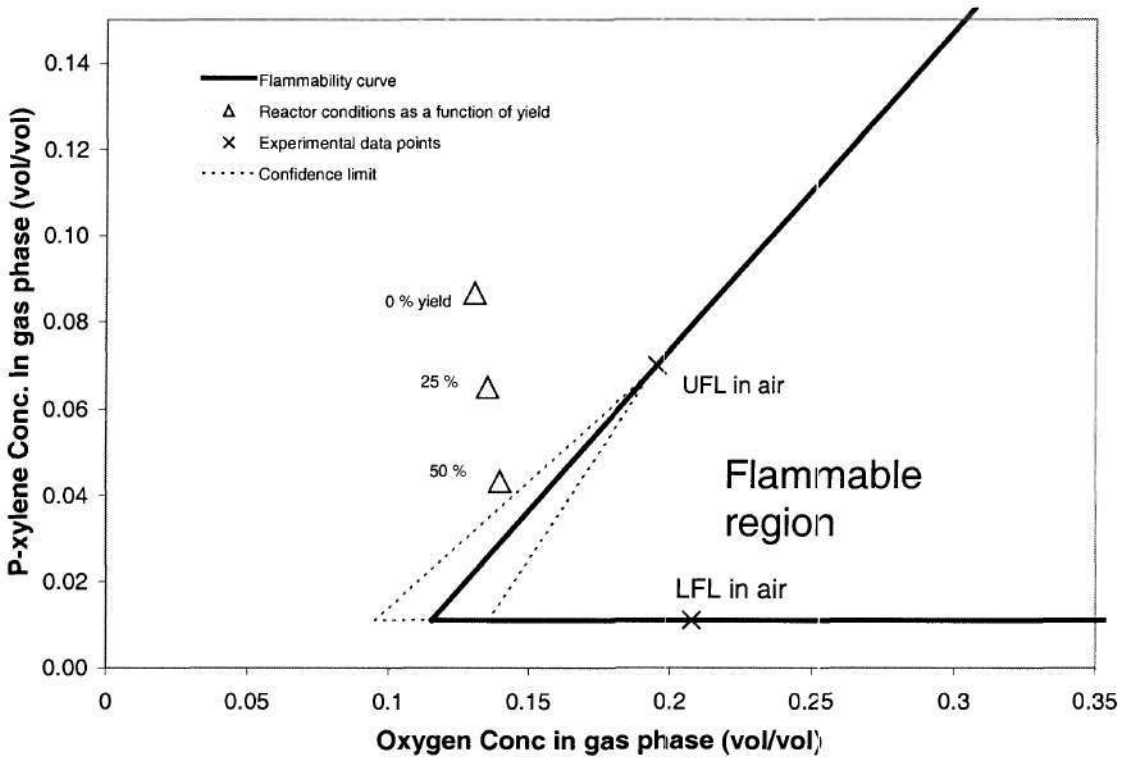

Figure D-1. Flammable region for oxidation of *p*-xylene in air.

References

Britton, L.G. Operating Atmospheric Vent Collection Headers Using Methane Gas Enrichment. *Proc. Safety Progr.* **1996**, *15*, 194-212.

Clark, D.G.; Sylvester, R.W. Ensure Process Vent Collection System Safety. *Chem. Eng. Progress*, **1996**, 65-77.

APPENDIX E

AUTOCATALYTIC MECHANISM FOR PHASE-TRANFER CATALYTIC OXIDATION OF P-XYLENE

Proposed Mechanism

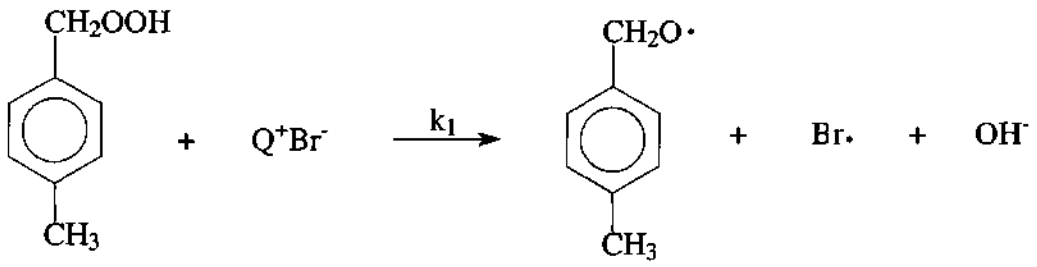

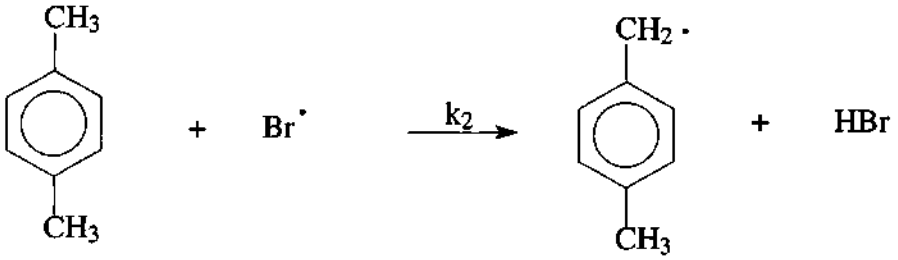

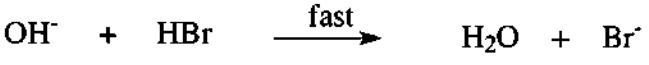

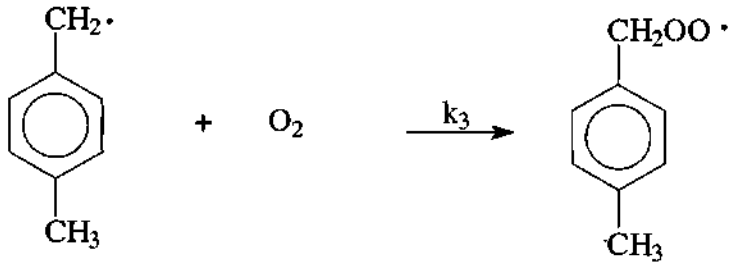
CH2·
+
O2
k3
CH2OO·
CH3
CH3

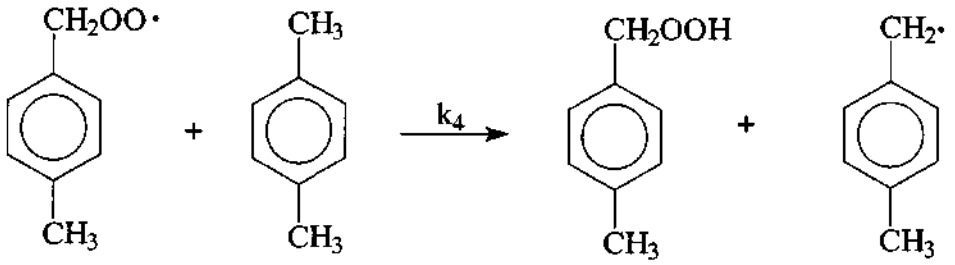
CH2OO·
CH3
+
CH3
k4
CH2OOH
+
CH2·
CH3
CH3
CH3

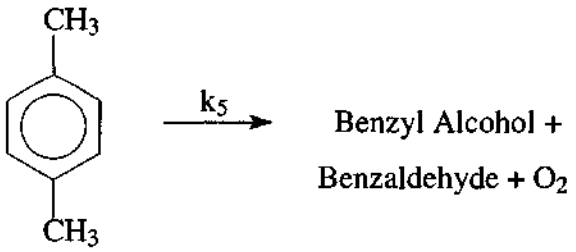
CH3
k5
Benzyl Alcohol +
Benzaldehyde + O2
CH3

Kinetic Analysis

Rate of disappearance of p-xylene:

$$\frac{-d(RH)}{dt} = k_2(RH)(Br\bullet) + k_4(RO_2\bullet)(RH)$$

For a long chain process,

$$\frac{-d(RH)}{dt} = k_4(RO_2\bullet)(RH)$$

Change in concentration of ROO• and R•:

$$\frac{d(RO_2\bullet)}{dt} = k_3(R\bullet)(O_2\bullet) - k_4(RO_2\bullet)(RH) - k_5(RO_2\bullet)^2$$

$$\frac{d(R\bullet)}{dt} = k_2(RH)(Br\bullet) - k_3(R\bullet)(O_2\bullet) + k_4(RO_2\bullet)(RH)$$

Steady-state approximation:

$$\frac{d(RO_2\bullet)}{dt} = 0$$

$$\frac{d(R\bullet)}{dt} = 0$$

$$(RO_2\bullet) = \sqrt{\frac{k_2(RH)(Br\bullet)}{k_5}}$$

Change in concentration of Br•:

$$\frac{d(Br\bullet)}{dt} = k_1(RO_2H)(Br^-) - k_2(RH)(Br\bullet)$$

Steady-state approximation:

$$\frac{d(Br\bullet)}{dt} = 0$$

Rate of disappearance of p-xylene:

$$\frac{-d(RH)}{dt} = k_4(RH)\sqrt{\frac{k_1(RO_2H)(Br^-)}{k_5}}$$

If

$$k' = k_4\sqrt{\frac{k_1(Br^-)}{k_5}},$$

a equals the initial concentration of p-xylene, and b equals the initial concentration of p-xylene hydroperoxide, then the following autocatalytic rate expression describes the disappearance of p-xylene:

$$\frac{-d(a-x)}{dt} = k'(a-x)(b-x)^{1/2}.$$

APPENDIX F

PRODUCT COMPOSITION VERSUS TIME FOR PHASE-TRANFER CATALYTIC OXIDATION OF P-XYLENE

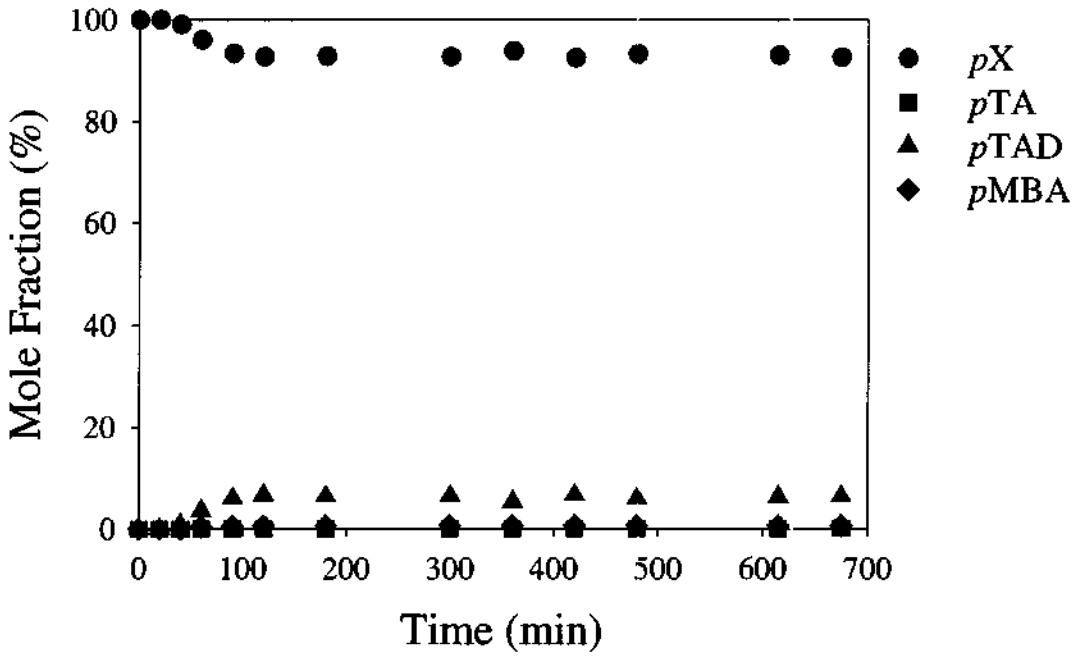

Figure F-1. Product distribution as a function of reaction time for batch-wise *p*X oxidation at 130°C and 120 psig. Agitation was 1600 rpm. Reactor was loaded with 0.972 mol *p*X, 1.667 mol H_2O, 0.00170 mol TBAB, 0.0129 mol KBr, and 0.0208 mol pentachlorobenzene.

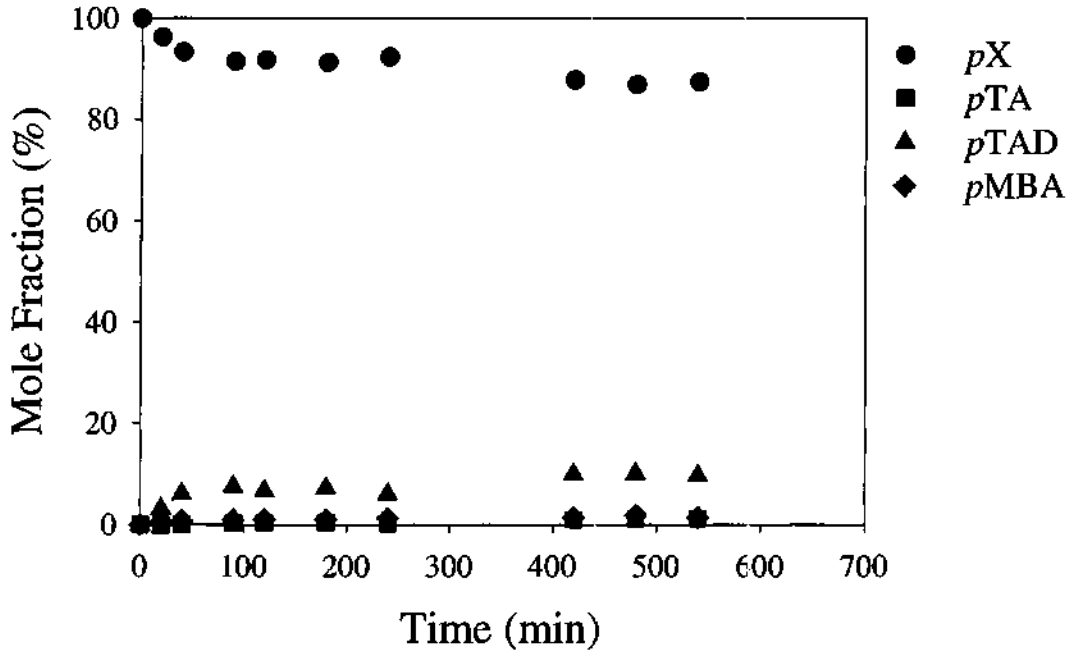

Figure F-2. Product distribution as a function of reaction time for batch-wise *p*X oxidation at 130°C and 120 psig. Agitation was 1600 rpm. Reactor was loaded with 0.546 mol *p*X, 0.833 mol H_2O, 0.00085 mol TBAB, 0.00648 mol KBr, and 0.0104 mol pentachlorobenzene.

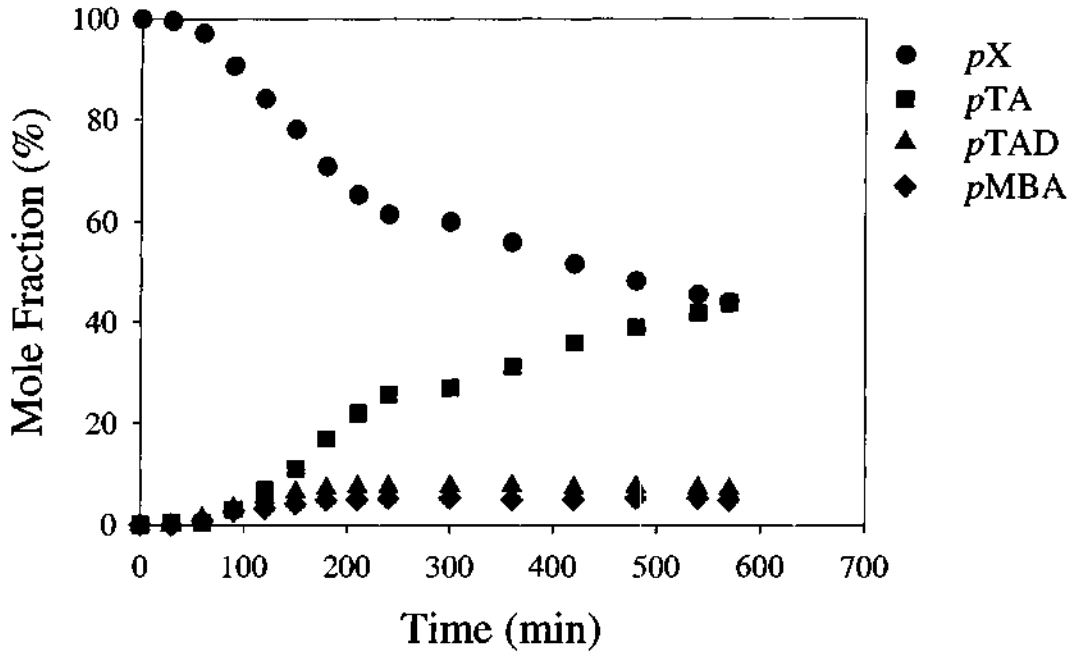

Figure F-3. Product distribution as a function of reaction time for semi-batch *p*X oxidation at 130°C and 120 psig. Air flow rate was 0.38 L/min. Agitation was 1600 rpm. Reactor was loaded with 0.489 mol *p*X, 0.888 mol *o*DCB, 2.222 mol H_2O, 0.00230 mol TBAB, 0.0175 mol KBr, and 0.00720 mol pentachlorobenzene.

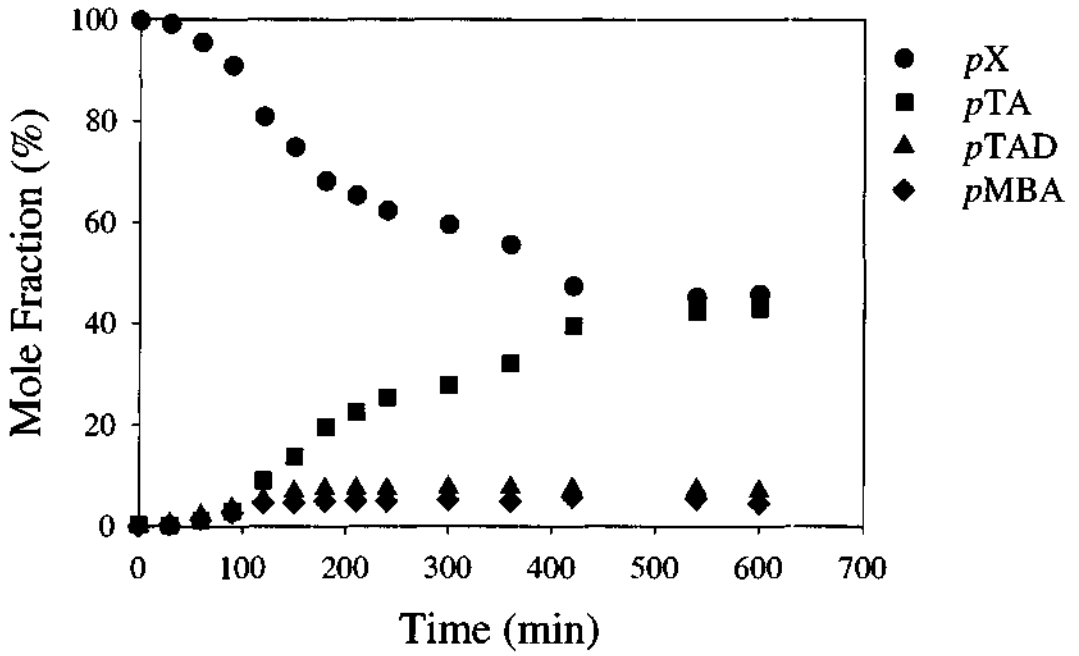

Figure F-4. Product distribution as a function of reaction time for semi-batch *p*X oxidation at 130°C and 120 psig. Air flow rate was 0.38 L/min. Agitation was 2200 rpm. Reactor was loaded with 0.489 mol *p*X, 0.888 mol *o*DCB, 2.222 mol H_2O, 0.00230 mol TBAB, 0.0175 mol KBr, and 0.00720 mol pentachlorobenzene.

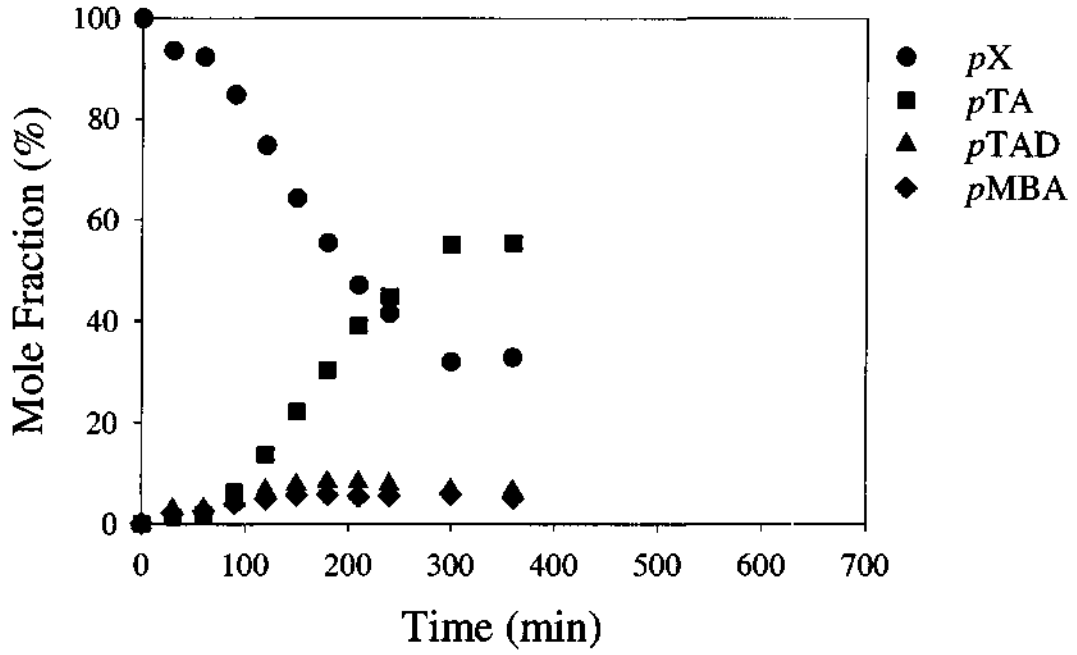

Figure F-5. Product distribution as a function of reaction time for semi-batch *p*X oxidation at 140°C and 120 psig. Air flow rate was 0.38 L/min. Agitation was 1600 rpm. Reactor was loaded with 0.489 mol *p*X, 0.888 mol *o*DCB, 2.222 mol H_2O, 0.00230 mol TBAB, 0.0175 mol KBr, and 0.00720 mol pentachlorobenzene.

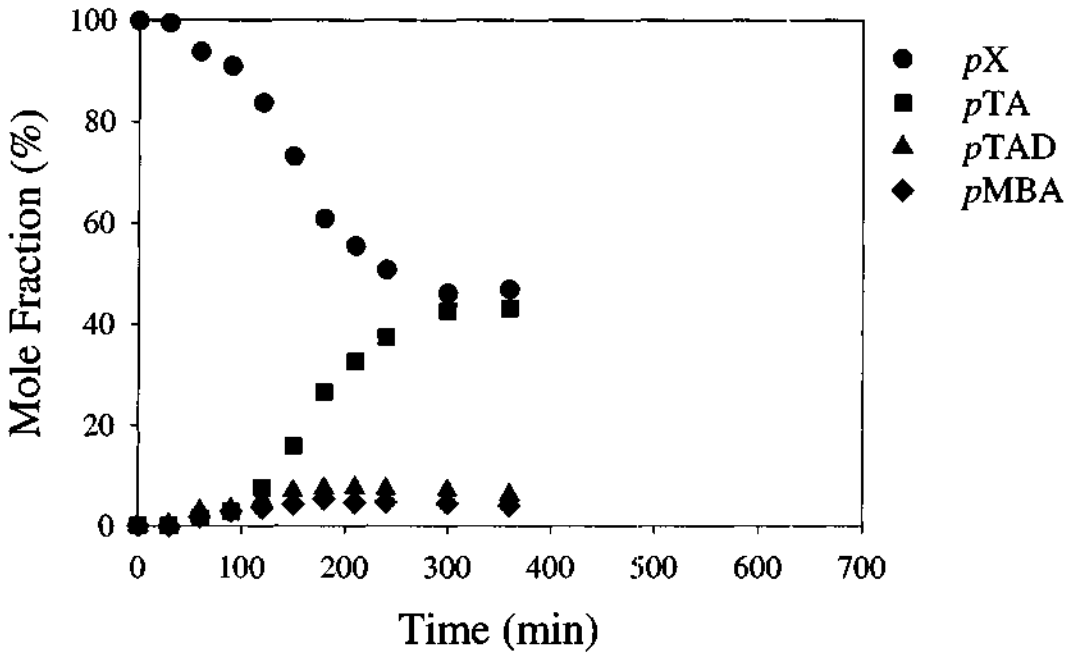

Figure F-6. Product distribution as a function of reaction time for semi-batch *p*X oxidation at 130°C and 120 psig. Air flow rate was 0.38 L/min. Agitation was 1600 rpm. Reactor was loaded with 0.428 mol *p*X, 0.777 mol *o*DCB, 3.333 mol H_2O, 0.00346 mol TBAB, 0.0262 mol KBr, and 0.00630 mol pentachlorobenzene.

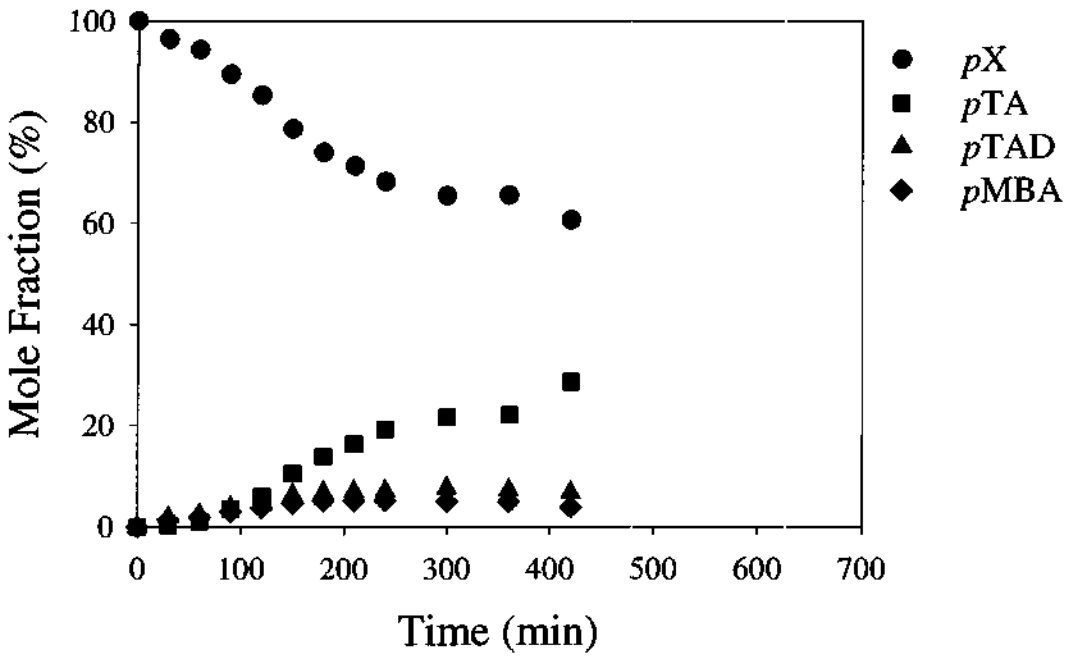

Figure F-7. Product distribution as a function of reaction time for semi-batch *p*X oxidation at 130°C and 120 psig. Air flow rate was 0.38 L/min. Agitation was 1600 rpm. Reactor was loaded with 1.305 mol *p*X, no *o*DCB, 2.222 mol H_2O, 0.00230 mol TBAB, 0.0175 mol KBr, and 0.00720 mol pentachlorobenzene.

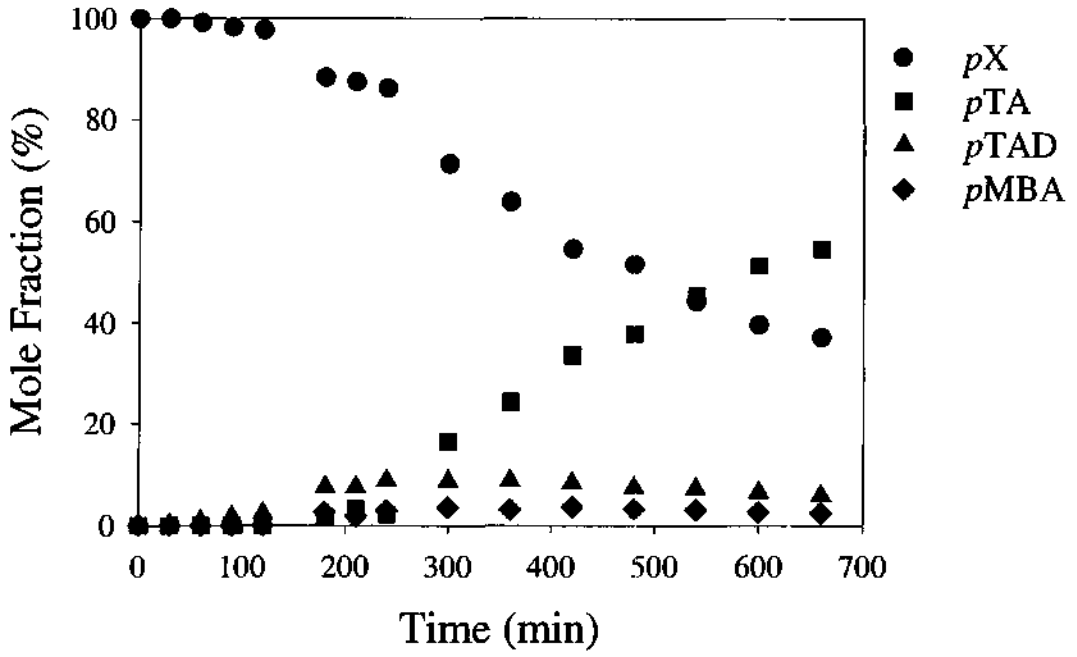

Figure F-8. Product distribution as a function of reaction time for semi-batch *p*X oxidation at 130°C and 120 psig. Air flow rate was 0.38 L/min. Agitation was 1600 rpm. Reactor was loaded with 0.220 mol *p*X, 1.182 mol *o*DCB, 2.222 mol H_2O, 0.00230 mol TBAB, 0.0175 mol KBr, and 0.00720 mol pentachlorobenzene.

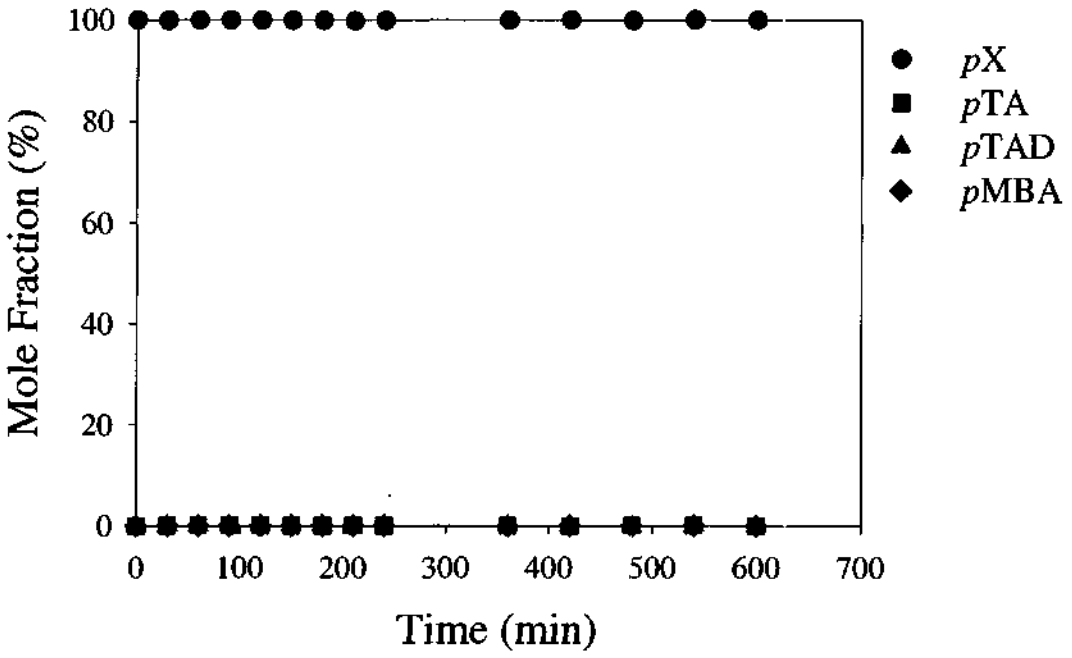

Figure F-9. Product distribution as a function of reaction time for semi-batch *p*X oxidation at 130°C and 120 psig. Air flow rate was 0.38 L/min. Agitation was 1600 rpm. Reactor was loaded with 0.489 mol *p*X, 0.888 mol *o*DCB, 2.222 mol H_2O, 0.00230 mol EHQB, 0.0175 mol KBr, and 0.00720 mol pentachlorobenzene.

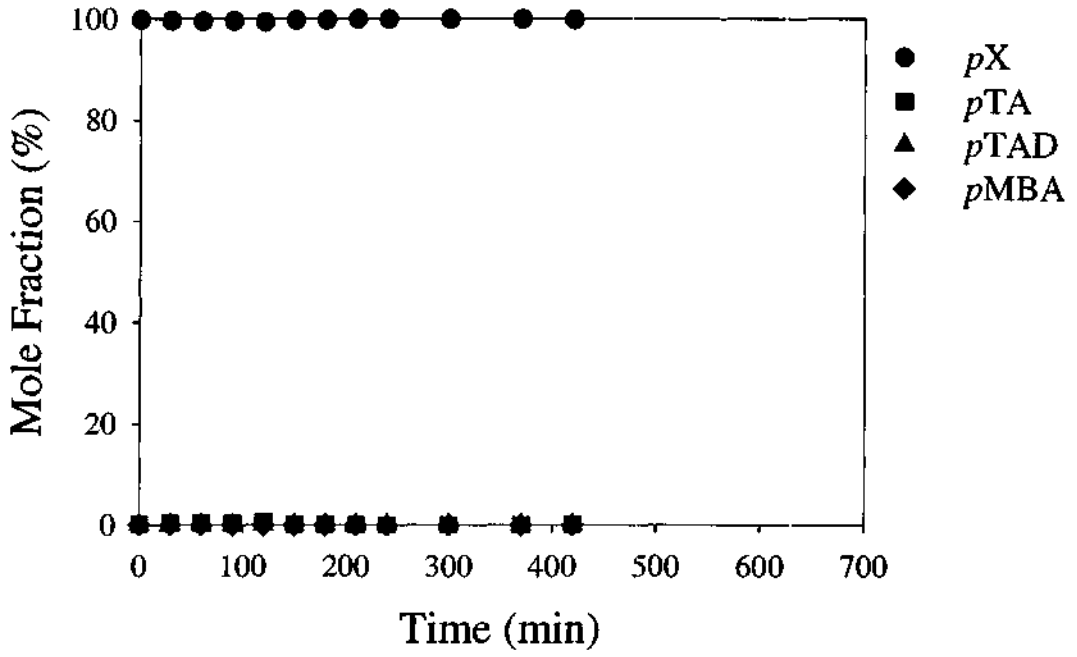

Figure F-10. Product distribution as a function of reaction time for semi-batch *p*X oxidation at 130°C and 120 psig. Air flow rate was 0.38 L/min. Agitation was 1600 rpm. Reactor was loaded with 0.489 mol *p*X, 0.888 mol *o*DCB, 2.222 mol H_2O, 0.00243 mol nicotinic acid inner salt, 0.00244 mol HBr, 0.0175 mol KBr, and 0.00720 mol pentachlorobenzene.

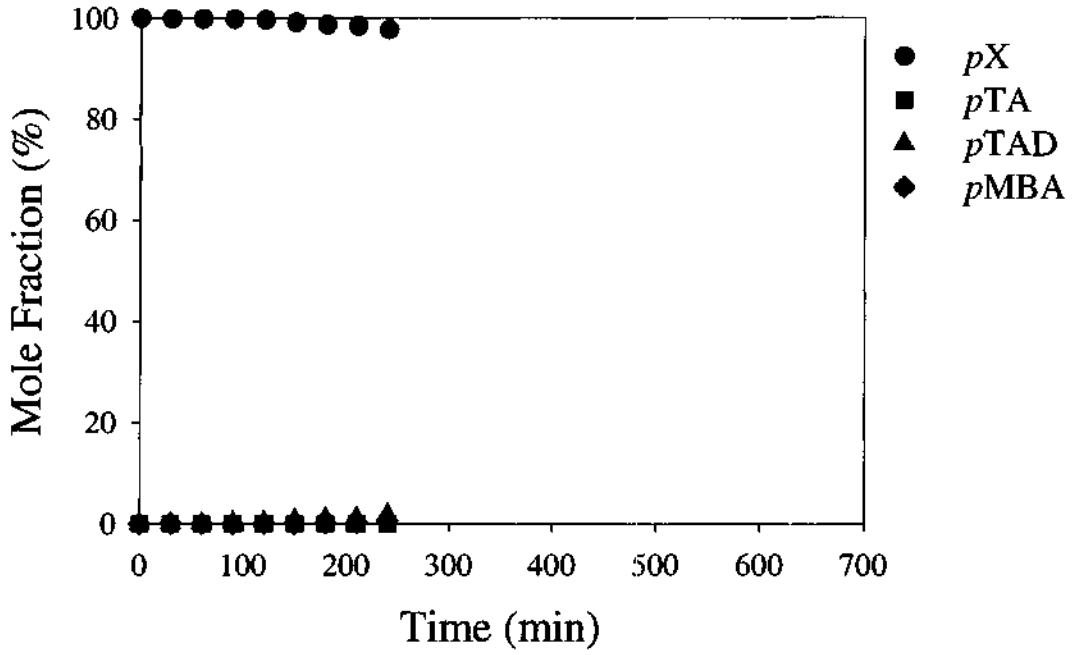

Figure F-11. Product distribution as a function of reaction time for semi-batch *p*X oxidation at 130°C and 120 psig. Air flow rate was 0.38 L/min. Agitation was 1600 rpm. Reactor was loaded with 0.489 mol *p*X, 0.888 mol *o*DCB, 2.222 mol H_2O, no PTC, 0.0175 mol KBr, and 0.00720 mol pentachlorobenzene.

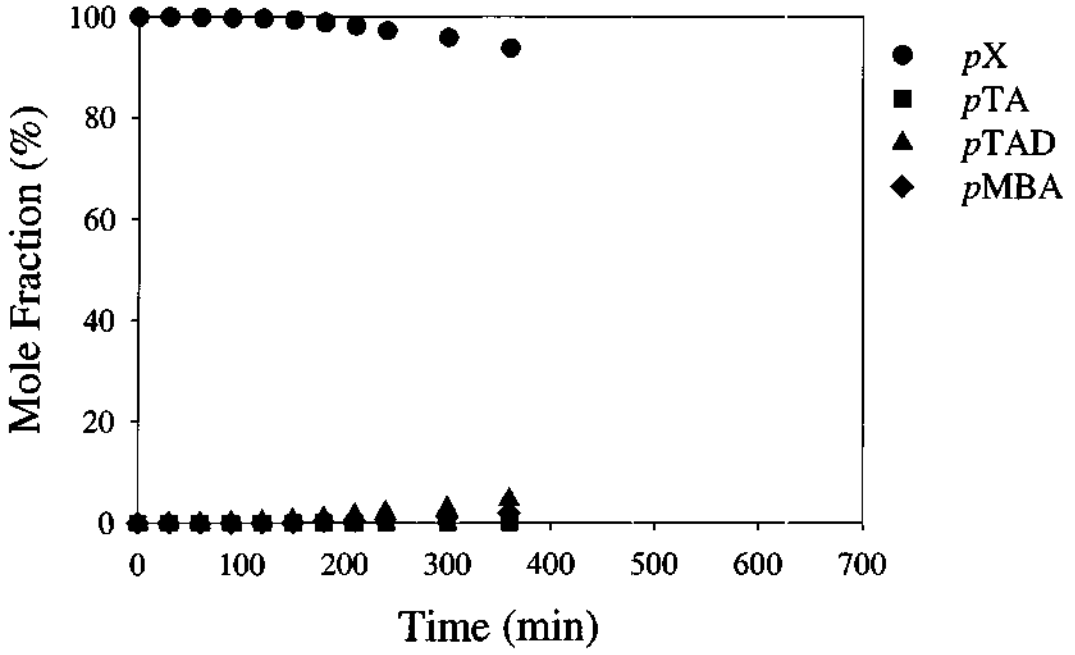

Figure F-12. Product distribution as a function of reaction time for semi-batch *p*X oxidation at 130°C and 120 psig. Air flow rate was 0.38 L/min. Agitation was 1600 rpm. Reactor was loaded with 0.489 mol *p*X, 0.888 mol *o*DCB, 2.222 mol H_2O, 0.00230 mol tetraethylammonium bromide, 0.0175 mol KBr, and 0.00720 mol pentachlorobenzene.

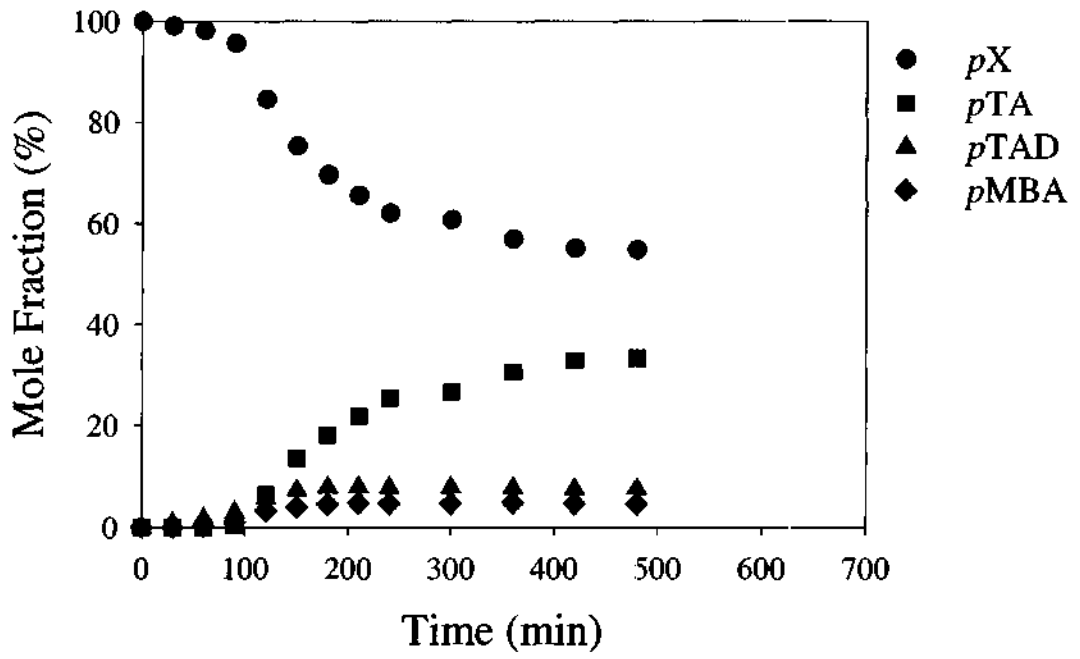

Figure F-13. Product distribution as a function of reaction time for semi-batch *p*X oxidation at 130°C and 120 psig. Air flow rate was 0.38 L/min. Agitation was 1600 rpm. Reactor was loaded with 0.489 mol *p*X, 0.888 mol *o*DCB, 2.222 mol H_2O, 0.00230 mol tetrahexylammonium bromide, 0.0175 mol KBr, and 0.00720 mol pentachlorobenzene.

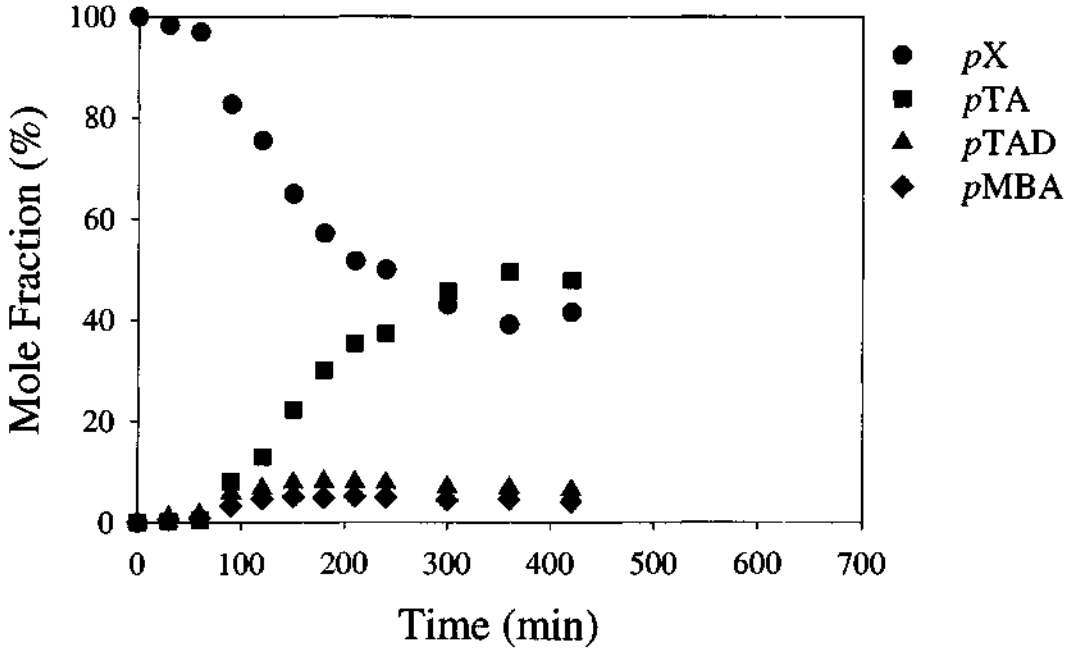

Figure F-14. Product distribution as a function of reaction time for semi-batch *p*X oxidation at 130°C and 120 psig. Air flow rate was 0.38 L/min. Agitation was 1600 rpm. Reactor was loaded with 0.489 mol *p*X, 0.888 mol *o*DCB, 2.222 mol H_2O, 0.00462 mol TBAB, 0.0175 mol KBr, and 0.00720 mol pentachlorobenzene.

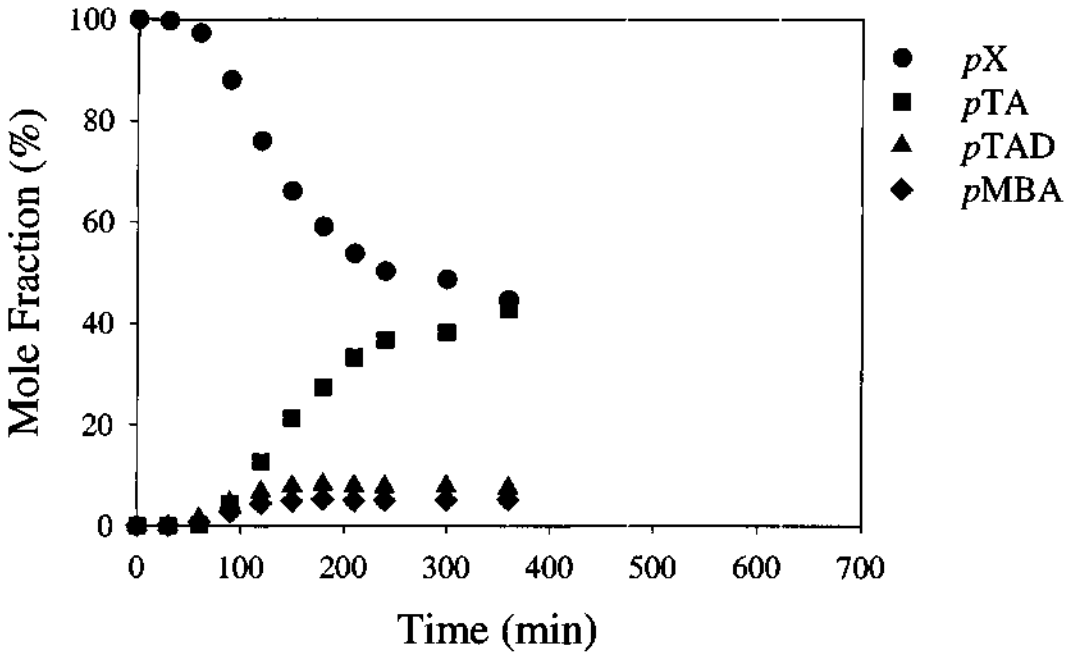

Figure F-15. Product distribution as a function of reaction time for semi-batch *p*X oxidation at 130°C and 120 psig. Air flow rate was 0.38 L/min. Agitation was 1600 rpm. Reactor was loaded with 0.489 mol *p*X, 0.888 mol *o*DCB, 2.222 mol H_2O, 0.00462 mol TBAB, 0.0350 mol KBr, and 0.00720 mol pentachlorobenzene.

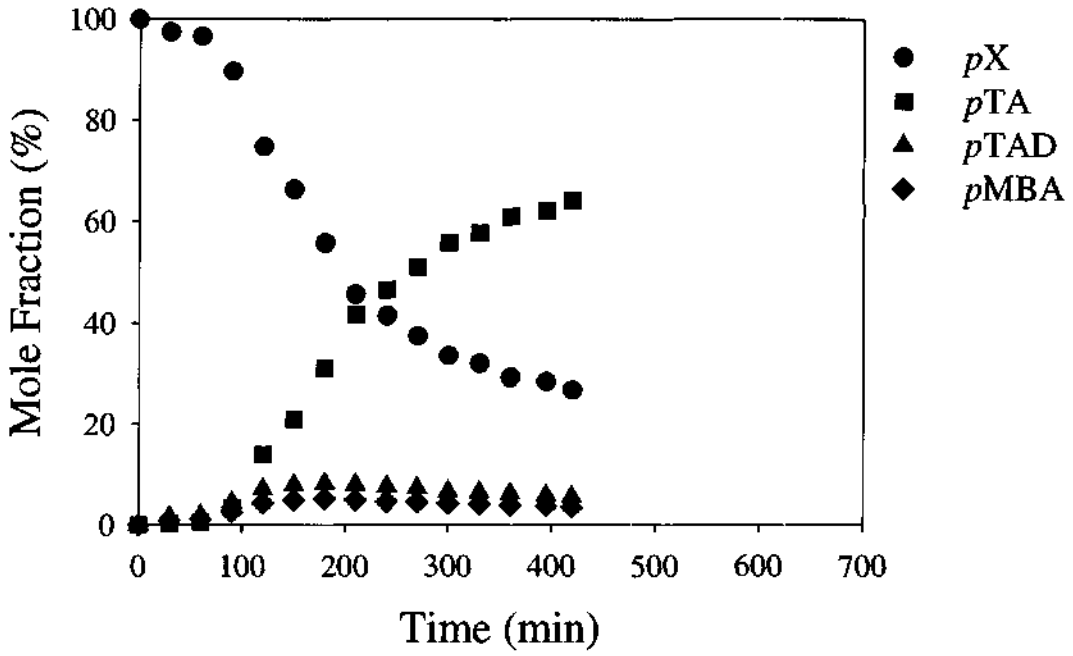

Figure F-16. Product distribution as a function of reaction time for semi-batch *p*X oxidation at 130°C and 120 psig. Air flow rate was 0.38 L/min. Agitation was 1600 rpm. Reactor was loaded with 0.428 mol *p*X, 0.777 mol *o*DCB, 3.333 mol H_2O, 0.00346 mol TBAB, 0.0524 mol KBr, and 0.00630 mol pentachlorobenzene.

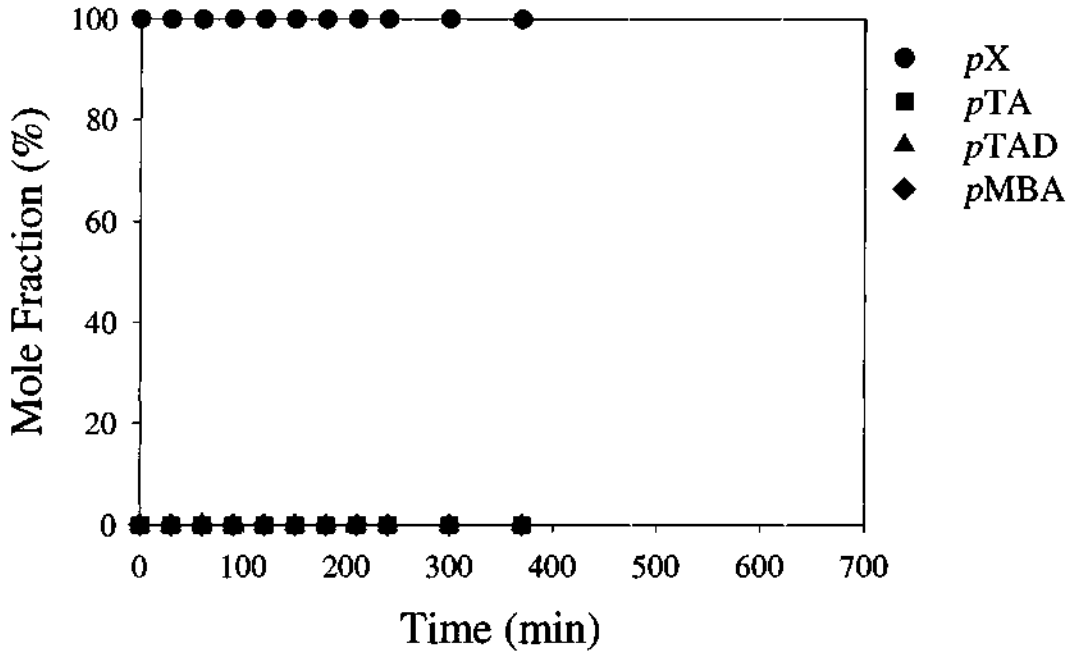

Figure F-17. Product distribution as a function of reaction time for semi-batch *p*X oxidation at 130°C and 120 psig. Air flow rate was 0.38 L/min. Agitation was 1600 rpm. Reactor was loaded with 0.119 mol *p*X, 1.297 mol *o*DCB, 2.222 mol H_2O, 0.00230 mol TBAB, 0.0175 mol KBr, 0.0175 mol cobalt(II) acetate tetrahydrate, 0.119 mol acetic acid, and 0.00720 mol pentachlorobenzene.

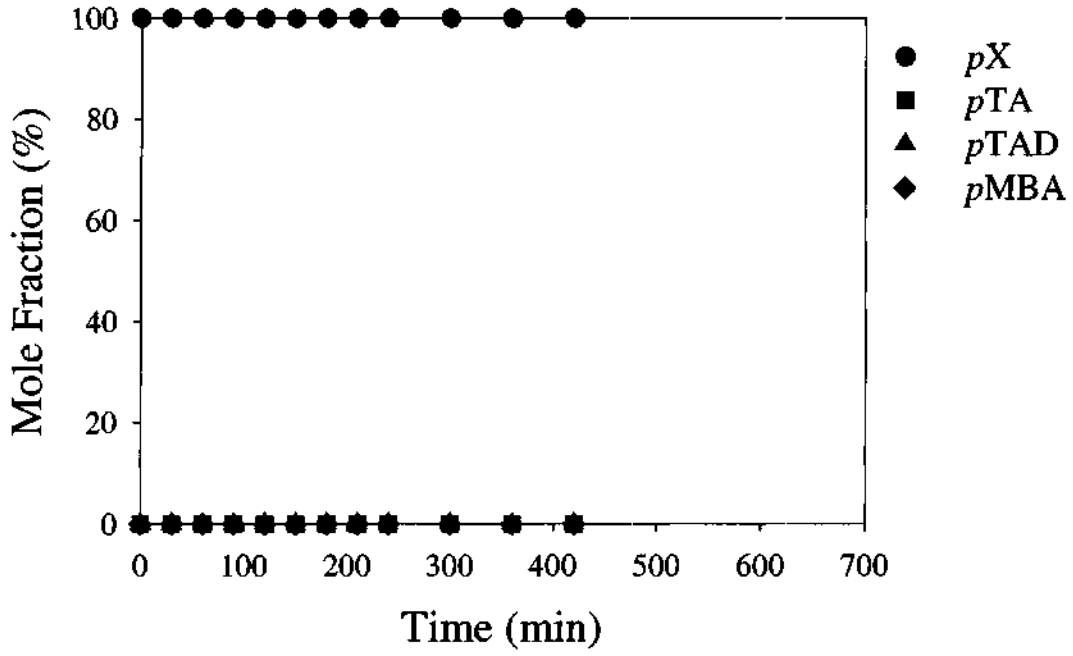

Figure F-18. Product distribution as a function of reaction time for semi-batch *p*X oxidation at 130°C and 120 psig. Air flow rate was 0.38 L/min. Agitation was 1600 rpm. Reactor was loaded with 0.489 mol *p*X, 0.888 mol *o*DCB, 2.222 mol H_2O, 0.00230 mol TBAB, 0.0175 mol KBr, 0.0175 mol cobalt(II) acetate tetrahydrate, 0.119 mol acetic acid, and 0.00720 mol pentachlorobenzene.

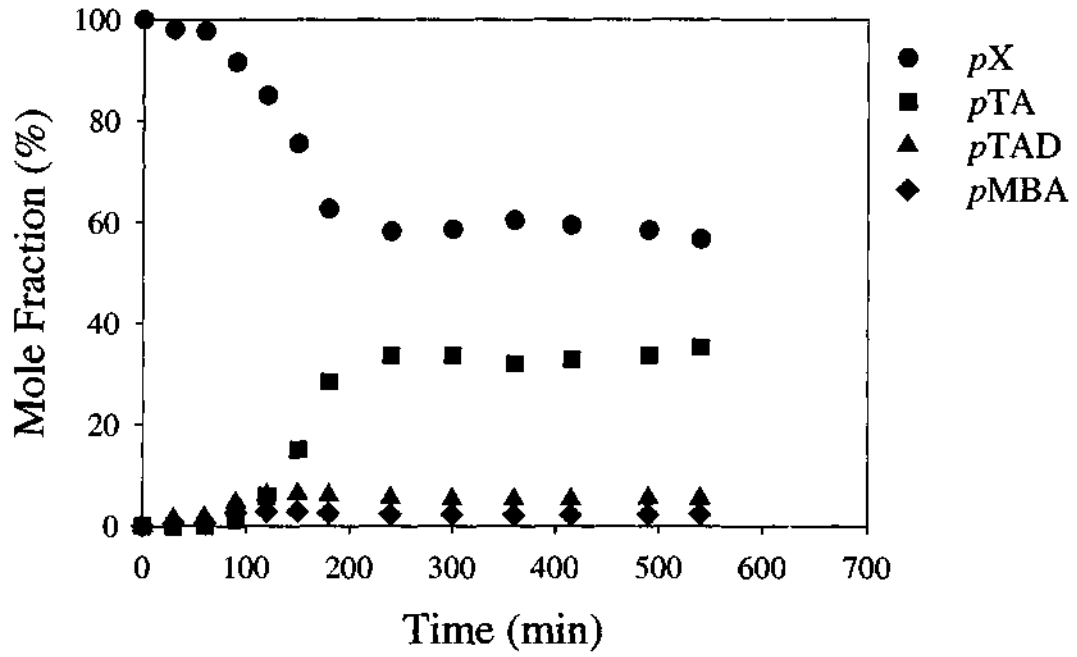

Figure F-19. Product distribution as a function of reaction time for semi-batch *p*X oxidation at 130°C and 120 psig. Air flow rate was 0.38 L/min. Agitation was 1600 rpm. Reactor was loaded with 0.489 mol *p*X, 0.888 mol *o*DCB, 2.222 mol H_2O, 0.00230 mol TBAB, 0.0175 mol KBr, 0.00230 mol cobalt bromide, and 0.00720 mol pentachlorobenzene.

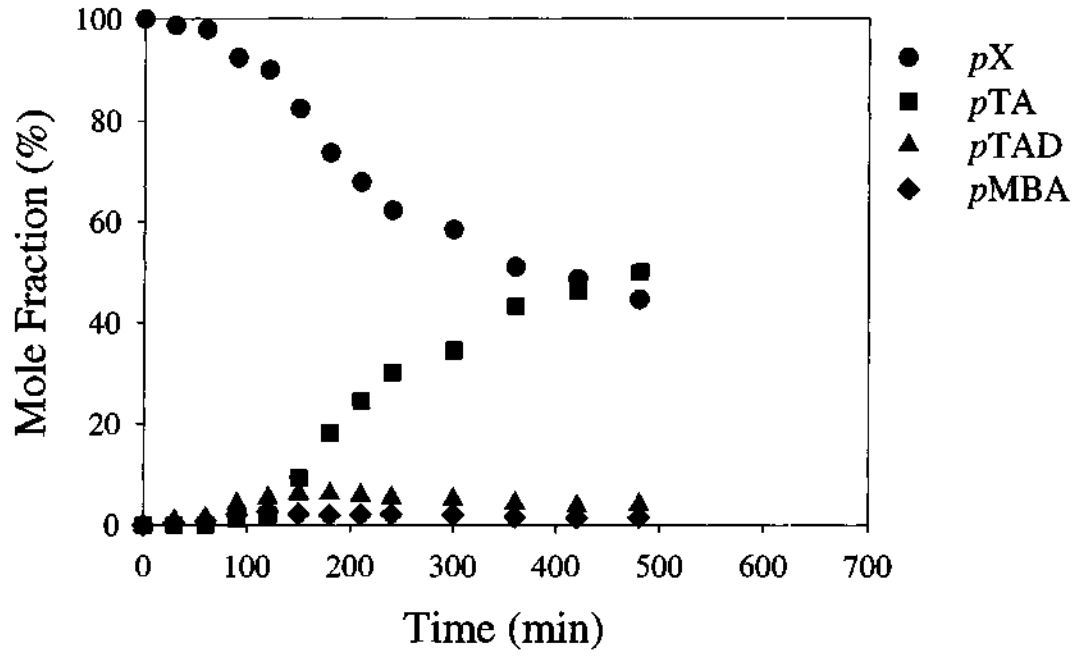

Figure F-20. Product distribution as a function of reaction time for semi-batch *p*X oxidation at 130°C and 120 psig. Air flow rate was 0.38 L/min. Agitation was 1600 rpm. Reactor was loaded with 0.489 mol *p*X, 0.888 mol *o*DCB, 2.222 mol H_2O, 0.00230 mol TBAB, 0.0175 mol KBr, 0.00230 mol cobalt(II) acetate tetrahydrate, 0.0157 mol acetic acid, and 0.00720 mol pentachlorobenzene.

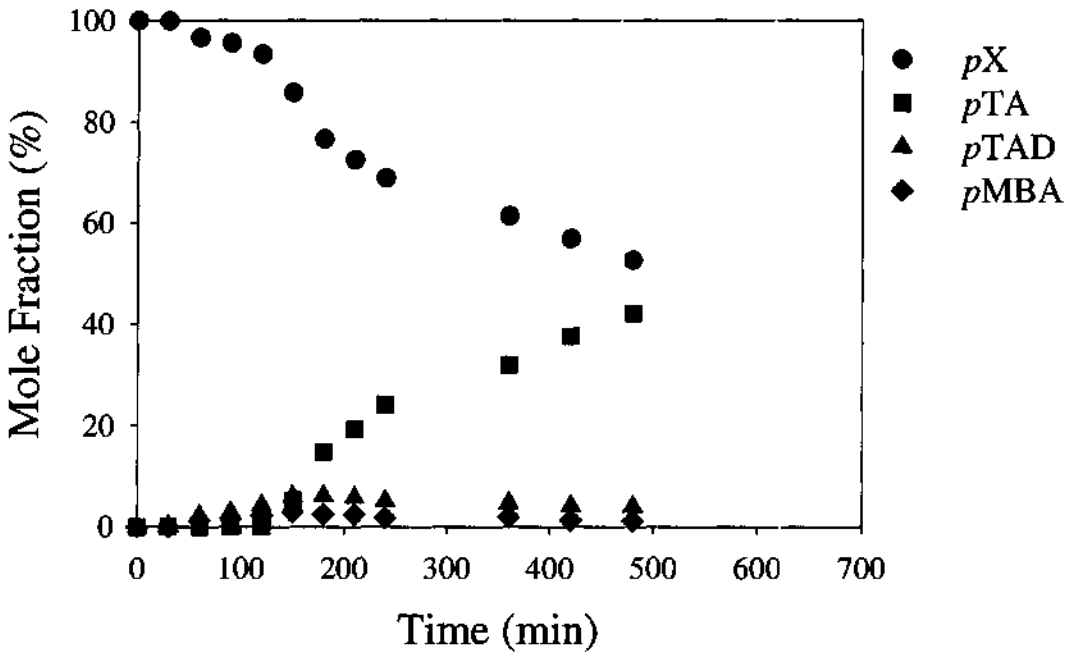

Figure F-21. Product distribution as a function of reaction time for semi-batch *p*X oxidation at 130°C and 120 psig. Air flow rate was 0.38 L/min. Agitation was 1600 rpm. Reactor was loaded with 0.489 mol *p*X, 0.888 mol *o*DCB, 2.222 mol H_2O, 0.00230 mol TBAB, 0.0175 mol KBr, 0.00230 mol cobalt(II) acetate tetrahydrate, 0.119 mol acetic acid, and 0.00720 mol pentachlorobenzene.

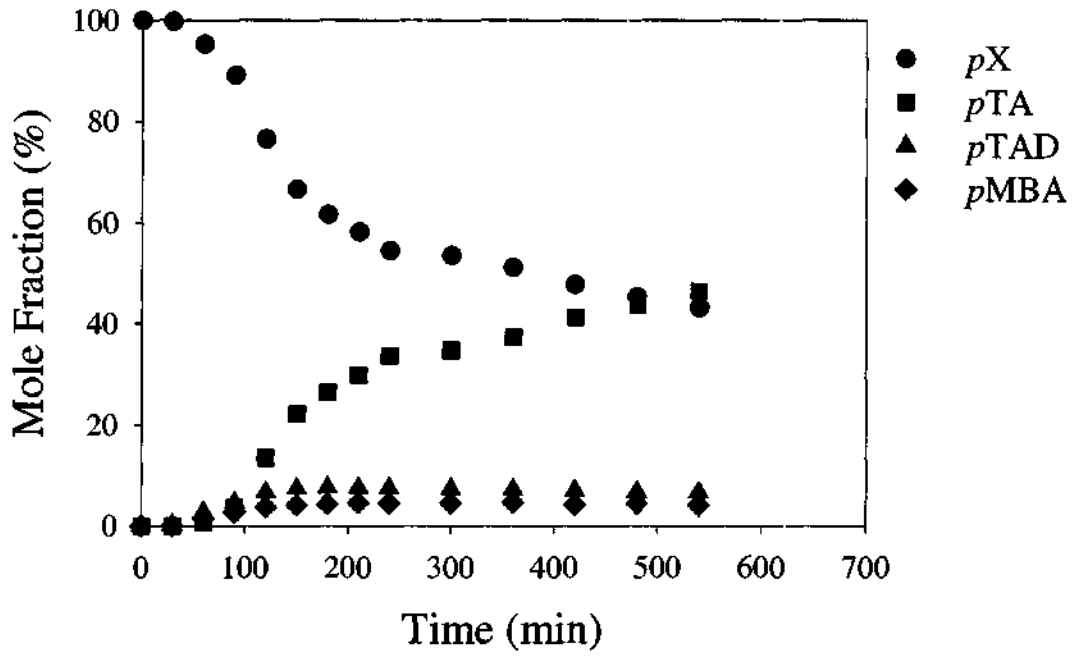

Figure F-22. Product distribution as a function of reaction time for semi-batch *p*X oxidation at 130°C and 120 psig. Air flow rate was 0.38 L/min. Agitation was 1600 rpm. Reactor was loaded with 0.489 mol *p*X, 0.888 mol *o*DCB, 2.222 mol H_2O, 0.00230 mol TBAB, 0.0175 mol KBr, 0.00015 mol cobalt bromide, and 0.00720 mol pentachlorobenzene.

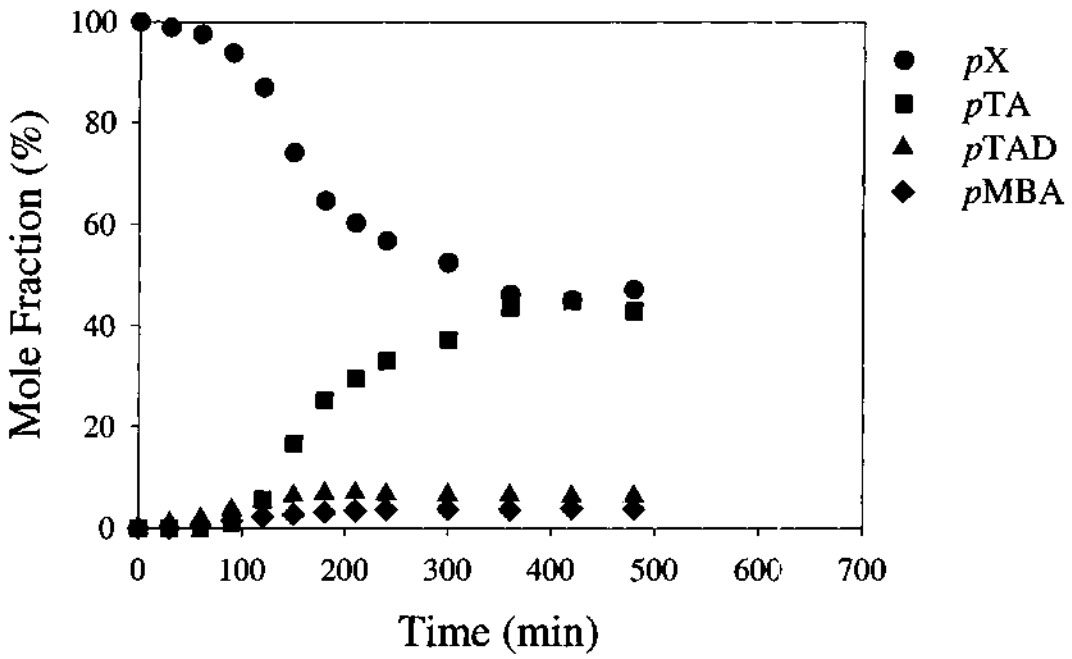

Figure F-23. Product distribution as a function of reaction time for semi-batch *p*X oxidation at 130°C and 120 psig. Air flow rate was 0.38 L/min. Agitation was 1600 rpm. Reactor was loaded with 0.489 mol *p*X, 0.888 mol *o*DCB, 2.222 mol H_2O, 0.00230 mol TBAB, 0.0175 mol KBr, 0.00046 mol cobalt bromide, and 0.00720 mol pentachlorobenzene.

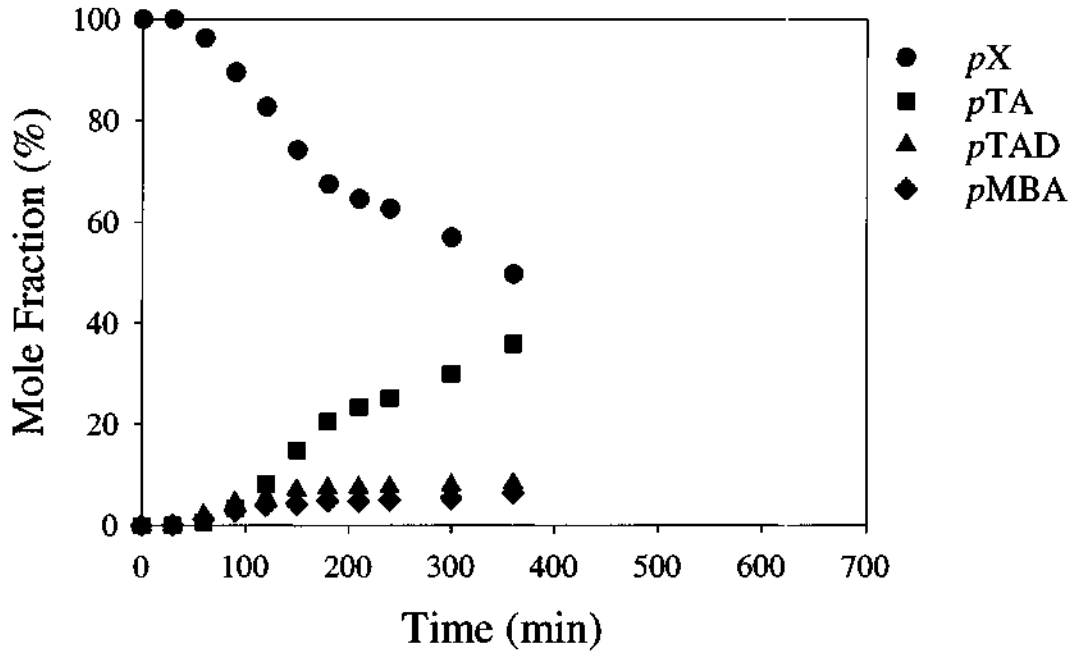

Figure F-24. Product distribution as a function of reaction time for semi-batch *p*X oxidation at 130°C and 120 psig. Air flow rate was 0.38 L/min. Agitation was 1600 rpm. Reactor was held at temperature for 3 hours before air was introduced. Reactor was loaded with 0.489 mol *p*X, 0.888 mol *o*DCB, 2.222 mol H_2O, 0.00230 mol TBAB, 0.0175 mol KBr, and 0.00720 mol pentachlorobenzene.

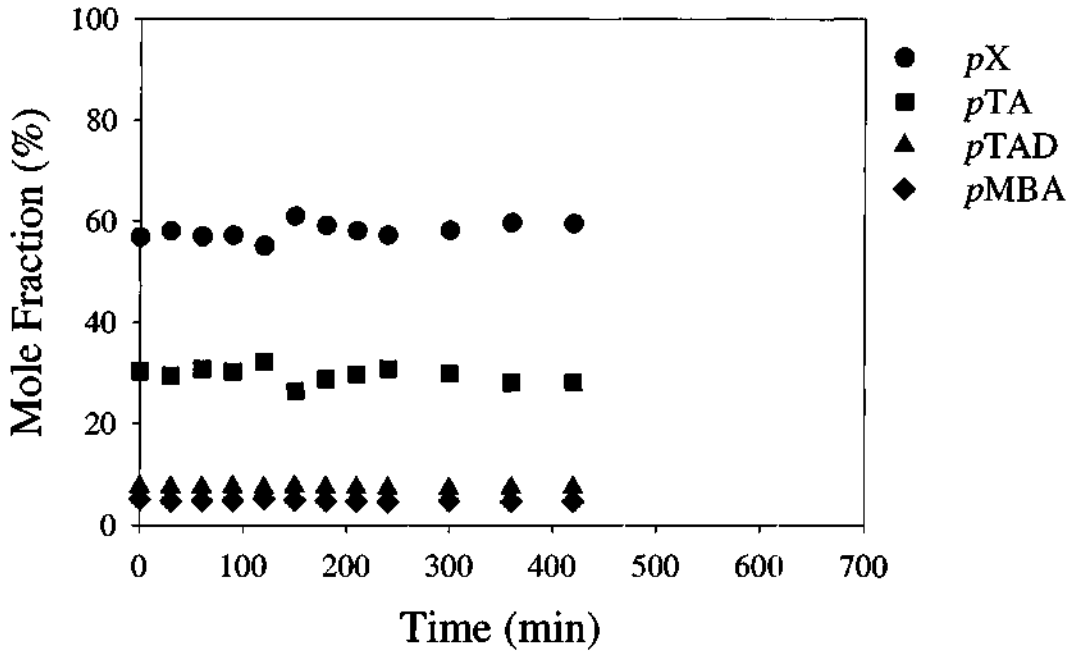

Figure F-25. Product distribution as a function of reaction time for semi-batch *p*X oxidation at 130°C and 120 psig. Air flow rate was 0.38 L/min. Agitation was 1600 rpm. Reactor was loaded with 0.294 mol *p*X, 0.109 mol *p*TA, 0.0376 mol *p*TAD, 0.0248 mol *p*MBA, 0.888 mol *o*DCB, 2.222 mol H_2O, 0.00230 mol TBAB, 0.0175 mol KBr, and 0.00720 mol pentachlorobenzene.

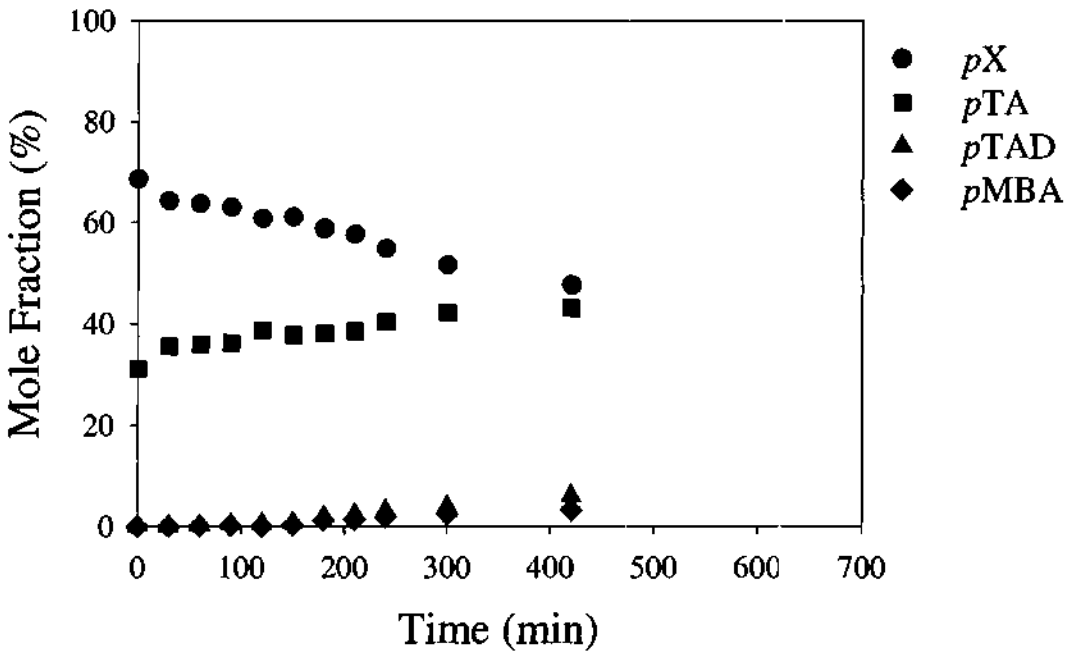

Figure F-26. Product distribution as a function of reaction time for semi-batch *p*X oxidation at 130°C and 120 psig. Air flow rate was 0.38 L/min. Agitation was 1600 rpm. Reactor was loaded with 0.294 mol *p*X, 0.161 mol *p*TA, 0.888 mol *o*DCB, 2.222 mol H_2O, 0.00230 mol TBAB, 0.0175 mol KBr, and 0.00720 mol pentachlorobenzene.

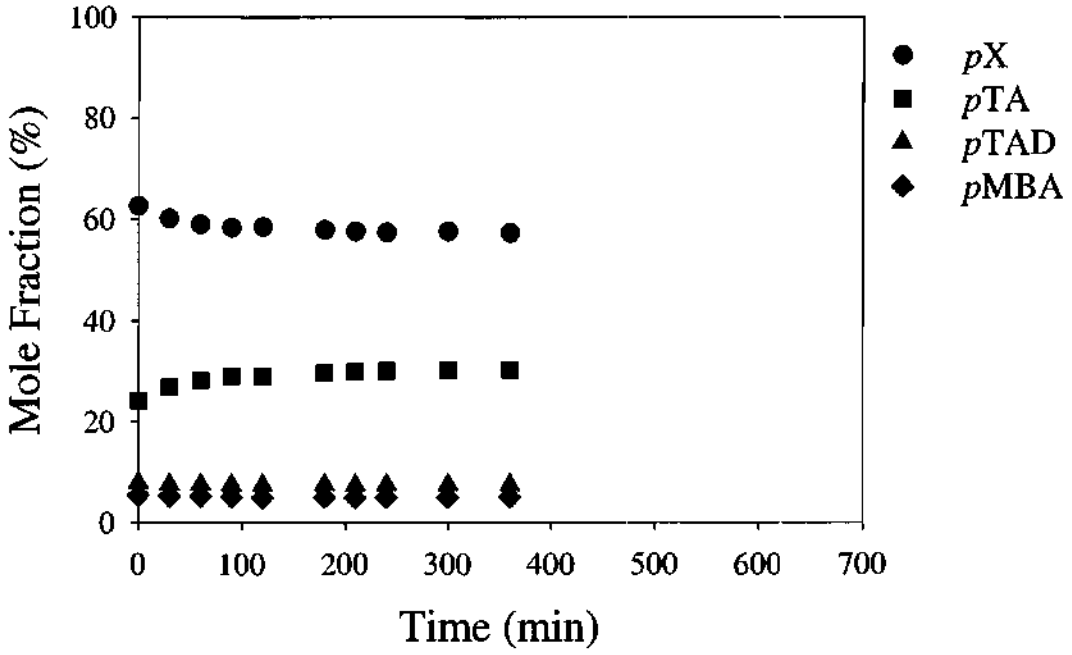

Figure F-27. Product distribution as a function of reaction time for semi-batch *p*X oxidation at 130°C and 120 psig. Air flow rate was 0.38 L/min. Agitation was 1600 rpm. Reactor was loaded with 0.294 mol *p*X, 0.109 mol *p*TA, 0.0376 mol *p*TAD, 0.0260 mol *p*MBA, 0.888 mol *o*DCB, 2.222 mol H_2O, 0.00230 mol TBAB, 0.0175 mol KBr, 0.0175 cumene hydroperoxide, and 0.00720 mol pentachlorobenzene.

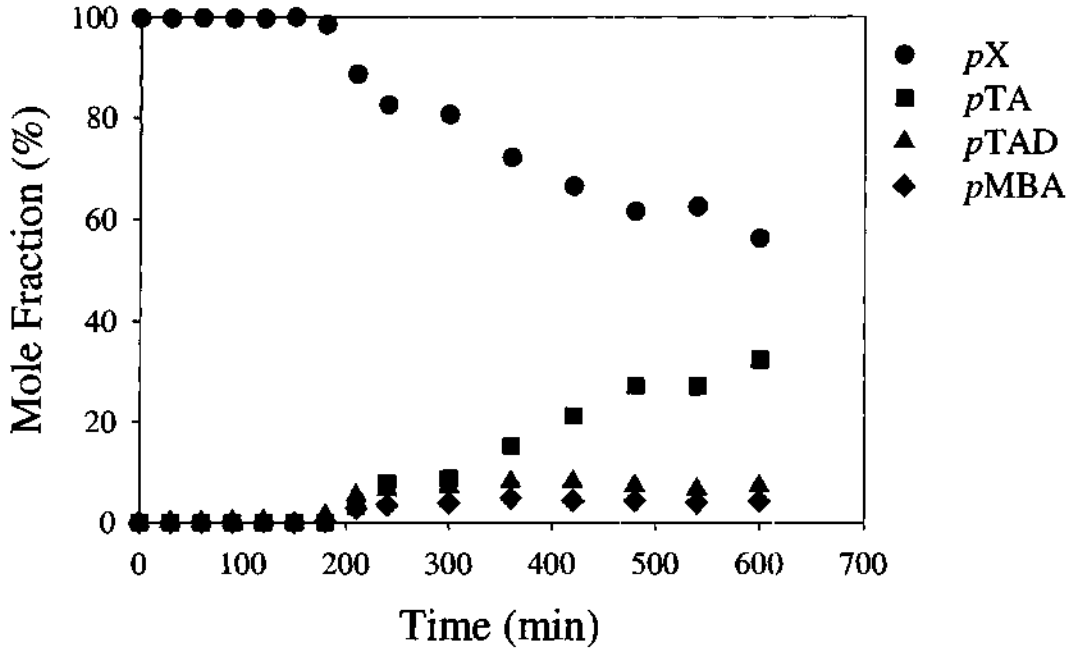

Figure F-28. Product distribution as a function of reaction time for semi-batch *p*X oxidation at 130°C and 120 psig. Air flow rate was 0.38 L/min. Agitation was 1600 rpm. Reactor was loaded with 0.489 mol *p*X, 0.888 mol *o*DCB, 2.222 mol H_2O, 0.00230 mol TBAB, 0.0175 mol KBr, 0.00224 mol NaOH, and 0.00720 mol pentachlorobenzene.

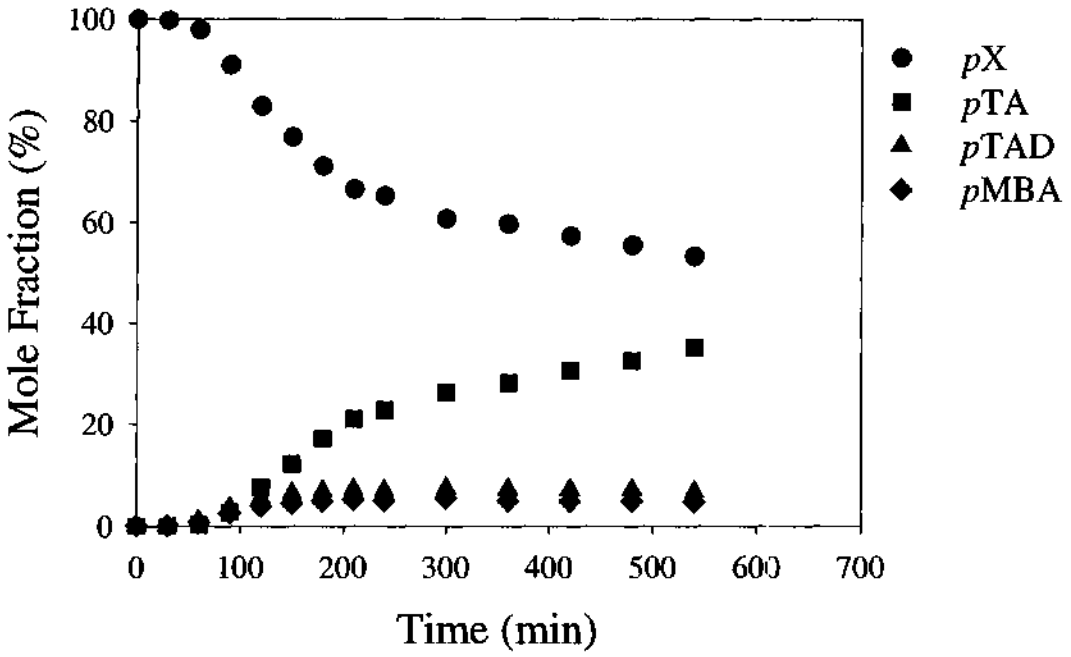

Figure F-29. Product distribution as a function of reaction time for semi-batch *p*X oxidation at 130°C and 120 psig. Air flow rate was 0.38 L/min. Agitation was 1600 rpm. Reactor was loaded with 0.653 mol *p*X, 0.711 mol *o*DCB, 2.222 mol H_2O, 0.00230 mol TBAB, 0.0175 mol KBr, and 0.00720 mol pentachlorobenzene.

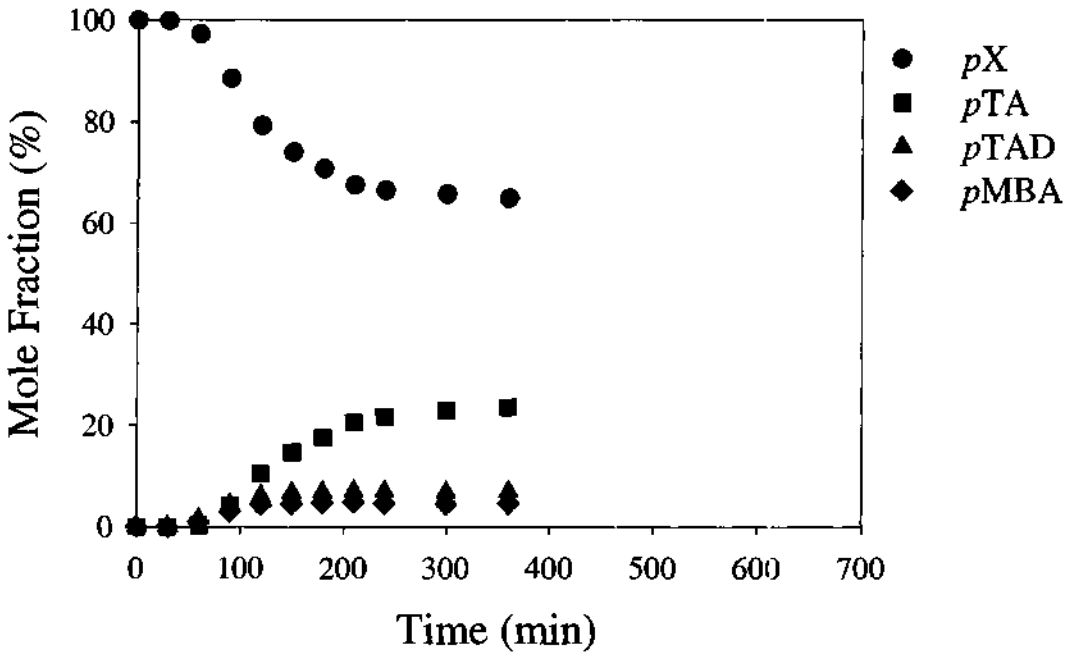

Figure F-30. Product distribution as a function of reaction time for semi-batch *p*X oxidation at 130°C and 120 psig. Air flow rate was 1.2 L/min. Agitation was 1600 rpm. Reactor was loaded with 0.653 mol *p*X, 0.711 mol *o*DCB, 2.222 mol H_2O, 0.00230 mol TBAB, 0.0175 mol KBr, and 0.00720 mol pentachlorobenzene.

VITA

Heather Patrick Lesutis was born in Montgomery, Alabama on May 2, 1971 to Hilda and Pat Patrick. After spending a few years in Oceanside, California, she lived with her parents and sister Bonnie in Atlanta, Georgia until her graduation from Pace Academy in May, 1989. She then matriculated at Princeton University, where she attained a B.S.E. in Chemical Engineering and graduated Cum Laude in June, 1993. On September 4, 1993, she married Michael Lesutis, a fellow Princeton University student. That fall, Heather joined the faculty of Pace Academy as an Upper School Mathematics and Physics teacher. Two years later, she entered graduate school at Georgia Institute of Technology under the research direction of Professor Charles A. Eckert. She has authored and coauthored one patent and three papers and has presented papers at two national meetings. After finishing her Ph.D. in May, 2000, she and her husband will remain in Atlanta, where she will continue her teaching career at Oxford College of Emory University.

Patents and Publications

Brown, J.S.; Chandler, K; Eckert, C.A.; Hurley, J.S.; Lamb, D.R.; Lesutis, H.P.; Liotta, C.L.; Schiraldi, D.A. Method for Esterification of Carboxylic or Polycarboxylicacid in the Presence of Supercritical Fluids and Catalysts Therefor. Patent Filed/Pending, Application Filed 10/98.

Lesutis, H.P.; Gläser, R.; Liotta, C.L.; Eckert, C.A. Acid/Base-Catalyzed Ester Hydrolysis in Nearcritical Water. *Chem. Comm.* **1999**, *20*, 2063-2064.

Brown, J.S.; Lesutis, H.P.; Lamb, D.R.; Bush, D.; Chandler, K.; West, B.L.; Liotta, C.L.; Eckert, C.A.; Hurley, J.S.; Schiraldi, D.A. Supercritical Fluid Separation for Selective Quaternary Ammonium Salt Promoted Esterification of Terephthalic Acid. *I&EC Res.* **1999**, *38*, 3622-3627.

Lesutis, H.P.; Gläser, R.; Griffith, K.; Liotta, C.L.; Eckert, C.A. Nearcritical Water: A Benign Medium for Catalytic Reactions. In Press.

Presentations

Lesutis, H.P.; Gläser, R.; Liotta, C.L.; Eckert, C.A. Acid/Base-Catalyzed Ester Hydrolysis in Nearcritical Water. Presented at the AIChE Annual Meeting, Dallas, TX, November, 1999.

Lesutis, H.P.; Liotta, C.L.; Eckert, C.A. Novel Process Applications for Quaternary Ammonium Salts. Presented at the Georgia Institute of Technology Chemical Engineering Seminar Series, Atlanta, GA, March, 1999.

Lesutis, H.P.; Brown, J.S.; Lamb, D.R.; Bush, D.; Chandler, K.; West, B.L.; Liotta, C.L.; Eckert, C.A.; Hurley, J.S.; Schiraldi, D.A. Interrupting a Reaction Sequence by Supercritical Fluid Extraction. Presented at the AIChE Annual Meeting, Miami Beach, FL, November, 1998.